

The Ocean Engineering Committee Final Report and Recommendations to the 29th ITTC



1. GENERAL

1.1 Membership and Meetings

The Committee appointed by the 28th ITTC consisted of the following members:

- Prof. Claudio Alexis Rodríguez Castillo (Chairman), Laboratory of Ocean Technology (LabOceano), Federal University of Rio de Janeiro, Brazil;
- Prof. Longfei Xiao, Shanghai Jiao Tong University, China;
- Dr. Viacheslav Magarovskii, Krylov State Research Center, Russia;
- Dr. Rae Hyoung Yuck, Samsung Heavy Industries Co. Ltd, Korea;
- Dr. Halvor Lie, SINTEF Ocean, Norway;
- Prof. Qing Xiao, University of Strathclyde, United Kingdom;
- Prof. Ayhan Menten, Istanbul Technical University, Turkey;
- Prof. Yasunori Nihei, Osaka Prefecture University, Japan.

Two in-person committee meetings were held:

- University of Strathclyde, Glasgow, United Kingdom, January 24-26, 2018;
- Samsung Heavy Industries, Daejeon, Korea, September 12-14, 2018.

1.2 Tasks based on the Recommendations of the 28th ITTC

The Ocean Engineering Committee is responsible for the issues in relation with moored and dynamically positioned ships and floating structures. For the 29th ITTC, the modelling and simulation of waves, wind and current is the primary responsibility of the Specialist Committee on Modelling of Environmental Conditions, with the cooperation of the Ocean Engineering, the Seakeeping, and the Stability in Waves Committees.

The following terms of reference were determined by the 28th ITTC:

- (1) Update the state-of-the-art for predicting the behaviour of bottom founded or stationary floating structures, including moored and dynamically positioned ships, emphasizing developments since the 2017 ITTC Conference. The committee report should include sections on:
 - a. the potential impact of new technological developments on the ITTC;
 - b. new experimental techniques and extrapolation methods;
 - c. new benchmark data;
 - d. the practical applications of computational methods to prediction and scaling;
 - e. the need for R&D for improving methods of model experiments, numerical modelling, and full-scale measurements.
- (2) Review ITTC Recommended Procedures relevant to ocean engineering, including CFD procedures, and
 - a. identify any requirements for changes in the light of current practice, and, if approved by the Advisory Council, update them;
 - b. identify the need for new procedures and outline the purpose and contents of these.
- (3) Review the state-of-the-art in offshore aquaculture systems (deeper water, further from shore, not in sheltered waters), including harsher conditions, larger volumes and scaling of whole structure vs scaling forces acting on nets.
- (4) Review the state-of-the-art in model tests of cable/pipe dynamics close to the sea surface

(substantial wave and current forces) (e.g. electric cables, hoses offloading). Rationale:

- a. Different from mooring lines: closer to surface (subject to wave forces) and flexible;
- b. Different from risers: S-shape risers usually at very deep water, no need to consider wave forces;
- c. Need to know more on the external forces for fatigue damage assessment / design;
- d. Investigate dynamic interactions between 2 floating platforms and connecting flow lines.

(5) Review the state-of-the-art in hybrid testing - software-in-the-loop tests for modelling wind forces. Rationale:

- a. Dominant frequencies are higher than those in hybrid mooring tests (wind change faster, quicker dynamics to be represented);
- b. Reference cases/tests to verify system – cases available are too different to be compared;
- c. Liaise with the SC on Hydrodynamic Testing of Marine Renewable Energy Devices for effects on wind turbine testing.

(6) Extend experimental wave run-up benchmark tests (four squared vertical cylinders) to measure wave run-ups and global forces on cylinders and to investigate scale effect.

(7) Carry out CFD benchmark study on two-body interactions, focusing on the investigation of viscous effects on the gap surface elevation using the benchmark experimental results produced by the 28th ITTC OE committee.

(8) Review the state-of-the-art for large diameter flexible risers used for deep water mining.

(9) Re-write Model Construction Procedure with focus on model construction issues (materials, tolerances, production methods, quality control, acceptance testing, etc.).

2. STATE-OF-THE-ART REVIEWS IN OFFSHORE STRUCTURES

2.1 Bottom Founded Structures

Bottom founded structures are widely used as production or oil recovering platform in shallow waters but have been also applied as offshore wind turbine supporting structures in the recent years.

Although the current trend in oil and gas industry is to explore and extraction in deeper waters which require more floating platforms, there is a high demand for life extension of existing fixed steel platforms in different regions, such as Gulf of Mexico, North Sea, Malaysian and Australian waters, that are now reaching, or have exceed, their design life. Deghani and Aslani (2019) have reviewed and discussed the various loads on these structures. Fatigue loading exerted by wave and wind actions is one of the main loading experienced by these platforms. Fatigue and vessel impact are reported to be responsible for almost half of the damages to steel offshore platforms. Corrosion having the highest rate in splash zone accelerates the initiation and growth of fatigue cracks that usually occur at the weld toe at the intersection of the chord and brace members. Horn and Leira (2019) have presented a methodology for evaluating the fatigue reliability of a bottom-fixed offshore wind turbine with stochastic availability. Fatigue damage was calculated in the foundation of an offshore bottom-fixed monopile-mounted large wind turbine. A detailed metocean model was used to evaluate the long-term fatigue damage distribution in both operational and idling conditions. It is shown that a deterministic

availability model may yield pessimistic fatigue life estimates compared to a stochastic model.

Luo-Theilen and Rung (2019) have presented hydrodynamic simulations of complex offshore installation procedures using mechanical couplings. To overcome the challenge of large relative motions, implicitly coupled overset-grids were applied. Special seaway boundary conditions combining viscous solutions in the near-field and inviscid solutions in the far-field were used to avoid undesirable reflections from the boundaries and allowed for the use of relatively compact domain sizes. With the help of the mechanical joints, three-phase (air-water-soil) flow simulations including structure-seabed interactions have been modelled realistically. The algorithm was successfully validated and applied to the installation process of a gravity foundation and a jack-up rig.

With the growing number of offshore wind installations, particular attention should be paid to the safe operation of assets. These assets are subject to extreme environmental conditions and high dynamic stresses caused by wind, waves, and currents. They are also largely exposed to hazards associated with collision with either commercial ships or infield support vessels. Moulas et al. (2017) have developed a numerical nonlinear finite element analysis (NLFEA) approach to evaluate the damage to wind turbine foundations when stricken by an offshore support vessel. Various accident scenarios were identified and the resulting damage to wind turbine foundations were analysed. Based on the results, an insight on how the next generation of wind turbine foundations can be designed in a more “collision-friendly” way has been provided. Chong (2017) have analysed the long-term offshore foundation that undergoes numerous mechanical cycles. A semi-empirical numerical scheme was used to simulate two offshore foundations subjected to repetitive loads (i.e., monopile and shallow foundation). Numerical results show that the most pronounced displacements occur during early cycles ($N <$

100), yet their incremental rate approaches toward an asymptotic value.

More recently, T. Yu et al. (2019) have developed a physical model for the scour induced by waves and current around a composite bucket foundation. Foundation models with scales of 1:40 and 1:60 were placed in a flume, and the scour process was monitored. The experimental results showed that the combined wave–current condition induced a greater scour range than the wave-only or current-only condition, but it did not necessarily induce a greater equilibrium scour depth than the current-only condition. The effects of dimensionless parameters such as the Keulegan–Carpenter number, ratio of velocities and Froude number on the maximum equilibrium scour depth were considered.

Wu et al. (2019) have reviewed the present state of knowledge concerning geotechnical and structural issues affecting foundation types under consideration for the support structures of offshore wind turbines, and provided recommendations for future research and development. Cheng et al. (2019) presented an experimental and numerical study of the combined bearing capacity of a recent hybrid foundation concept that merges a skirted footing with a deeper caisson (Figure 1). A significant increase in capacity was observed in all directions compared to a circular skirted mat of the same size due to the inclusion of the caisson.

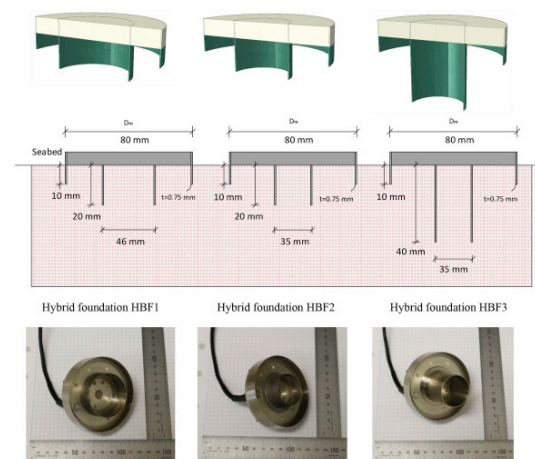


Figure 1: Hybrid foundation geometries (Cheng et al., 2019)

A structural optimization design method for jacket platform structure has been developed based on topology optimization theory (Tian et al., 2019). The method is applicable at an early design stage, which can determine the initial structure and force transmission path to maximize the structural stiffness. A set of constraints based on multi-criteria design assessment was applied according to standard requirements, which include stress, deformation, vibration, and design variable constraints (Figure 2). Results showed that the optimized structure had a 13.7% reduction in the global mass, 46.31% reduction in the maximum equivalent stress, and large ultimate carrying capacity ability under environmental loads.

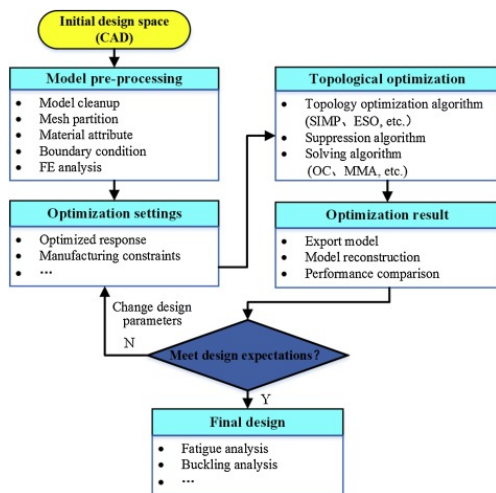


Figure 2: Flowchart of topology optimization solution (Tian et al., 2019)

Offshore wind turbines (OWTs) have played an important role in the field of renewable energy. The main issues in design of OWTs in regions of recent development have been aero- and hydro-dynamic loads; however, earthquake is a design concern in seismic areas such as East Asia and Western United states. Kaynia (2019) reviewed the state of practice in seismic design of offshore wind turbines. It was demonstrated that wind turbines are vulnerable to vertical earthquake excitation due to their rather high natural frequencies in vertical direction; however, inclusion of the radiation damping could contribute considerably to reduce the earthquake loads. Moreover, it was

demonstrated how soil nonlinearity could lead to settlement and permanent tilting of offshore wind turbines on caisson foundations or tripods. Ju and Huang (2019) have provided an analysis framework for OWT support structures subjected to seismic, wind, and wave loads using the finite element method with soil-structure interaction, and a conservative soil liquefaction analysis. The NREL 5-MW jacket-type OWT under IEC 61400-3 was analysed. The results indicate that seismic loads combined with wind and wave loads during power production often control the design, especially near the rated wind speed. For PGA over 0.52 g, almost all the members are controlled by the seismic loads, and the increase in the steel design weight can be over 40%. First-mode tuned mass dampers for jacket-type support structure with deep piles are efficient to reduce the vibration coupled from wind, wave, and seismic loads even with 20-m soil liquefaction. Z. X. Li et al. (2019) experimentally investigated the earthquake-induced added mass and inertial coefficient in the Morison equation through a dynamic test system with a water tank and actuator on four cylindrical steel tubes

Karimirad and Bachynski (2017) performed sensitivity analyses to investigate the importance of limited actuation of aerodynamic and generator loads for the responses of a 5 MW bottom-fixed turbine. Normal operational, parked and fault conditions have been considered. The aerodynamic yaw moment was only important for the yaw/torsional responses, but the sensitivity was quite high (up to 80% changes in the dynamic responses). In severe conditions with a parked turbine, aerodynamic damping had a significant effect on the responses. Removing the aerodynamic pitch moment induced errors up to 20% for some important load actions, i.e., pile and tower fore-aft bending moments.

Ghassempour et al. (2019) dealt with vibration mitigation via tuned mass damper in bottom-fixed, horizontal-axis offshore wind turbines. Focusing on a baseline 5-MW turbine mounted on a monopile, equipped with an

omnidirectional tuned mass damper inside the nacelle, the study explored a wide range of potential tuning frequencies, mass, and damping ratios, in both operational and parked rotor conditions. Due to inherent non-linearity of rotor dynamics, their results demonstrated that a conventional design of the tuned mass damper based on the natural frequencies of the support structure modes may not be suitable for offshore wind turbines.

O’Leary et al. (2019) investigated the application of lightweight fibre reinforced composite materials in the construction of offshore wind turbine support structures. A composite tower design suitable for the NREL 5 MW reference wind turbine was presented. The design was based on the most automated and low-cost composite manufacturing methods (pultrusion and filament winding). The mass of the tower was minimized using gradient based optimization approach. The cost of a composite tower was calculated and levelized cost of energy (LCOE) projections were discussed in comparison with the existing steel tower cost. The study determined that while the composite tower is technically feasible and has a lower mass than a comparable steel tower, uncertainty remains in how it compares economically in terms of LCOE.

2.2 Stationary Floating Structures

Stationary floating structures addressed in this section include FPSOs, semisubmersibles, TLPs, spars, FLNGs, and their riser/mooring and dynamic positioning systems. Unless specified, this section is focused on platforms for oil and gas industry, while some platforms for the offshore wind energy industry are given in Section 2.2.5.

2.2.1 FPSO Vessels

In number of units, FPSOs platforms continue to be leading type of floating offshore structures for oil and gas production. Among the different concerns associated to this type of platforms, green water and wave impacts have

been the issues that have attracted more attention in the recent years. Several works reporting experimental as well as numerical investigations have been found. In the latter, CFD simulations have been the main numerical tool adopted. For instance, green water on FPSOs subjected to beam and quartering irregular seas have been investigated through experimental model tests (Figure 3) and CFD simulations (Figure 4) in Silva et al. (2017a, 2017b). The model tests were performed for a 1:70 ship-type FPSO, with measurements of water elevations and loads during green water events. Many green water events have been monitored and critical regions for extreme elevation and loads have been identified along the deck edge. For the CFD simulations, extreme green water events at beam and quartering waves were selected and the whole wave vessel interaction was simulated, including the water on deck propagation. The applied methodology allowed access to high spatial resolution free surface position, water velocities and load distribution, aspects usually not available from experiments.



Figure 3: Evolution of a beam sea extreme green water event during model tests (Silva et al., 2017a)

Numerical prediction of green water was also carried out on a spread mooring FPSO (Wang et al., 2017). The numerical approach was based on 3D panel method and accounts for linear and nonlinear effects caused by bilge keel, mooring lines, and risers. The calculation is conducted in frequency domain with an iterative approach. Analysis of the results indicated a good agreement with model experiments and that the relative wave elevation at sides of the FPSO in oblique waves was strongly affected by bilge keel, mooring, and risers.

Hu et al. (2017) described numerically and experimentally the physical processes involved in offshore wave-breaking impacts on a truncated wall (representing the vertical section of a FPSO). Four types of wave impact were identified in the tests, and are referred to as slightly-breaking, flip-through, large air pocket and broken wave impacts (Figure 5).

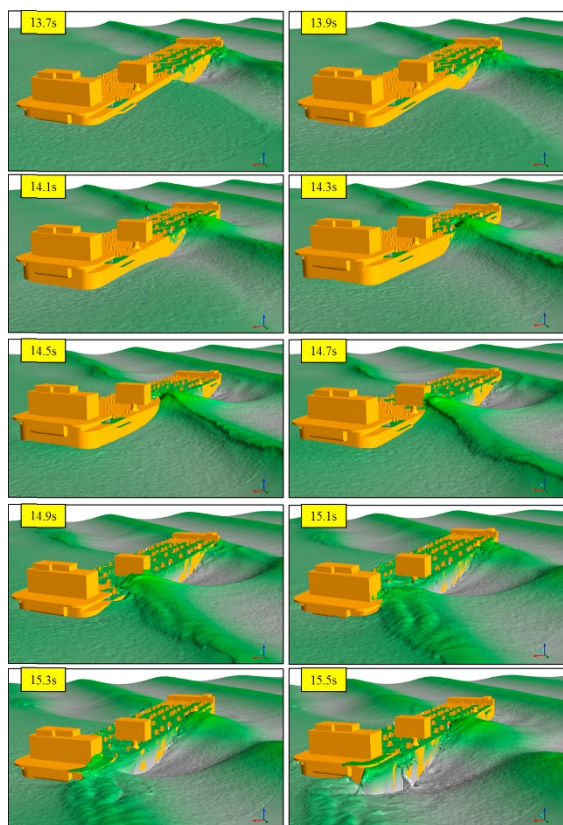


Figure 4: 3D simulation of a quartering sea green water event (Silva et al., 2017b)

Numerical prediction of green water was also carried out on a spread-moored FPSO (Wang et al., 2017). The numerical approach was based on 3D panel method and accounted for linear and nonlinear effects caused by bilge keel, mooring lines, and risers. The calculation is conducted in frequency domain with an iterative approach. Analysis of the results indicated a good agreement with model experiments and that the relative wave elevation at sides of the FPSO in oblique waves was strongly affected by bilge keel, mooring, and risers.

Hu et al. (2017) described numerically and experimentally the physical processes involved in offshore wave-breaking impacts on a truncated wall (representing the vertical section of a FPSO). Four types of wave impact were identified in the tests, and are referred to as slightly-breaking, flip-through, large air pocket and broken wave impacts (Figure 5).

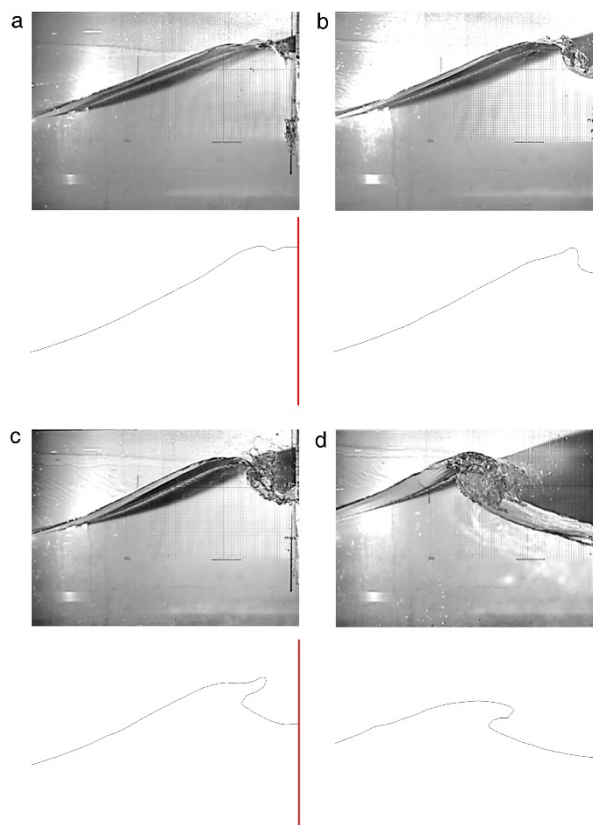


Figure 5: Wave profiles: numerical wave profiles (upper) and wave profiles (lower) (a) slightly-breaking (b) flip-through (c) large air pocket (d) broken wave (Z. Z. Hu et al., 2017)

Rosetti et al. (2019) performed an experimental analysis on green water events in a wave flume with a fixed model representing the middle-body of an FPSO hull, emulating the incidence of beam waves on such structure. Water elevations and impact loads on a deck structure were measured and water velocities were calculated with the purpose of correlating this information. Despite the variability in the peak impact forces observed from cycle to cycle, good agreement between mean values and deviation obtained in CFD and experiments evidenced that, in a statistical sense, numerical

model captured the essence of the phenomena. Wang et al. (2019) have studied the effects of the asymmetric riser and bilge keel arrangements on the motion response and relative wave elevation of a FPSO. A coupling effect between roll and heave has been identified, due to nondiagonal inertia terms associated to the asymmetric riser system.

Yan et al. (2019) have investigated, experimentally and numerically, plunging wave impacts on a box-shape structure focusing on three typical scenarios with distinct features, i.e. the wave impact occurs after, upon and before wave breaking. The wave elevations at typical positions, the wave impact pressures on the front and bottom of the platform, and the wave profiles of the transient wave impact process have been measured.

Hu et al. (2020) have experimentally and numerically studied the interaction between (nonbreaking) extreme waves, generated by focusing NewWave group, and a simplified FPSO. Both the two-phase incompressible CFD solver, OpenFOAM, and the fully nonlinear potential theory (FNPT) based solver, QALE-FEM, have been applied. The wave run-up and pressure on the FPSO surface, the wave load on and the response of the moored FPSO were examined. Viscous/turbulent effects were insignificant for the wave generation and propagation. Cases with a fixed FPSO were considered for quantifying the main sources of the error on the wave runup and the wave loading. The results revealed that a better reproduction of the incident wave by the self-correction wavemaker generally secures a higher overall accuracy on predicting the wave runup and the wave loading in a non-breaking extreme sea. Viscous effect played an important role in extreme motion response of an FPSO subjected to a focusing wave group, especially in cases with higher significant wave height. It is concluded that the QALE-FEM can accurately model the wave with high computational efficiency but may fail to achieve a reliable result when significant wave run-up or structure motions (especially the rotational

motions) occur. In contrast, the two-phase OpenFOAM has capacity of modelling violent wave impact and aeration, can well capture the viscous/turbulence effect, but shows limitation on large-scale wave propagation due to its extensively high computational cost. To take advantages from each and minimize their disadvantages, one may develop a hybrid model combining the QALE-FEM and the OpenFOAM, as suggested by Li et al. (2018).

Ha et al. (2021) have conducted an experimental investigation of the characteristics of the slamming impact loads on the bow of a ship-type FPSO under breaking and irregular wave conditions for three heading angles: 180°, 165°, and 150°, with the largest slamming impact loads observed for 150°. The slamming impact loads can be categorized as loads with one peak and two peaks. For a heading of 180°, more slamming impact loads with two peaks were detected, while those with one peak are more frequent for a heading of 150°. In loads with two peaks, the second peak is smaller due to the damping effect of the first slam. Depending on the heading angle, sway, roll, and pitch motions appear as the more important factors for the slamming impact loads.

Issues associated to side-by-side configurations of FPSOs or box-shaped structures have also attracted a growing concern. For instance, Li (2020) studied the hydrodynamic interaction of side-by-side vessels based on the gap resonant modes theoretically derived by Molin et al. (2002). The hydrodynamic associated wave elevations, coefficients, and wave forces were analysed for a real hull shaped FPSO and a ship under parallel and nonparallel configurations for different wave headings. The numerical simulations of vessel motions, RAOs by white noise test and relative motion under irregular waves were validated by measurement in model tests. The shielding effect was also evaluated numerically and experimentally by exchanging vessels on lee-side and weather-side. Results indicate that the first mode which is superior under beam sea may become less significant

under oblique and head seas. Higher resonant mode shifts to lower frequency in the nonparallel configuration. The shielding effect only suppresses the motion caused by the gap resonance, the natural frequency resonance like roll remains without change. A numerical investigation of viscous effects on the gap resonance between side-by-side boxes have shown that flow separation accounts for most of the energy loss during the process of gap resonance (Feng et al., 2017).

Jiang et al. (2020) have also numerically investigated the hydrodynamic behaviour of box-systems with and without narrow gaps, by employing a numerical wave flume. Their results indicate that the wave resonance in the narrow gap increases the horizontal and vertical wave forces on each box around resonant frequency. The fluid resonance in the narrow gap can also significantly affect the total vertical wave forces on two-box systems; while the influence on total horizontal wave forces is not remarkable.

A two-dimensional numerical wave tank based on OpenFOAM was used to investigate the effect of heave motion on the gap resonance formed between two boxes under the action of regular waves (Gao et al., 2021). Two series of numerical experiments were conducted to compare the effects of upstream box motion on gap resonance. In the first series, the two boxes are fixed in the wave flume. In the second series, Box A heaves freely under incident wave actions, while Box B remains fixed. The heave motion of the upstream box leads to a lower wave height amplification inside the gap and a higher fluid resonant frequency (close to the natural frequency of the heave free decay).

Other issues associated to the behaviour of FPSOs in the presence the waves, wind and/or currents are reported in the following works:

Zangeneh et al. (2017) reported model tests of a turret-moored FPSO at 1:120 scale conducted with regular waves under two wind speeds (12 and 25 m/s full scale). Free-decay tests were also conducted to investigate the

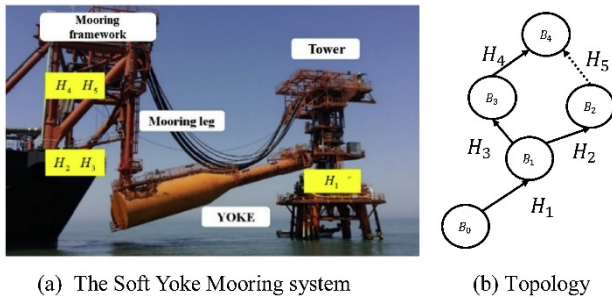
contribution of the wind damping to the total damping. Measured results show that in the presence of wind, the damping values are higher than those estimated due to hydrodynamics only. This wind induced damping on FPSOs, can result in smaller heading angles and play a large role in the station-keeping dynamics of moored-tankers.

Fonseca and Stansberg (2017) presented a method to estimate realistic surge and sway wave drift force coefficients for the Exwave FPSO. Model test data is used to identify the difference frequency wave exciting force coefficients based on a second order signal analysis technique. The process also identifies the linearized low frequency damping. Comparisons with empirical mean-wave drift coefficients showed that potential flow predictions underestimate the wave drift forces, especially at the lower frequency range where severe sea states have most of the energy.

Sanchez-Mondragon et al. (2017) have investigated the piston mode effects in moonpool on the motion behaviour in a turret-moored FPSO under regular waves. Two series of experimental test have been conducted in two different configurations: one using a turret that prevents water inflow, and the other using a turret that allows water inflow between the moonpool and the internal cylinder.

Kang et al. (2017) investigated the model test method of the FPSO and offloading system by using the development mode of “FPSO + CALM + TANKER” working in a 1700-m depth of offshore West Africa (Figure 6a). An equivalent design based on static and dynamic similarity criteria for oil offloading line (OOL) was discussed, and a type of creative method for the equivalent design of OOL in a model test was proposed. It was observed that the calculated results of the truncated system (Figure 6b) are basically consistent with those of the prototype system, and the design of the model test scheme is demonstrated to be robust and reliable.

alternating loads influence the service life of hinge joints.



(a) The Soft Yoke Mooring system

(b) Topology

Figure 7: Topological graph of the SYMS (Lyu et al., 2019)

Reynolds scale effects and shielding effects on current loads of offshore vessels in side-by-side configuration have been addressed by Koop (2020). Based on CFD calculations, those loads could be obtained with acceptable accuracy for most headings. The results for the current coefficients at full-scale Reynolds number are found to be lower than at model-scale Reynolds number, which implies that results from model tests are conservative for the current loads. However, current load coefficients may be used to estimate hydrodynamic damping and a lower coefficient implies lower damping.

Towing- and course-stability of a FPSO towed by a tug-boat was experimentally investigated by Park et al. (2021) using the conventional experimental method (CEM) in which the lateral motions of the tug-boat are neglected (Figure 8) and, a new experimental method (NEM) in which the lateral motions of the tug-boat are modelled as a sinusoidal motion using a forced oscillation device changing frequency and amplitude (Figure 9). Higher lateral speed of tug-boat compared to the towed FPSO or relatively large tension on the towline may cause poor course stability. The towed point had strong influence on the towing stability under the CEM.

Roll damping prediction for FPSO hulls have also attracted the attention of several authors during this ITTC term and several works have addressed this problem numerically, experimentally and/or a combination of both

approaches (Asgari et al., 2020; Avalos and Wanderley, 2018; Fernandes et al., 2018; Ji et al., 2019; Kim et al., 2020; Rodríguez et al., 2020).

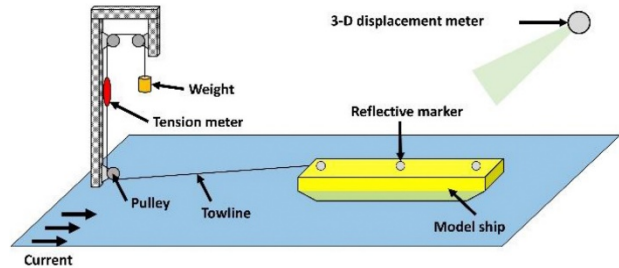


Figure 8: Layout of conventional experimental method (CEM) - (Park et al., 2021)

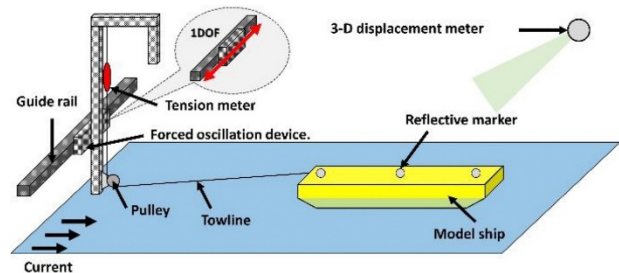


Figure 9: Layout of new experimental method (NEM) - (Park et al., 2021)

2.2.2 Semi-submersibles

Semi-submersibles have attracted much more attention in the recent years due to their suitability in reducing wave-induced motions of the floating system. However, there are various challenges related to vortex induced motions (VIM). Size of columns, corner shape and helical strakes help in the mitigation of dynamic responses in waves, but their effects need to be further investigated in terms of VIM performance. Hydrodynamic loads evaluation continues to be another big challenge.

X. Hu et al. (2017) carried out numerical studies on vortex-induced motions of a deep draft semi-submersible with four columns based on improved delayed detached eddy simulation (IDDES) model. The transverse motions for 22.5° current incidence are larger than those for 0° and 45° current incidences in the study. The mean drag force coefficients for these simulated current incidence angles tend to grow as the

transverse motion amplitudes increase. In addition, parametric studies have also been performed to examine the effects of the column corner radius on VIM.

Tan et al. (2017) presented a vortex-induced motion performance of a dry tree Heave and VIM Suppressed (HVS) semi-submersible designed to possess low VIM and low heave responses (Figure 10). VIM performance was estimated using model testing and Computational Fluid Dynamics (CFD) analysis. From model tests, VIM suppression was observed in the HVS semisubmersible due to the presence of the column steps. CFD simulations of the model tests showed results comparable to the measured data. Additional CFD analysis was performed to account for the external damping effect of the mooring lines and risers on the VIM performance of the HVS semisubmersible.

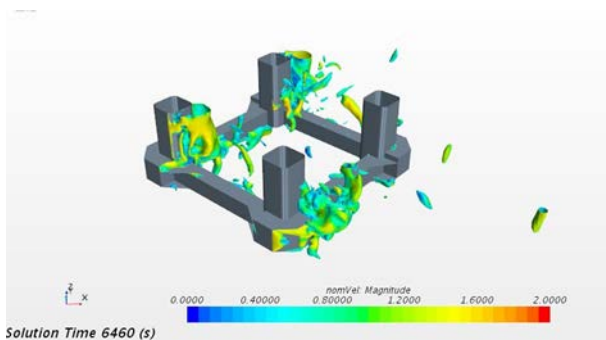


Figure 10: VIM Performance of HVS Semi-submersible (Tan et al., 2017)

Liao et al. (2017) presented numerical analysis of wave impact loads on semi-submersible platform which can result in structural damage. In the method, the FDM (Finite Difference Method) is applied for solving flow field, and the THINC/SW (Tangent of Hyperbola for INterface Capturing with Slope Weighting) model, which is kind of VOF (Volume-of-Fluid) model, is adopted to capture the free surface.

Yu et al. (2017) attempted to assess the ultimate strength of a new large-sized semi-submersible platform with lateral brace structures and square cross-section columns using a three-dimensional nonlinear finite

element model under different loading conditions. Results showed that the time dependent dynamic explicit method was reliable and feasible for the calculation of ultimate strength of such complicated structure. For the target platform, the bracings and upper hull structure were the main bearing component and were critical for the ultimate strength of the whole structure. High stress occurred in connection areas and special attention shall be paid for.

M. Liu et al. (2017a) conducted a numerical study using CFD method on vortex-induced motions of semi-submersibles (SS) with various types of columns (Figure 11). Four semi-submersibles with different column designs: a SS model with four rounded square columns (SRC-SS), a SS model with four circular columns (CC-SS), a SS model with two tandem rounded square columns and two tandem circular columns (SRCT-CCT-SS), and a SS model with two staggered rounded square columns and two staggered circular columns (SRCS-CCS-SS) were considered with the current headings ranged from 0° to 180° . The most significant transverse motions of the CC-SS model occur at the 0° current heading with the largest nominal transverse amplitudes around 74% of the column diameter. On the other hand, the maximum amplitudes in the transverse direction of the SRC-SS model, approximately 63% of the column width, are observed at the 45° current heading. It is suggested that the VIM responses could be mitigated when the semi-submersible consists of combined circular-section and square-section columns.

Cahay et al. (2017) presented ice load calculation on semi-submersible platform using Ice-MAS which uses a multi-agent technology and can simulate ice loadings on complex geometry by user input file like semi-submersible floaters with pontoon and columns. The study was focused on the results obtained for different geometries subject to ice sheet loading through different incidence angles. The

issues related to the anchoring of the platform were addressed in a simplified way.

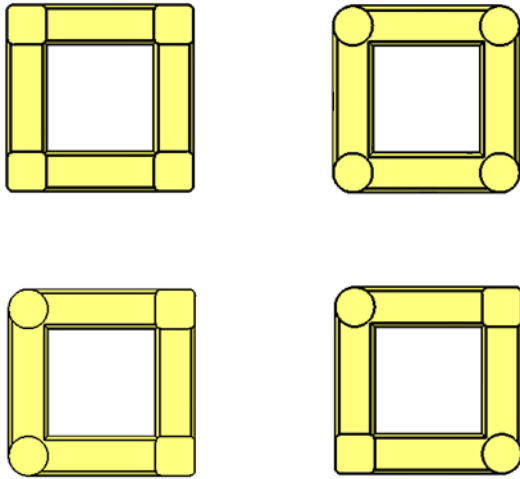


Figure 11: Different column designs for VIM study (M. Liu et al., 2017a)

Liang et al. (2017) presented an experimental study and numerical simulation with the aim to investigate the VIM effects on the overall hydrodynamics of the structure and study the fluid physics associated with VIM of a deep-draft semi-submersible (DDS), respectively. Good correlation has been demonstrated among the vortex shedding patterns, the fluctuating forces on the structure, and the VIM trajectory. Besides, the differences of the mooring line settings between the experiments and numerical simulations may affect the forces on the structures.

M. Liu et al. (2017b) presented an experimental study and three-dimensional simulations to analyse the pontoon effect on the VIM of two semi-submersible and a four-column structure. The results show that the presence of pontoons delays the onset of VIM to a higher reduced velocity in the cases of the four-pontoon DDS. Additionally, the four-column structure with no pontoons shows the most significant transverse response and yaw motions owing to the largest fluctuating lift forces induced by the well-established wake.

M. Liu et al. (2017c) conducted numerical simulations by the detached eddy simulation

method validated by experimental data and then were used for parametric analysis of the VIM performance of various semi-submersibles with different column rounded ratios (Rc/L) and pontoon rounded ratios (Rp/Lp). The results show that the effect of pontoon shape on the transverse response is negligible for semi-submersibles with sharp square columns, while for semi-submersibles with rounded square columns or circular columns, the sharp rectangular pontoons greatly mitigate the VIM response.

Pessoa et al. (2018) presented an experimental and numerical study of the free surface elevation over the pontoons of a semi-submersible platform in waves. It was shown that the maximum free surface elevation over the pontoons in front of upwave columns can be severely overestimated if calculated with the current state of the art numerical models, which are based on linear diffraction-radiation theory. The observed discrepancy in this case can be explained primarily by a very high linear predicted amplification induced by the shallow pontoon, with resulting high local steepness leading to local breaking and dissipation. Such pontoon effects should be addressed in semi-submersible platform air-gap analysis.

Batalla Toro et al. (2018) summarized the challenges of integrated decommissioning of a pentagon shaped production semisubmersible in the UK. The decommissioning process of the Buchan Alpha in the UK after more than 40 years since being built and more than 35 years of successful operation was explained. Significant challenges for the decommissioning team included the requirement to preserve the operational status of the subsea infrastructure for potential future field redevelopment and the diver disconnection of the subsea wells.

The float-over operation is less time-consuming and has larger lifting capacity, especially for large and medium sized offshore platforms. The float-over installation process of a deep-water semisubmersible platform topside was analysed by Gang et al. (2018). The calculation results show that the float movement

condition meets float-over installation requirements of topside. The analysis can provide a reference for the project of the float-over installation in the future.

Larsen et al. (2018) presented results from small-scale model testing of three semi submersibles together with an overview of damping contributions of low frequency motions. The main parameters of the semis such as displacement, number of columns and diameter of columns were intentionally varied to assess the effects on total wave drift forces and corresponding damping. For accurate prediction of low frequency motions of moored semi submersibles in extreme sea states, a damping level in the range 40–70% of critical damping should be applied for surge and sway when the empirical correction formulas for wave drift forces are applied.

Yang et al. (2018) presented numerical predictions of low frequency horizontal motions of a semi-submersible in combined high waves and current condition. Low frequency surge responses calculated by the simulation model are compared with model tests for waves only and for combined collinear and noncollinear wave and current conditions.

He et al. (2018) presented a set of VIM CFD simulations for a semi-submersible with and without helical strakes (Figure 12). The Vortex Induced Motion (VIM) of semi-submersible with and without helical strakes was compared against each other for different reduced velocities (U_r). The flow characteristics of the semi-submersible platform is studied based on the characteristics of vortex shedding. For different current incident angles, time histories, trajectories, and vorticity of the semi-submersible at different reduced velocities were reported.

Zhu et al. (2018) investigated the fatigue damage of stiffened plates in splash zone for a semi-submersible. A global analysis model of the Gjøa semi-submersible, is built and the local response for the side structure was investigated. The contribution of fatigue damage due to

global and local load effects are compared and presented.

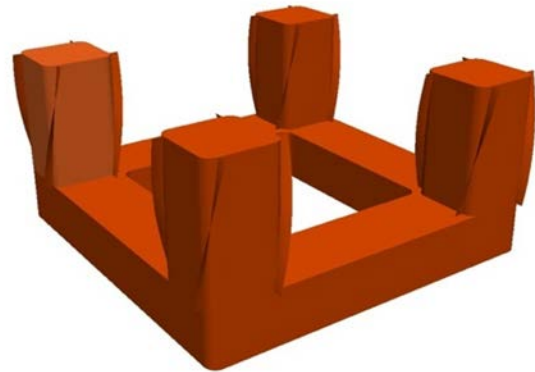


Figure 12: Semi-submersible with helical strakes (He et al., 2018)

Zhu (2018) designed a four column semi-submersible with low heave motions based on genetic algorithm. The geometry of a ring-pontoon four-column semi-submersible was generated by parametric modelling. The heave transfer functions at the centre of gravity were calculated using WADAM. Genetic algorithm was used to find the most favourable heave responses. The parameters that influence the heave motions have been discussed.

Zhao and Wan (2018) presented a parametric study of geometrical variations on the vortex-induced motions (VIM) of a deep-draft semi-submersibles (DDS) - Figure 13. Paired-Column semi-submersible (PC-Semi) design involved paired-column gaps and column cross-section and these parameters could be tuned to mitigate dynamic response to waves and currents. A geometry model scaled at 1:54 from MARIN was selected as the baseline model for parametric study and CFD code validations. VIM characteristics of paired-column, gaps and other geometrical variations were numerically investigated. The ability of a CFD method in optimizing geometric design parameters for the mitigation of VIM response for a deep-draft semi-submersible was demonstrated.

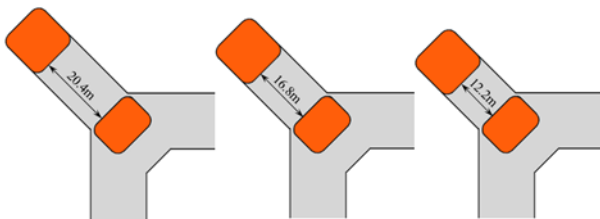
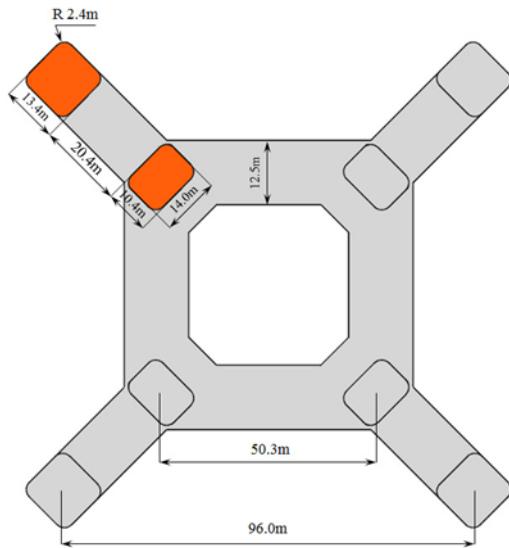


Figure 13: Geometrical Variations to mitigate VIM for PC-Semi (Zhao and Wan, 2018)

D.-J. Li et al. (2018) discussed the structural configuration selection and optimization design of 7th generation semi-submersible drilling unit (CSDU) based on the profound investigation on the load-resistance characteristics of the overall structures and considering the stress distribution variation of the deck box with the integration of different lower hull configurations. The study also investigated the effects of different types of upper and lower hull joints on the structural strength and fatigue in way of the main connection regions and provides the major connection optimization design.

Liang and Tao (2018) concentrated on the hydrodynamics around a deep-draft semi-submersible (DDS) to investigate the corner shape effects. Three models based on a typical DDS design with different corner shapes were numerically investigated under 45° incidence. It is demonstrated that, as the corner shape design changed, the hydrodynamic characteristics alter drastically. The flow patterns examined

revealed some insights of the fluid physics due to the changing of different corner shape designs.

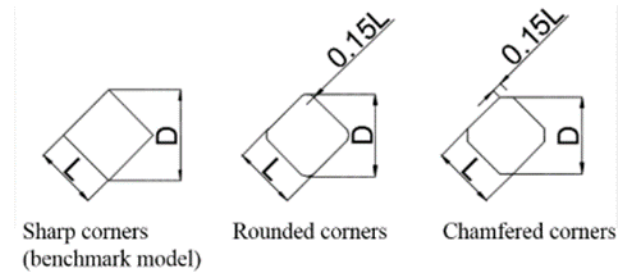


Figure 14: Corner shape effects for DDS (Liang and Tao, 2018)

Kim et al. (2019) conducted experimental and numerical study of horizontal wave impact loads for a semi-submersible drilling unit (Figure 15). A semi-submersible drilling unit model was tested to estimate horizontal wave impact loads on vertical side of deckbox following the procedure recommended by DNVGL OTG-14. The model test data showed that there is clear difference in the relationships between upwell and horizontal wave impact pressure between near column/pontoon and around centreline. The CFD simulation results clearly showed that the flows in front of column are strongly accelerated in vertical direction by blocking effect of column and pontoon, eventually producing strong run-up jets.

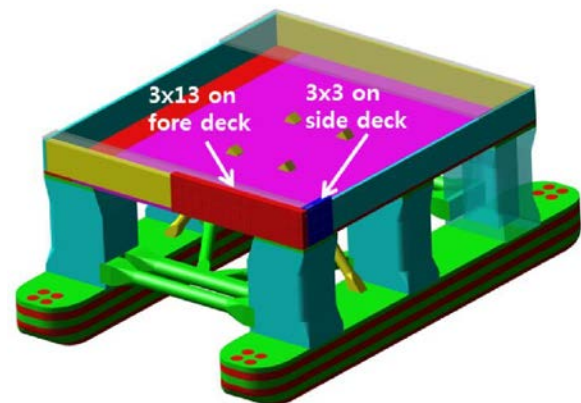


Figure 15: Semi-submersible drilling unit with force sensors to measure wave slamming loads (Kim et al., 2019)

Seo et al. (2019) also conducted experimental evaluation of wave impact loads on a semi-submersible structure according to trim angle. To evaluate wave impact loads on the semi-submersible structure, a series of experiments were conducted in a 2D wave flume. In the experimental test, a half-model semi-submersible was used, and 11 uniaxial force sensors were installed on deck side, column side, and deck bottom. To generate horizontal and bottom wave impact on the test model, focusing wave was applied. The model was fixed without any motion during each test, while the trim angle of the model was changed to examine the effect of trim angle on wave impact load. Through this, the characteristics of the wave impact force at each position were investigated.

Gonçalves et al. (2020) conducted an experimental study of the effect of the pontoon dimensions on flow-induced motions (FIM) of a semi-submersible platform with four square columns (Figure 16). FIM is an essential topic on multi-column platforms due to the effect on the mooring line fatigue life. Vortex-Induced Motions (VIM) or galloping behaviour can be observed for an array of four columns with square sections. The presence of pontoons showed to be important for changing the flow around the array and promoting different amplitude behaviours of the motions in the transverse direction.

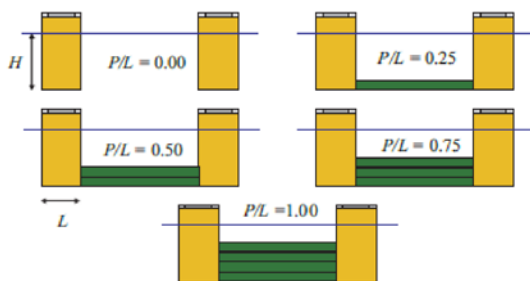


Figure 16: Five different pontoon ratios tested by Gonçalves et al. (2020)

Although some model-scale experiments have been conducted, there are still limited experimental studies especially pertaining to VIM and hydrodynamic loading estimation for

semi-submersible floaters. Most of the studies are limited to CFD evaluations for a general description of the phenomenon. Therefore, it is recommended to conduct state of the art benchmark experiments to validate the use of different column designs and use of helical strakes in columns for VIM study.

2.2.3 TLPs

During the review period, TLPs behaviour has been investigated numerical and experimentally with special focus on responses under extreme wave conditions. For instance, Abdussamie et al. (2017) provided detailed experimental information on the global behaviour of a TLP due to wave-in-deck events in abnormal waves. The wave events that produced the maximum and minimum tendon tension generally did not correspond to the largest wave crest or the largest wave steepness; this indicates that selection of the design wave event or wave train, in the same sea state, may require special attention (Figure 17). Lim and Kim (2019) investigated the statistical behaviour of the airgap of a TLP based on potential flow theory up to second order to model wave elevation around the platform and eigen-value method to estimate the extreme airgap. The effect of short-crestedness and the platform set-down were investigated. Yu et al. (2019) investigated numerically a series of tendon one-time failure and progressive failure for a whole TLP with top-tension risers under an extreme cyclone. Different directions of environment load that include extreme wind, wave and current and tendon failure positions were considered.

Also of interest is the dynamic interaction of TLPs with other bodies, such as moored vessels, auxiliary platforms, etc. Choi et al. (2018) have conducted experimental and numerical analyses to investigate the coupled behaviour of a TLP combined with a tender semi-submersible platform with focus on the multi-modal behaviours. Free decay tests showed that the TLP and semi-submersible system had complex coupled behaviours with multiple natural mode

frequency components. Dong et al. (2019) have systematically investigated the TLP - Tender Assisted Drilling coupled system under 0° , 45° and 90° headings by numerical and experimental analyses (Figure 18). The focus was on the global motion performance of the multi-body system, relative motion between gangway connection points, characteristics of dynamic gangway responses with predictions for extreme values and the definition of extreme sea conditions. Experiments with a 1:40 scale including decay tests, static offset tests, white noise wave tests, and irregular wave tests has been performed to validate the numerical model and addressed the difficulty of modelling of tendons, risers of TLP, hawsers and mooring lines.

maximum surge motion, and the minimum airgap.



Figure 18: Experiment of TLP-TAD coupled system (Dong et al., 2019)

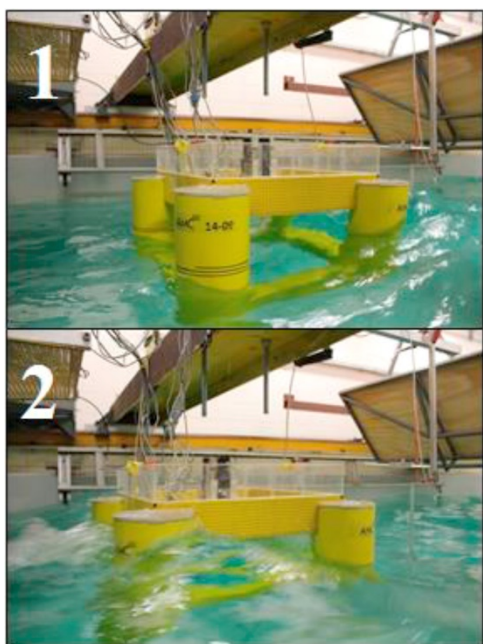


Figure 17: Wave impact at the TLP model: (1) water entry; (2) water exit (wave propagating from right to left) - Abdussamie et al. (2017)

Concerning TLPs design, Zhang et al. (2018) have proposed Innovative TLP Optimization Program (ITOP) to solve the multi-objective optimization problem for a TLP. Hull draft, column spacing, column diameter, pontoon height, and pontoon width are selected as design variables. The objective functions include the maximum dynamic tendon tension and the total weight of the platform, with three constraints being the maximum heave motion, the

2.2.4 Spar platforms

Recently, spar platform has become one of the most attractive deep-water development concepts thanks to its superior stability and powerful operability in deep water offshore regions. Benefits of the deep drafted first-generation classic spar, such as excellent stability and hydrodynamic performances that allow dry tree drilling and production, large capacity of the mid hull section for oil storage, cost efficiency for construction and save in-service operations, are combined to provide a competitive solution from moderate deep water of 300 m to ultra-deep water of 3000 m. COOEC (China Offshore Oil Engineering Company) has made a great breakthrough to the new Spar Drilling Production Storage Offloading Platform (SDPSO) and therefore has successfully mastered the water-oil replacement technology (Figure 19). The integrated innovation technology creates a new model of integrating the drilling, production, storage, and exporting, and will lead the "second" deep-water technology revolution if applied successfully in engineering. The oil-water replacement technology is a core and key technology for SDPSO underwater wet storage (W. Liu et al., 2017).

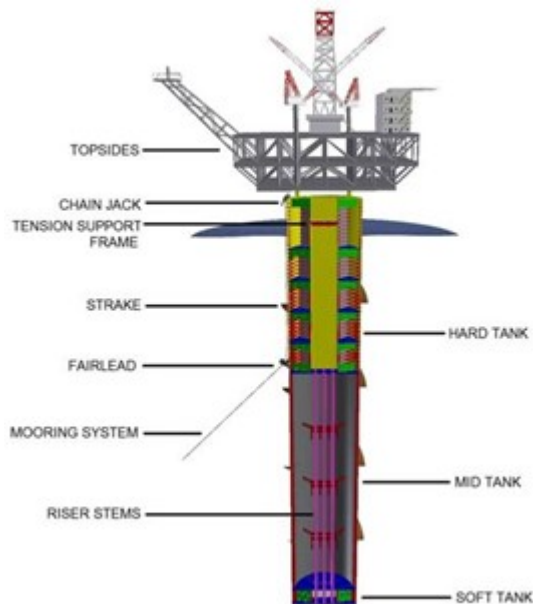


Figure 19: SDPSO Model (W. Liu et al., 2017)

Research has been carried out to address the global motions of spar platforms in waves, currents, and wind. Soeb et al. (2017) investigated the response of a fully coupled spar platform under a regular ocean environment. Considering the coupling effect of the platform and its mooring system, the responses of the spar platform were extracted and evaluated in time histories along with Response Amplitude Operator (RAO). The behaviours of coupled spar platforms were investigated under real sea environments for increasing water depth to ultra-deep together with the load variability employing sea current for surge, heave, pitch, and mooring tension responses. They modelled the integrated spar hull and mooring line in finite element code ABAQUS/AQUA. Motions showed consistency in the behaviour of spar platform responses. Surge response indicated the static offset of the platform due to the static current force under wave plus current and the current force compressed oscillations and reduced heave and pitch magnitude. For larger water depth, the platform responses were reduced significantly due to the increased damping of the mooring line.

Jin et al. (2018) focused on the influence of small-scale cylinders on the motion response under wave action to estimate the response more

accurately. A mooring truss spar platform was used with a second-order wave-body interaction numerical model in the time domain based on the Laplace equation. This numerical model simulated the large amplitude slow drift motion of the truss spar platform under bi-chromatic waves. The results showed that small-scale cylinders influence damping. At the same time, the existence of small-scale cylinders increased the added mass of the platform, thus the nature frequency was changed and moved to lower frequency, which led to large amplitude slow drift motion of the structure.

VIV and VIM are phenomena that affect several offshore compliant structures such as spars. Harsh environmental conditions can induce VIV and VIM and cause the failure of these structures. In the recent years, several investigations have addressed those problems and ways to mitigate them. Sun et al. (2018) employed the discrete vortex method (DVM) based on the stream function equation and vorticity formulation to study large vortex-induced motions (VIM). Sway and surge displayed similar periodic vibration. As the reduced velocity increased, surge displacement got larger and changed from irregular-amplitude to stable-amplitude motions with a well-defined period. As the Reynolds number (Re) increased, initially, the sway displacement was in direct proportion to the Re , but then its amplitude ratio (amplitude/diameter) exceeded 1.0, and after, decreased to less than 1.0, evidencing the “lock-in” phenomenon. The VIM trajectory was not clear and regular at low reduced velocities. With the increase of Re , the trajectory exhibited an obvious shape of “8” that gradually become more regular, i.e., periodic, and repeatable. Kumar et al. (2018) focused on the experimental investigations of an elastically mounted circular cylinder shrouded with a net substructure called Ventilated Net (VN) to suppress VIV. The VN was an omnidirectional, economical, customizable net substructure comprising flexible hollow tubes in a systematic arrangement. This device could be retrofitted to the offshore structures/risers to attenuate VIV. Various configurations have been tested to

address the reduction of VIV and drag forces acting on the oscillating cylinder shrouded with VN. VIV amplitudes have been measured at high Re regime, ranging from $(0.22-2.50) \times 10^5$. The effect of spaces between the flexible hollow tubes and shrouding radii of VN around the cylinder was also addressed. It was observed that a cylinder with VN of dense mesh at a radial spacing of twice the diameter of the bare cylinder, suppresses VIV by 98% and drag force by 40%, at Re of 1.2×10^5 .

Samadi and Ghodsi Hassanabad (2017) analysed the catenary mooring of a non-classical spar truss platform in the Caspian Sea. The hydrodynamic analysis including the mooring system was based on the three-dimensional diffraction method. The effect of removing mooring lines was also investigated. Under that condition, roll and pitch motions were not significantly affected and kept their stability but sudden changes in surge motions were observed.

W. Li et al. (2018) investigated the nonlinear coupling internal resonance of heave, roll, and pitch motions of a spar platform when their frequencies are in the ratio of 2:1:1 under wave and vortex exciting loads. Three degree-of-freedom (DOF) nonlinear coupled equations were established by considering a time-varying wet surface with a first-order wave force in heave and pitch and a vortex-induced force in the roll motions equation. The first-order steady-state response was solved using the multi-scale method. Multiple solutions of the motion equations using an analytic method and a numerical simulation were discussed. The jump phenomenon and regions of multiple solutions depending on the values of damping and detuning parameter were detected.

O'Connell et al. (2018) developed a Computational Fluid Dynamics (CFD) model for a free heaving Oscillating Water Column (OWC) spar buoy with non-linear Power Take-Off (PTO). A comprehensive system comprising of the 3D numerical wave tank, 1-DOF set-up, and non-linear PTO allowed the development of a heave-only OWC spar buoy model with a non-linear PTO. Experiments

completed by the UCC MaREI centre in LIR-NOTF ocean wave basin under the FP7 MARINET project were detailed and used to validate the comprehensive model. A range of regular waves was applied, and responses of heave and chamber pressures were compared to experimental data.

Yang and Xu (2018) analysed the parametric instability of a spar platform in irregular waves. A Hill equation was derived in this work, which can be used to analyse the parametric resonance under multi-frequency excitations. The derived the Hill equation for predicting the instability of a spar included non-harmonic excitation and random phases. The stability charts for multi-frequency excitation in irregular waves were given and compared with that for single-frequency excitation in regular waves. Three-dimensional stability charts with various damping coefficients for irregular waves were also investigated. The results showed that the stability properties in irregular waves have notable differences compared with those in the case of regular waves.

Banik et al. (2019) investigated the effect of the directionality of waves on the responses of a spar-type floating offshore platform restrained by four catenary mooring cables. The numerical model and simulation were validated based on experimental results (natural periods, RAOs, and response statistics).

Montasir et al. (2019) presented the effect of mooring diameters, fairlead slopes, and pretensions on the dynamic responses of a truss spar platform in intact and damaged line conditions. The spar was modelled as a rigid body with three degrees-of-freedom. The implicit Newmark Beta technique was used to analyse its motions in time-domain. The mooring restoring force-excursion relationship was evaluated using a quasi-static approach. To eliminate the conventional trial and error approach in the mooring system design, a numerical tool was settled and described.

Wang and Zhou (2020) carried out numerical simulations and experiments about

the scale effect of internal solitary wave loads on spar platforms. The scale effect on the viscous pressure-difference force is important while the scale effect on the wave pressure-difference force is not clear for the horizontal force. Morison equation with the same set of inertia and drag coefficients is not applicable to estimate the internal solitary wave loads for both the prototype and experimental model. Those coefficients should be modified to account for the scale effect. It is possible to get dimensionless vertical forces measured in model scale and use directly on the prototype based on Froude similitude. However, for the dimensionless horizontal force, the measured values in the laboratory will overestimate the corresponding values on the prototype if the Froude extrapolation laws are directly applied.

Subbulakshmi and Sundaravadivelu (2021) investigated the heave and pitch responses of spar platforms with single and double damping plates under regular waves. Damping plates are generally used to decrease the response of the floating platform by increasing the added mass and damping. Regular wave experiments were conducted on a 1:50 scale spar hull with damping plates. Heave and pitch response amplitude operators (RAOs) were numerically predicted using ANSYS-AQWA and compared with model test results. Parameters of scaling ratios such as damping plate diameter to spar diameter ratio, damping plate position to spar draft ratio and spacing between the double damping plates to spar draft ratio were considered for the analysis. Heave and pitch RAOs reduced with an increase in scaling ratio. Diameter ratios of 1.2–1.4, position to spar draft ratio of 0.16, and spacing to spar draft ratio of 0.16 were suggested for reducing the heave response. Similarly, diameter ratios of 1.2–1.4, position to spar draft ratio of 0.12 and spacing to spar draft ratio of 0.2 were recommended for pitch response reduction.

2.2.5 Floating LNG Production Storage and Offloading Vessels

The concept of Floating Liquefied Natural Gas (FLNG) has been developed over the past few decades with the increasing demands in LNG. Although the FLNG hull is usually designed to be a typical ship type which is similar to an FPSO, it owns great volume of displacement and large LNG tanks. In addition, FLNG has higher centre of gravity due to the low density of LNG and larger waterline area. Therefore, hydrodynamic characteristics of the FLNG are different from those of the FPSO.

Z.-Q. Hu et al. (2017) performed experimental analysis and numerical modelling with aims to address the inner-tank sloshing effect on motion responses of a FLNG system (Figure 20). The results show that LNG-tank sloshing has a noticeable impact on the roll motion response of the FLNG and a moderate tank filling level is less helpful in reducing the roll motion response.



Figure 20: FLNG vessel model test setup in the basin (Z.-Q. Hu et al., 2017)

Zhao et al. (2017) presented an experimental investigation on dynamic responses of the connection system in the FLNG system during side-by-side offloading operations. Three typical irregular wave cases are used in the model test. Relationships between relative vessel motion and the load born by the connection system are obtained, and features of dynamic connection system responses are summarized. The results show that hawsers and fenders at different locations are sensitive to

different motion patterns; loads on connection systems have distinct dynamic properties, and snap loading crucial to the safety of offloading processes can be induced. Moreover, FLNG is subjected to large low-frequency responses in side-by-side configurations due to hydrodynamic interactions and sloshing effects.

Y. Jin et al. (2018) presented numerical investigations of hydrodynamic interactions of a conceptual FLNG-LNG offloading system in regular head sea waves by using an unsteady Reynolds-Averaged Navier-Stokes solver. The gap wave responses and wave loads on the FLNG and LNG vessels were studied for different wave frequencies and varying lateral separations. The gap wave resonance appears when the incident wave frequency approaches the natural frequency of the gap fluid, resulting in significant variation of wave loads in the directions of sway, heave, pitch, and yaw.

Vieira et al. (2018) set up an experimental arrangement (Figure 21) to investigate the influence of the liquid inside the tanks in the wave behaviour of FLNG. The study comprised the vessel evaluation both in isolated and in side-by-side configurations. The latter considered the vessel operating close to an LNG carrier, emulating an offloading operation. The study shows that the analysis of coupled systems considering all the above effects is very important for the correct definition of the dynamics of the vessels. Not considering one of these effects may underestimate the vessels motions and consequently underestimate the efforts regarding mooring lines, fenders, and the necessary power to carry out the operations with tugboats.

Zhao et al. (2018) developed a numerical code based on potential flow to investigate the coupling interaction between 6 degrees of freedom vessel motions and internal nonlinear sloshing. The impulsive response function (IRF) method and the boundary element method (BEM) is adopted to resolve vessel motions and internal liquid sloshing, respectively. The results show that significant coupling effects can be induced in beam sea conditions between

sway and roll motions and internal sloshing; heave motion is slightly affected by internal sloshing. Besides, coupling effects will increase rapidly when the natural sloshing frequency is close to the main response frequency region of the ship.

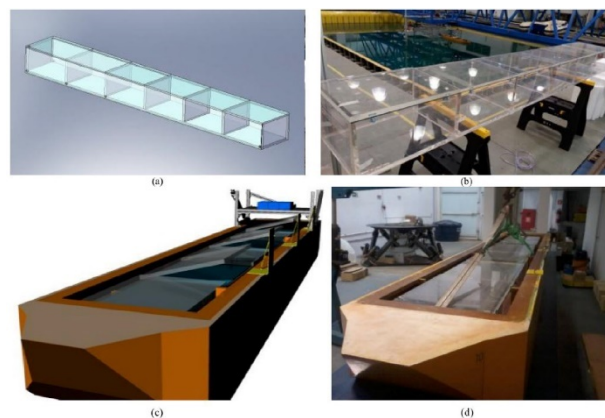


Figure 21 FLNG scaled model. Legend: (a) FLNG tanks (CAD), (b) FLNG acrylic tanks, (c) FLNG complete model (CAD), (d) FLNG complete model (Vieira et al., 2018)

Jin et al. (2019) investigated the hydrodynamics of a FLNG-LNG offloading system in a side-by-side configuration by using potential flow solver ANSYS AQWA. Time domain analyses are carried out for the FLNG-LNG system coupled with hawser, fender, and mooring systems under the combination of wind, current and waves. And the effects of varying hawser pretension and stiffness on the hydrodynamic performance are investigated.

Kawahashi et al. (2019) performed model experiments in an ocean model basin and discussed the coupling influence of FLNG motions with internal liquid sloshing. To verify the liquid cargo effect, the FLNG model was tested under two conditions: a liquid cargo condition and a fixed solid-cargo condition. The results show that the effect of internal liquid is significant for sway and roll motion (Figure 22).

Meng et al. (2021) developed a two-dimensional computational fluid dynamics (CFD) model for the structural packed column which is applied in FLNG in offshore platforms. The results show that the sloshing angle has

significant effects on the liquid volume fraction in the central region of the column.

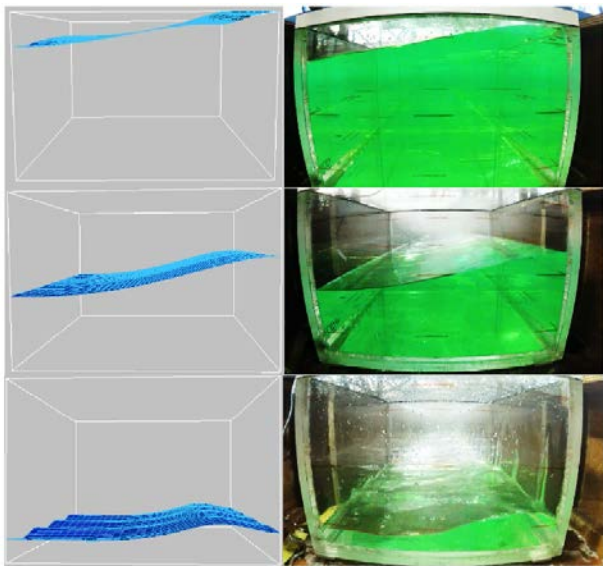


Figure 22 Free surface deformations in resonant period for different filling conditions: top: 90%, middle: 50%, bottom: 15% (Kawahashi et al., 2019)

2.2.6 Floating Offshore Wind Turbines (FOWT)

The application of floating stationary platforms as basis for wind turbines continues to attract the attention of the ocean engineering community. Semisubmersibles and TLPs have concentrated the major interest.

Some of the concepts related to semisubmersibles are:

Murai and Takahashi (2017) reported a study on the influence of arrangement of an array of semi-submersible type FOWTs (Figure 23). The study focused on hydrodynamic response of a wind farm and the investigation of how the arrangement of the array impacts on the hydrodynamic response including the motion of the nacelle. The change of the expected efficiency of the generator by change of the array arrangement in each sea area around Japan was discussed as an example scenario.

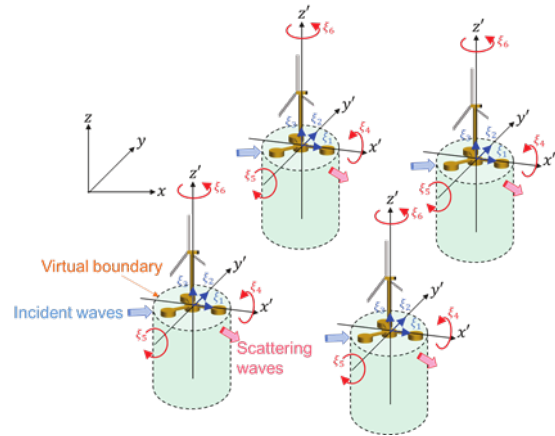


Figure 23: Hydrodynamic response of array of semi-submersibles (Murai and Takahashi, 2017)

Karimirad et al. (2017) compared real-time hybrid model testing (ReaTHM®) and numerical simulations of a braceless semi-submersible wind turbine. The experimental data was from a 1:30 scaled model of a semi-submersible wind turbine. Coupled aero-hydro-servo-elastic simulations were performed in MARINTEK's SIMA software. Low-frequency hydrodynamic excitation and damping are seen to be important, but these loads include a combination of viscous and potential forces. For the braceless semi-submersible concept, the second order potential flow forces have limited effects on the responses.

Krishnan and Seeninaidu (2017) investigated the hydrodynamic analysis of three column semi-submersible with vertical axis wind turbine (VAWT) in parked condition under regular and random waves. Free decay experiments were conducted for using scale model (1:75) in a laboratory wave basin and numerical simulations of hydrodynamic motion response of the floater were carried out using potential flow theory based on commercial software (ANSYS AQWA). The damping values obtained from experiments were used in numerical simulations to obtain motion response and Response Amplitude Operator (RAO).

Hegseth et al. (2018) presented the comparisons and validations of hydrodynamic load models for a semi-submersible floating

wind turbine. A simplified method to include distributed, large volume hydrodynamics in the global analysis was considered. Furthermore, frequency-dependent loads from potential theory were applied on a finite element (FE) model of the hull in a strip-wise manner. The method is compared to a conventional load model for a braceless 5 MW semi-submersible FWT and validated against experimental results from model tests with focus on internal loads and rigid body motions in the main wave-frequency range. In combined wave-wind conditions, the measured bending moments are significantly increased because of the wind-induced mean angle of the platform.

Robertson et al. (2018) attempted to assess the sources of experimental uncertainty in an offshore wind validation campaign focused on better understanding the nonlinear hydrodynamic response behaviour of a floating semisubmersible. The test specimen and conditions were simplified compared to other floating wind test campaigns to reduce potential sources of uncertainties and better focus on the hydrodynamic load attributes.

Kvittem et al. (2018) carried out a study focusing on the process of calibrating a numerical model to the experimental results of a 1:36 scale model of the public version of the 10 MW OO-Star Wind Floater semi-submersible offshore wind turbine. The hull was considered as rigid, while bar elements were used to model the mooring system and tower in a coupled finite element approach. First-order frequency-dependent added mass, potential damping, and excitation forces/moments were evaluated across a range of frequencies using a panel method. Distributed viscous forces on the hull and mooring lines were added to the numerical model according to Morison's equation. Potential difference-frequency excitation forces were also included by applying Newman's approximation.

Thys et al. (2018) presented the real-time hybrid model (ReaTHM®) tests that were performed on a 10-MW semi-submersible floating wind turbine in the Ocean Basin at

SINTEF Ocean in March 2018. The physical model was subjected to physical waves, while the rotor and tower loads were simulated in real-time and applied on the model by use of a cable-driven parallel robot. Recent advances in the ReaTHM test method allowed for extended testing possibilities and load application up to the 3p frequency and the first tower bending frequency.

The study by Zhao et al. (2020) proposed a method for the structural control of an ultra-large semi-submersible floating offshore wind turbine. A 10 MW wind turbine braceless semi-submersible with an ideal tuned mass damper (TMD) installed in the nacelle of the FOWT was proposed to dynamically compensate the vibrations and reduce the structural loads. A fully coupled time-domain simulation of the FOWT with active TMD subjected to a set of environmental conditions was conducted using FAST, and the effect of the TMD on the load reduction of the FOWT was analysed.

Concerning TLPs equipped with FOWT, the following works may be of interest:

Oguz et al. (2018) describe an experimental and numerical investigation of the Iberdrola TLP wind turbine concept, TLPWIND, in realistic wind and wave conditions. The TLP was coupled to the NREL 5 MW reference turbine and was designed to operate in a water depth of 70 m. The test campaign included free oscillation tests, tests in regular and irregular waves and simulated wind conditions. A software-in-the-loop approach was adopted to account for the time-varying aerodynamic forces produced by the turbine during the physical experiments. The effect of wind was found to have a significant contribution to the overall response of the platform whilst variation in wave conditions was found to have a relatively small effect on the platform response.

Kiamini et al. (2018) proposed the stabilization control of a 5 MW tension leg platform used as FOWT. The TLP was structurally controlled based on fuzzy controller and its structural behaviour was evaluated in the

presence of uncertainty, time delays and disturbances.



Figure 24: Extreme irregular wave test (Oguz et al., 2018)

Ren et al. (2018) presented a new concept by combining a 5 MW monopile type wind turbine and a heave-type wave energy converter, referred as the ‘MWWC’ (Monopile-WT-WEC-Combination) system (Figure 25). Hydrodynamic responses of the MWWC system under typical operational seas cases have been investigated by using both time-domain numerical simulations and scale model tests (1:50). For the numerical model, hydrodynamic loads of the monopile and the WEC are calculated by the AQWA code. For the scale test model, two air-dampers simulated the absorption effect of the wave energy (through the PTO damping force) without air compressibility effect.

Uzunoglu and Guedes Soares (2019) presented a systematic approach to the hydrodynamic design of a tension leg platform to host the NREL 5 MW turbine. Model development, hydrostatics, mooring setup, and estimation of motion dynamics in frequency domain were discussed. The time domain model built in FAST was used to compare simulations and the frequency domain calculations.

Manikandan and Saha (2019) proposed a novel controller technique and its application in tension leg platform(TLP) supported OWT to harvest optimized power. The TLP is mooring

line stabilized and has a 5 MW NREL wind turbine on top of it. The results showed that the proposed nonlinear quadratic regulator can control the power, generator torque and rotor speed effectively without additional increase in platform motions vis-à-vis existing conventional baseline controller.

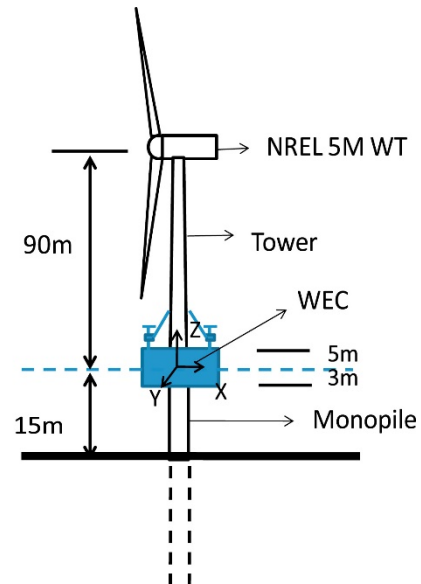


Figure 25: Sketch map of the MWWC concept system (Ren et al., 2018)

Chow et al. (2019) performed a validation study to test out the coupled 6-DoF rigid body motion solver, using the experimental results obtained for the floating wind turbine setup on a tensioned leg platform (Laugesen and Hansen, 2015). A modified restrain system was implemented to model the tendons with custom force-displacement functions and that also apply zero force when the ropes are slack.

2.3 Dynamically Positioned Floating Structures

In the recent years, advanced software-based protection systems to run DP with redundant power systems that are closer connected (closed bus-ties) are being introduced to produce more flexible designs to carry out efficient and environmentally friendly operations. Another trend is increased use of software to integrate more functions into larger software-dependent systems to ensure that DP vessels and operations

comply with acceptable safety standards. Some of the most relevant recent works are described as follows:

Sayed et al. (2017) performed comparisons between numerical simulations based on an ice dynamics model and an ice basin test of the dynamic positioning (DP) of a vessel in managed ice. The test case consisted of a vessel moving through a field of ice floes and brash ice (Figure 26). The set-up was intended to represent station keeping of a thruster-controlled vessel under the action of moving ice. Simulations were done to examine the effects of the ice basin set-up. The ice cover was driven using a uniform upstream velocity, while the vessel aimed to maintain position. The resulting thrust forces and offsets were close to those obtained with the set-up used in the ice basin test.

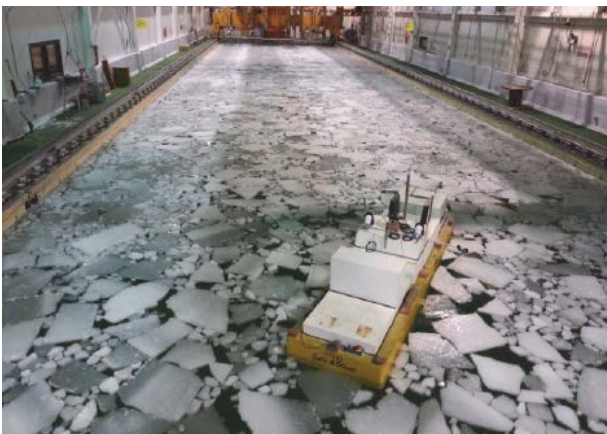


Figure 26: View of the ice basin and the model DP vessel (Sayed et al., 2017)

The positioning performances of the vessels with thruster failure modes was investigated by Xu et al. (2017) using time domain simulations. A novel synthesized positioning performance criterion was proposed to quantify the positioning performance including the aspects of positioning accuracy and power consumption. The synthesized criterion concerns how well the vessel is positioned rather than how large the environmental conditions the vessel can counteract. A semi-submersible employed with eight azimuth thrusters was adopted and six different thruster failure modes were considered. If the thruster system is well designed, thruster

failure may not affect the thrust system in supplying sufficient thrust force with two or less than two thrusters' failure for the semi-submersible.

Detlefsen et al. (2017) presented a static and a time domain method to assess the position-keeping capability of mono hull vessels. For the static analysis method, the equilibrium between mean environmental loads and available actuator forces is determined. In case of the dynamic assessment, the motions of the fully actuated ship in all degrees of freedom are simulated in time domain and evaluated by criteria regarding the position and heading of the ship. The developed time domain simulation method benefits from the computational efficiency of linear strip methods in frequency domain, whereas important nonlinear force contributions were directly handled in time domain. The simulation results have been compared with model tests that were performed by Potsdam Model Basin and included measurements of fixed and free models in regular and irregular waves as well as dynamic capability test with a fully actuated model of an offshore supply vessel.

Skjong and Pedersen (2017) studied a co-simulation case study of a marine offshore surface vessel in Dynamic Positioning (DP) operation, where the DP-controller is placed on an Arduino micro-controller. This enabled the use of suited modelling software for different types of dynamical systems, as well as hardware, such as micro-controllers for Hardware-In-the-Loop testing in Figure 27. Such an integrated and open simulation method facilitated the development of new products as well as shortening the iterative process in design phases. As for co-simulation standard, the Functional Mock-up Interface (FMI) for co-simulation was used, and a communication Functional Mock-up Unit (FMU) that communicated with hardware and handled the signal flow between the hardware and the co-simulation was developed. The total co-simulation model consisted of a vessel model, including e.g. propulsors and environmental forces such as irregular wave

forces and current forces, a nonlinear passive observer to filter out high frequent wave generated vessel motions, a serial communication model, a reference model, in addition to a DP-control law uploaded to the micro-controller. The simulation results showed that even though the micro-controller is set to communicate with a lower frequency than the rest of the co-simulation sub-models, the total co-simulation is stable and produced good results.

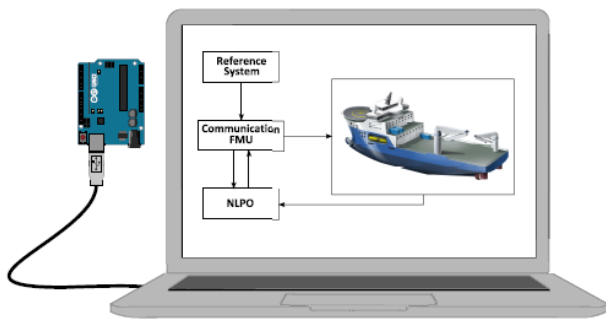


Figure 27: Co-Simulation of offshore marine vessel in DP operation using a hardware microcontroller as DP controller (Skjog and Pedersen, 2017)

Koop et al. (2017) presented the thruster-hull interaction effects for a drillship with 6 azimuth thrusters. The approaches investigated were the so-called Frozen Rotor approach, where the propeller rotation is modelled, the Actuator Disk approach with prescribed body forces and the unsteady Sliding Interface approach where the motion of the propeller was simulated in time. From the open-water calculations it was concluded that, using a Frozen Rotor approach, the propeller and nozzle thrust from the CFD correspond well with the experiments especially at bollard pull conditions. The thruster-hull interaction of one active thruster under the drillship was investigated using the three approaches. A comparison with experimental results was presented for the thruster-hull interaction coefficients. Using the Actuator Disk approach, a good agreement with the experiments was obtained. The results using the Actuator Disk and Sliding Interface were very similar to each other, but the computational costs for the Sliding Interface method were, at least, a factor of 20 higher. The results using the

Frozen Rotor deviated due to an unphysical wake behind the thruster.

Zhang et al. (2017) studied the flow interaction between a dynamic positioning (DP) thruster and a floating structure (semi-submersible) hull. The Spalart-Allmaras RANS model has been evaluated to simulate a single thruster rotating in open water, with OpenFOAM. The actual thruster geometry was meshed with structured grid, and the gap between the blade tip and nozzle was carefully treated. The Moving Reference Frame (MRF) method was used for steady state simulation, and the arbitrary mesh interface (AMI) method was applied to simulate the rotating blade for transient dynamic mesh simulation. Experimental data from a JIP project conducted at MARIN with a single straight thruster at different RPMs, advance coefficients and inflow angles were used to validate the numerical simulations. It was concluded that the OpenFOAM was capable to handle such complicated investigation with both MRF method and dynamic mesh method.

Bjørnø et al. (2017) studied a thruster-assisted position mooring (TAPM) system with different control functions for station keeping and motion damping for a moored offshore vessel assisted by thrusters. The thrusters were used to provide damping and some restoring to the vessel motion to compensate if a line breakage occurs. The mooring system absorbed the main loads to keep the vessel in place. The complete modelling, parameter identification, and control design for a 1:90 scaled TAPM model vessel was reported. The experiments focus on the set-point chasing algorithm, where the position setpoint slowly moved to the equilibrium position while the environmental loads were balanced by the mooring forces. This approach avoided conflicts between the mooring system and the control actions. If the environmental loads were too large so that the set-point exceeded a user-defined safety radius, the set-point was set to this radius and thruster forces grew to support the mooring system in counteracting the environmental loads to avoid

line breakage. The experiments using Statoil’s Cat I Arctic Drillship with six thrusters and mooring line (Figure 28) showed that the vessel and set point chasing control algorithm behaved as expected, minimizing thruster usage, and maximizing utilization of mooring system.



Figure 28: The model test for thruster-assisted position mooring (Bjørnø et al., 2017)

Cozijn et al. (2017) investigated the wave orbital motions that may cause variations in the inflow conditions of thrusters, that, in turn, result in variations in thrust and torque. Physical scale model tests were carried out to investigate these thruster-wave interaction effects, with an azimuth thruster running at constant RPMs. The observed effects included changes in the mean thrust, torque values, and associated wave frequencies. The test conditions were systematically varied to investigate the effects of the incoming waves, the presence of the hull and the vessel motions. First, measurements were carried out on an azimuth thruster in open water conditions. Thrust and torque in regular waves were compared with bollard pull conditions. Second, measurements were carried out on the azimuth thruster under the hull of a vessel, which was rigidly connected to the basin carriage. Third, measurements were carried out on the same azimuth thruster under the hull of the vessel in a soft-mooring system. In open water conditions the wave orbital motions caused a reduction of mean unit thrust and the observed effect was strongest in short waves. In the presence of the hull the thruster-wave interaction effects were much less pronounced. Furthermore, the thrust variations were larger in long waves. A reduction of the mean unit thrust was observed, as well as wave frequency thrust variations. The effects were stronger than in the captive tests, suggesting that both the wave orbital motions and the vessel motions played a role. The overall mean thruster interaction

losses were derived from a series of tests in regular waves and still water, with and without active thrusters. Depending on the wave period, thruster-wave interaction effects of 5-10% were found as shown in Figure 29.

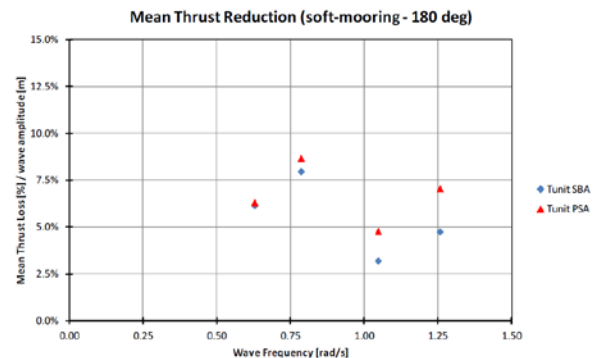


Figure 29: Mean thrust reduction due to thruster-wave interaction (Cozijn et al., 2017)

Pivano et al. (2017) presented the use of comprehensive dynamic operability analyses performed by time-domain simulations for understanding the vessel performance and limitations, providing reliable input to operational risk assessment and planning. The Dynamic Capability “DynCap” concept based on time-domain simulations (Level 3 in the new DNV GL standard) was introduced to overcome the traditional quasi-static approach. Full-scale validation of the DynCap concept was provided by comparing measurements from sea trials (with the platform supply vessel “Island Condor”) with corresponding simulations using the DynCap methodology. DP footprint including standard deviations and max excursions for different vessel headings showed that the DynCap analysis was within the expected uncertainties in sea state measurements and the limited duration of the full-scale time series. A full DynCap wind envelope and power envelope for Island Condor was presented (Figure 30), including the relevant full-scale data points. The results showed that DynCap simulations are comparable to full-scale measurements.

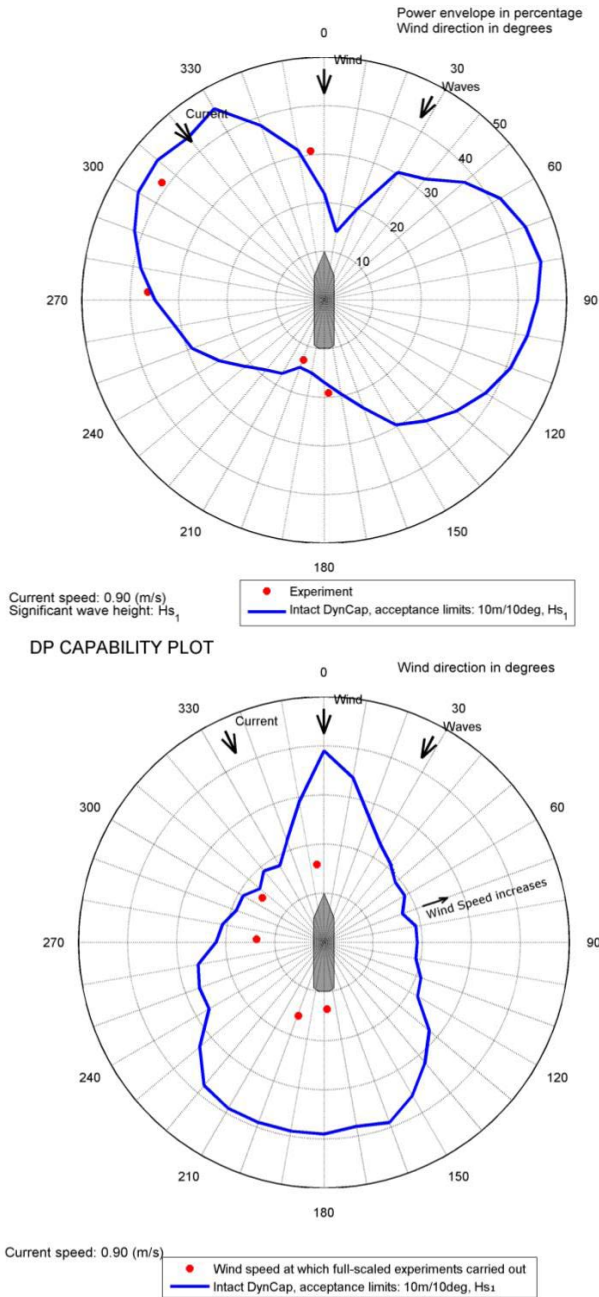


Figure 30: DynCap wind and power envelope comparison between experiments and simulations

Chen (2017) presented an overall framework for DP safety management in offshore marine operations. Three steps were considered: 1) identification of position loss scenarios, 2) risk analysis in terms of position loss frequency and consequences, and risk evaluation, 3) mitigation of risk via measures to eliminate the risk, or to reduce the likelihood of position loss, as well as to mitigate the consequences in marine operations given DP vessel position losses. Case

studies from DP shuttle tankers and DP mobile offshore drilling units were presented to illustrate the key principles of each step. The challenges associated with this approach were: frequency of position loss, reliability of DP operators, and risk acceptance criteria for DP operations.

Huang et al. (2017) studied the utilization of a hold back vessel to support a drilling rig during the DP operation. Firstly, an analytical study of a simplified model of two vessels connected by a cable with two degrees of freedom (one for each vessel, i.e., the force applied by the cable was unidirectional) was considered. Using control theory, the limiting stiffness of the cable was determined by analysing the poles of the system. Considering a catenary model for the connecting cable, the maximum force that could be transmitted between the vessels without the system becoming unstable, was determined. The influence of the Kalman Filter in the stability of the system was also studied. It was shown that the hold-back vessel could be maintained in DP mode only when in stand-by, with the minimum cable traction required to avoid interference with the thrusters. When a higher force was applied, it was unsafe to operate with the hold-back vessel in DP mode, considering typical sizes of the vessels and the forces that should be transmitted. In summary, connecting two vessels reduced the stability margins of the system, requiring full attention of the operators since the DP was not designed to consider this external force. However, it may be a contingency solution to avoid drilling interruption and disconnection.

Li et al. (2018) investigated the approach of using supervised learning algorithms to estimate thruster-thruster/current interactions between adjacent azimuth thrusters in tandem, based on scattered model test data. The model tests for thruster-thruster/current interaction study were conducted in a towing tank. As depicted in Figure 31, two ducted thrusters were mounted in tandem for thruster-thruster interaction and the inflow velocity ranged from 0.15 to 1.00 m/s for thruster-current interaction. The Gaussian

radial basis function (RBF) network and feedforward neural network were applied to approximate the thrust efficiency function with respect to both thruster azimuth and current inflow velocity. The training results demonstrated that RBF network was not an appropriate model, mainly because of the insufficiency of the training sample. On the contrary, feedforward neural network performed much better in approximating the thrust efficiency function of the aft thruster, revealing its capability for handling complex function approximation problems even when the training set is not a big one.

Xu et al. (2018) presented the nonlinear time-domain mating simulations. The major findings were successfully applied in the design of the installation devices and in the selection of the dominant design parameters. The float-over vessel was equipped with 7 thrusters: two forward azimuth thrusters, one forward tunnel thruster, two aft tunnel thrusters and two aft main propellers. The vessel used DP mode in training and pre-entry stage but use manual mode in entry stage. So, a conventional method was used to simulate the float-over, entry, mating and exit stages. The float-over process was simulated in AQWA software, including hydrodynamic analysis, simulation of fenders & LMU mechanics.

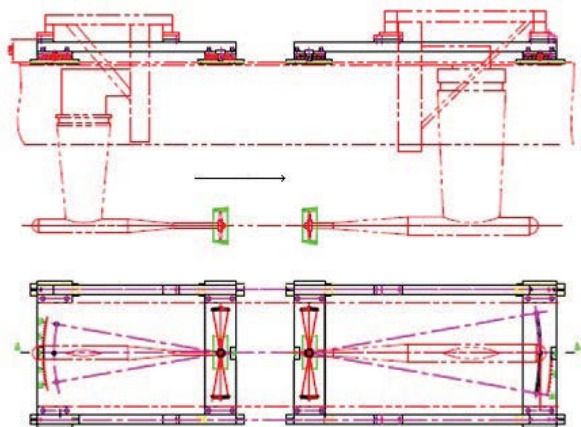


Figure 31: Test set-up for thruster-thruster/current interaction (Li et al., 2018)

X. Jin et al. (2018) presented a description of the DP float-over technology that was successfully applied in the float-over installation of the HZ25-8 DPP integrated topsides in South China Sea. A series of dynamic positioning (DP) model tests were conducted to assess the various float-over installation stages. Hydrostatic decay tests to calibrate the models, DP capacity tests at pre-defined survival conditions, docking tests and undocking tests at auto DP mode to ensure the feasibility at pre-defined operation conditions, and mating tests without DP operations were performed. A virtual simulation program was also developed to simulate the float-over installation of the 13000 Te integrated topsides with a dynamic positioning (DP2) semisubmersible vessel at a water depth of 100 m under a virtual reality environment of South China Sea.

Kerkeni et al. (2018) reported that standard DP systems may fail to perform in ice conditions and emphasized specific principles and position keeping philosophies that should be applied in ice covered waters. The tests were performed as a part of the station keeping trials performed in March 2017 in drifting ice in the Bay of Bothnia (Figure 32). Control algorithms limitations of Standard DP Systems were presented, showing the necessity of new control principles. The importance of crew training was also demonstrated along with the approaches to keep position in ice. The limitations of a standard open water DP system to handle severe ice conditions were assessed at full scale. Station-keeping in manual control was successfully performed by the application of Dynamic Ice Loading Dodging (DIL-Dodging) manoeuvre. It combines the use of thrusters wake and heading changes to dodge ice floes and clear ice accumulation on the sides. The importance of the skilled operator was clearly observed.



Figure 32: Full scale DP test in ice (Kerkeni et al., 2018)

Harmsen et al. (2018) presented the instabilities caused by heavy lifting operation with the DP vessel connected to another fixed or floating objects through hoist wires. These DP-instabilities are caused by the inability of the DP system to handle the relatively stiff external spring of the hoist wire correctly. When two vessels are lifting a single object together (e.g., QUAD lift), existing solutions to prevent this DP-instability are insufficient, as the nature of such lift requires a synchronous move on DP. Heerema Marine Contractors presented the DP-stability challenges to Kongsberg Maritime, and a joint effort resulted in an implementation of a modified Kalman filter in the Kongsberg Maritime DP system. Also, a dedicated engineering analysis to predict risk of DP-instabilities for specific lift configurations has been developed. The modified DP-system was tested in large number of simulations (both desktop and a full mission simulator) to test the ability of the updated DP-system to deal with a wide range of specific heavy lift conditions. The system is tested during a dedicated DP-trial program onboard Thialf. As the results of all these tests were very successful, the new High Kalman filter was made available onboard Thialf as a permanent option next to the original functionalities. Offshore tests with High Kalman setting demonstrated the difference in DP stability for the oscillation periods of interest. These tests also showed that this Kalman setting provides good positioning ability for noisy reference systems. The High Kalman option leads to more thruster RPM and azimuth fluctuations. To prevent higher wear and tear of the thrusters, it should only be used when needed for a limited period of time.

Gundersen et al. (2018) studied a hawserless tandem offloading operation between a

FPSO and a DP shuttle. The structural limits of the flexible loading hose allowed for larger operational sectors and heading flexibility which enable the shuttle tanker to point away from the FPSO and hence reduce the probability of collision. An analysis model with two representative vessels for offloading operations in the North Sea was developed to investigate the new concept. The model included a compiled version of the DP system core algorithm, extracted from the real time system of both vessels. The new offloading strategy, with heading offset away from the FPSO was implemented in an updated control algorithm for the shuttle tanker. The complete tandem offloading system (Figure 33) has been simulated in time domain with measured wind, waves and current from a Hindcast database. Heading and relative motion between the FPSO and the shuttle tanker was statistically evaluated to determine the time in which the shuttle tanker is directed towards the FPSO. The proposed strategy reduced that time to a minimum, and prevented the risk of collision between the vessels, in case of a drive-off incident.

Fernandez et al. (2018) proposed a new concept of Dynamic Positioning Reliability Index (DP-RI) and a state-of-the art advisory decision-making tool. This tool was developed based on information from various sources including Offshore Reliability Data (OREDA), International Marine Contractors Association (IMCA) Accident database, DP vendor equipment failure databases, DP System supplier's manuals, previous system level FMEA and HIL testing results, site specific risk analysis documents, project design specification and operator's operational experiences. The DP system was classified into various sub-systems using big data analysis and a correlation method. Each of the sub-systems has been given a weighting factor and a Reliability Index (RI) was calculated based on the DP class type, configuration, and mode of operation. DP-RI addressed the gaps found in the traditional reliability assessment methods of a DP system.

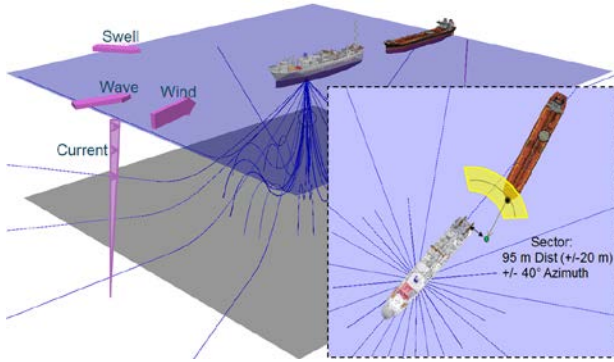


Figure 33: Time domain simulation model for FPSO and DP shuttle and tanker yellow restriction zone (Gundersen et al., 2018)

Lee et al. (2019) studied a heading control strategy to reduce the ice load acting on the arctic production platforms equipped with DP Assisted Mooring System. A heading control strategy considering real time tension under Arctic conditions was proposed for safe and fuel-efficient operation. The strategy calculated the target heading using a ratio of the most loaded line and second loaded line. The target heading was an estimated direction of ice drift. From the simulations, the advanced performance in station-keeping of heading compared with no heading control was validated with 4 different conditions of ice drift direction.

An et al. (2019) applied the exogenous Kalman filter (XKF) algorithm to DP station-keeping numerical simulations. The algorithm was a two-stage cascade of NLO (Nonlinear Observer) and linearized KF, which used the first-stage NLO estimated states as exogenous inputs for the second-stage linearized KF. XKF approach had both the stability property inherited from NLO and the optimality from the linearized KF. To verify the applied XKF approach, a high fidelity 6 degree-of-freedom station-keeping vessel simulator was also developed. At the normal DP station-keeping scenario (Figure 34), the vessel stayed around the desired equilibrium point with the DP control action and showed similar errors in motions and velocities between NLO and XKF. The advantage of XKF comparing to the NLO is the error covariance calculations that can be monitored by DP operators.

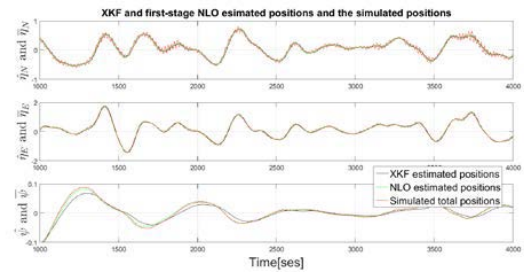


Figure 34: XKF Estimated vessel positions at normal DP station keeping simulation (An et al., 2019)

Moreno et al. (2019) developed a control system for an innovative configuration for oil transfer between a DP shuttle and a conventional tanker, using a modified tandem configuration. A control system design applied to the DP vessel inside the offloading site was investigated. This control applies two individual sliding mode controllers for rudder and thruster control, with coefficients obtained from numerical simulations, associated with a line-of-sight strategy for course and speed over ground controllers. Control performance and operation safety were evaluated through a set of real-time simulations of the transfer operation, where performance was evaluated through measurement of the Bow Loading System point position in both straight-line navigation and in a 10 km radius curve. Real-time simulations showed that a lateral and longitudinal distance of, both, 50 m was enough to provide a safe escape route in case of a control drive-off failure.

Yenduri et al. (2019) presented a novel DP system for a flotel operating aside a FPSO. The system included an adaptive controller combined with an optimized thruster allocation law and a sea state detector. An optimized allocation algorithm for lower fuel consumption, wear, and tear of the thruster equipment and to ensure the resultant command in the respective direction of the azimuth thrusters was designed. The simulation results showed that the flotel exhibits nearly same mean offset as the FPSO (Figure 35).

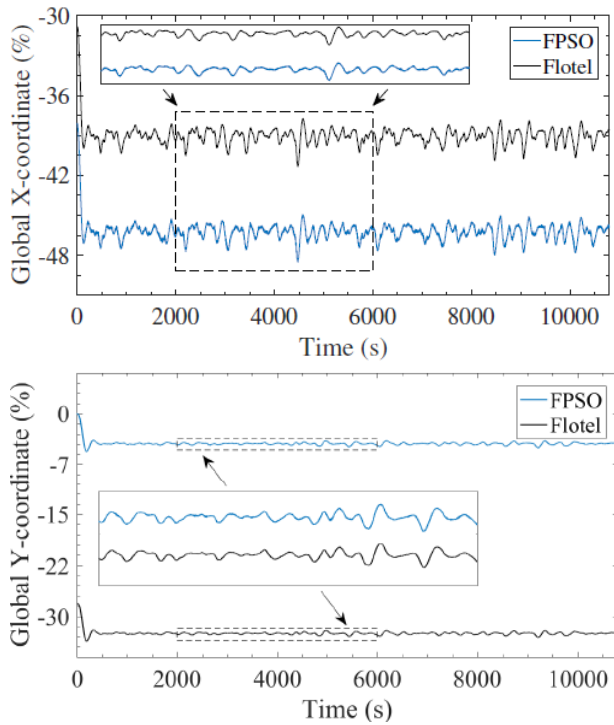


Figure 35: Demonstration of offset between flotel and FPSO by using DP system with adaptive neural network controller (Yenduri et al., 2019)

Fernandez et al. (2019) presented the Analytic Hierarchy Process (AHP) methodology for weight assignment among the DP subsystems. The developed DP-RI (Reliability Index) tool showed that the AHP technique was effective (Figure 36). Further, it eliminated the inherent uncertainty and level of inconsistency in the decision making during critical operations. The systematic assignment of weightings was attained through clear definition of criteria, objectives and data collection from experts and comparing against the results obtained through a machine learning algorithm with actual data from DP vessels.

A. M. Wang et al. (2019) presented a comprehensive description of an innovative training program and its successful simulation application, including virtual reality (VR) simulations of offshore field, numerical and visual modelling of met-ocean environment and DP2 float-over vessel, and performance of key personnel when executing float-over operations. The simulation scenarios are tested under normal/anticipated environmental conditions and extreme environmental conditions, as well

as several stressful conditions, such as thruster failure, adverse internal wave current, power blackout, etc. Two mathematic models of the float-over vessel, DP2 X-Class semisubmersible vessel HYSY278, were developed for the DP simulations. The simulation runs encompassed all the scenarios of various float-over operations, including a series of positioning trials, moving to standoff position, approaching to pre-installed jacket, docking into jacket slot, undocking operation, etc.

Dynamic Positioning - Reliability Index (DP-RI)



Figure 36: DP RI tool - Online (real-time / dynamic) reliability analysis (Fernandez et al., 2019)

Song et al. (2019) developed high performance DP thruster for extreme environmental conditions such as the ice DP model test for the Arctic condition. In the performance analysis, three duct shapes were used: 19A-mod, 19A and 37 (Figure 37). CFD simulations and model tests proved that the thrust produced by the duct was not significant, but by the propellers was remarkably different.

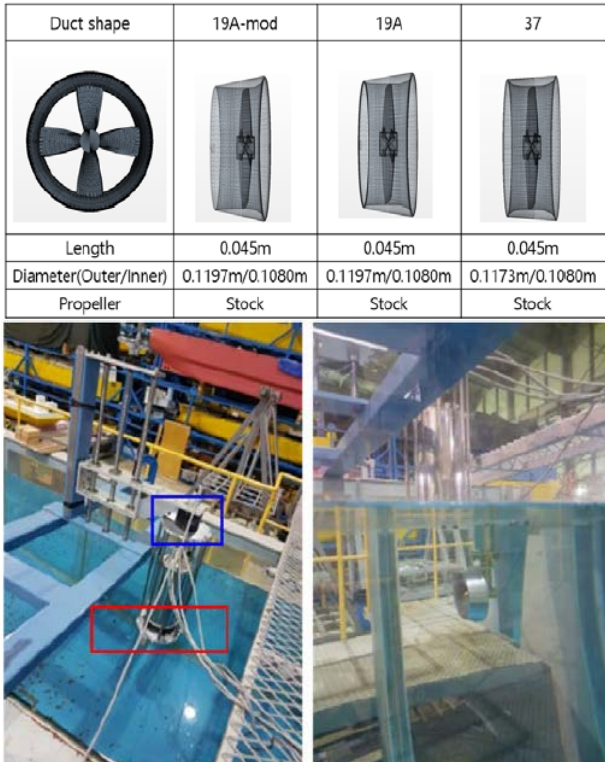


Figure 37: Study on duct shape to develop high performance DP thruster (Song et al., 2019)

Lee and Lee (2019) proposed an adaptive PD based on the Deep Deterministic Policy Gradient (DDPG) – which is one of Reinforcement Learning (RL) algorithms, to overcome the restriction of conventional PD controller – which is inefficient in time-varying environments. The DDPG was developed by Google Deepmind and is trained with sequences of prior experience from interaction with environments. The fully trained model at the end of the epoch showed good position keeping performance (Figure 38).

Kato et al. (2020) described the development of a side thruster system that can maintain the heading direction of autonomous surface vehicles (ASVs) for mud collection. The side thruster system is implemented in an ASV and conducted the operation tests at a port in Soma city, Fukushima. The test results confirmed no kinking of the wire during mud collection operation. Therefore, the side thruster system maintained the heading of the ASV and prevented kinking of the wire under relatively gentle wave and wind conditions.

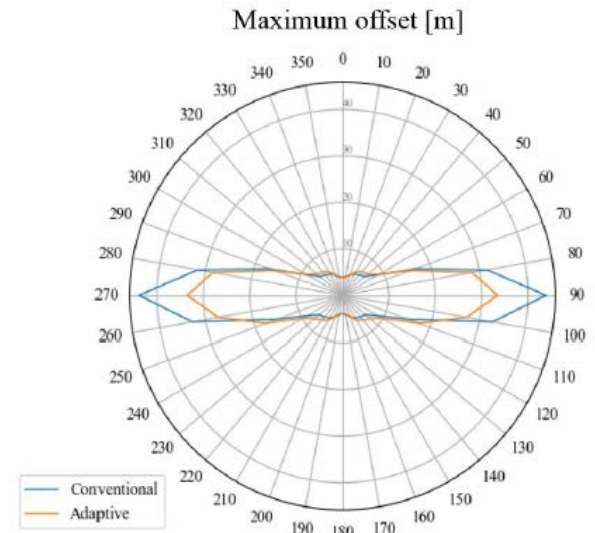
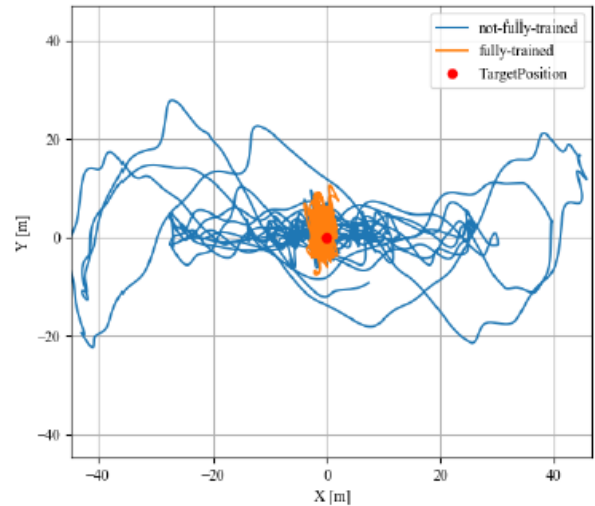


Figure 38: Enhancement of DP performance by using the adaptive PD control based on DDPG

L. Zhao et al. (2020) proposed a novel saturation protocol to refine the thrust allocation algorithm and improve the response speed to drastic changes in control force, under extreme wave conditions, i.e., when the DP system is in saturated state. When the thrust allocation modified strategy executes the saturation protocol, the limit of maximum thrust should be slackly set. The secondary thrust allocation makes the thrust of other unsaturated thrusters grow faster and improves the response speed of the propulsion system to the drastically changing control force (Figure 40).

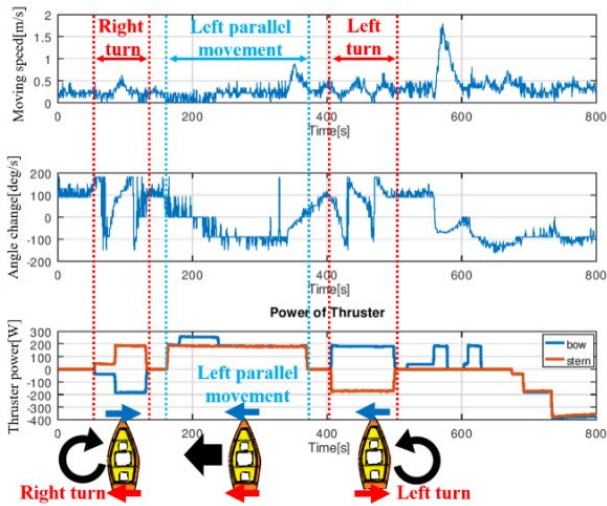


Figure 39: Test results of side thruster installed in ASV (Kato et al., 2020)

Lyu and Ding (2020) studied hydrodynamic characteristics such as thrust deduction of a submerged waterjet propelled vessel. Through a computational fluid dynamics method, the open water performance of the waterjet and the flow field around the hull were calculated. The results showed that when the advanced coefficient was in the range of 1.0 to 1.6, the open water efficiency of the submerged waterjet was more than 60%. Therefore, the waterjet showed potential to adapt to the multi-working conditions of transport vessels on inland rivers.

Fernandez et al. (2020) proposed a framework using Long Short Term Memory (LSTM) for prediction of reliability of DP sub-systems for computation of DP Reliability Index (DP-RI). The proposed framework included a mathematical computation approach and a data driven approach to predict the reliability at a sub-system level for evaluation of model performance and accuracy. The framework results demonstrated excellent performance under a wide range of data availability and guaranteed lower computational burden for real-time non-linear optimization. Numerical simulations were set-up using a state-of-the-art advisory decision-making tool with mock-up and real-world data to give insights into the model performance and validate it against the existing risk assessment methodologies.

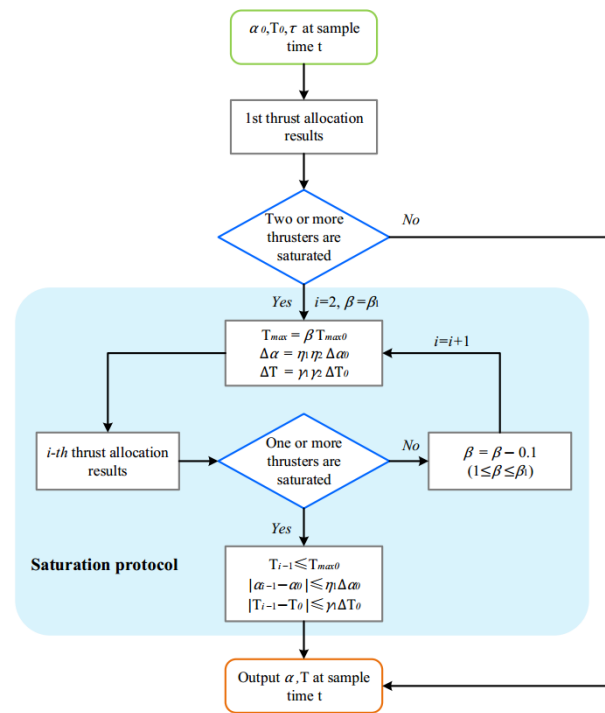


Figure 40: Flow chart of modified thrust allocation strategy in extreme operating condition (L. Zhao et al., 2020)

Tang et al. (2020) proposed an optimized thrust allocation algorithm based on Radial Basis Function (RBF) neural network and Sequential Quadratic Programming (SQP) algorithm, named RBF-SQP for the purpose of improving the traditional Forbidden Zone (FZ) method. The thrust coefficient was introduced to express the thrust loss in the mathematical model to remove forbidden zones. The training dataset of the RBF neural network was obtained from model tests of thrust-thrust interaction (Figure 41). Numerical simulations for the DP of a semi-submersible platform were conducted under typical operating conditions. The simulation results demonstrated that the demanded forces can be correctly distributed among available thrusters. Compared with the traditional methods, the proposed thrust allocation algorithm achieved a lower power consumption.

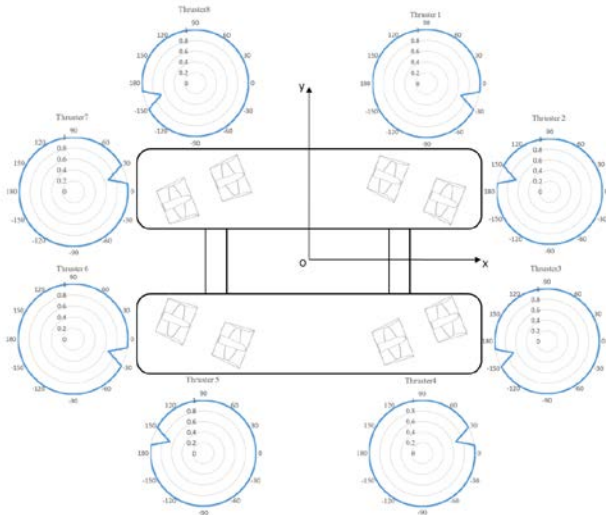


Figure 41: Thrust-thrust interaction as thrust coefficient of semi-submersible (Tang et al., 2020)

Rindarøy et al. (2020) presented SINTEF Ocean’s vessel simulator, VeSim, and its results in a numerical DP3 study of a windfarm support vessel operating in DP mode near a platform. These results were validated against model-scale test results, also performed by SINTEF Ocean in its Ocean Basin Laboratory. In these tests, VeSim used SINTEF Ocean’s in-house DP algorithm to control the model-scale vessel in a real-time hybrid testing environment. The proposed approach emphasised VeSim’s use in both a hardware-in-the-loop and software-in-the-loop testing environment. Figure 42 displays maximum and minimum yaw angles from both simulations and model tests.

Fu et al. (2020) proposed a new concept to remove large and heavy structures with a single lift, utilizing three semi-submerged vessels. It requires high positioning accuracy especially under environmental disturbances to ensure the safety of transportation. To ensure efficiency and safety, a DP system was developed and model tests were performed for such twin-lift operation (Figure 43). The test results showed that twin vessels can achieve station keeping and low-speed manoeuvring capabilities, with PID controller and optimization-based thrust allocation.

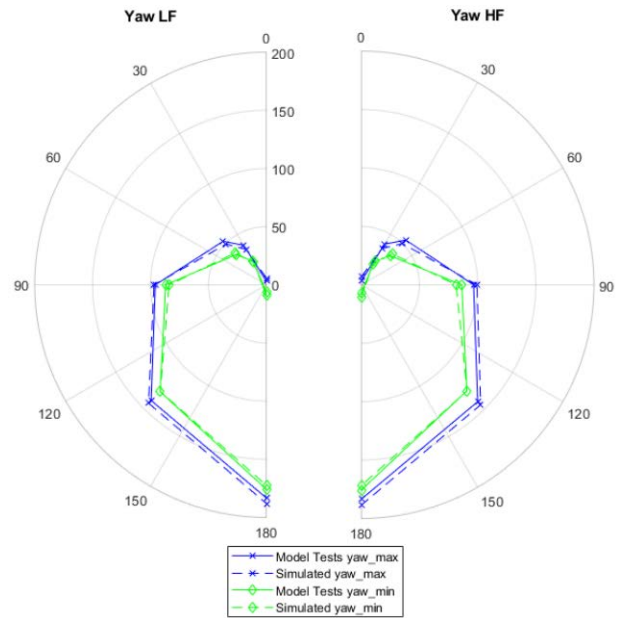


Figure 42: Comparison of maximum and minimum yaw angle for simulator and model tests (Rindarøy et al., 2020)

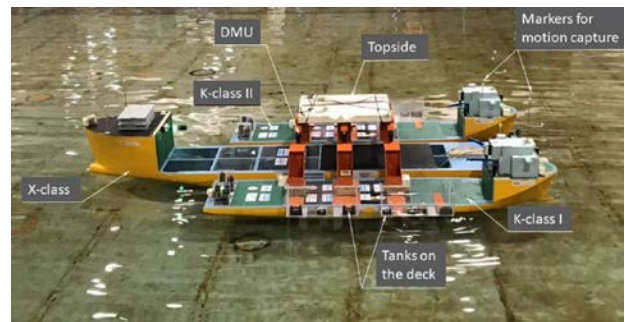


Figure 43: Sketch of wave tank test for twin-lift decommissioning operation (Fu et al., 2020)

Sauder and Tahchiev (2020) presented an active positioning system aimed at replacing the classical passive soft horizontal mooring system used in seakeeping tests of floating structures. An active positioning system was able to apply low frequency (LF) linear restoring and damping loads in surge, sway, and yaw, without directly affecting wave frequency (WF) motions, and motions in the vertical plane. Furthermore, this system enabled changes of heading, stiffness, damping, and decay tests, to be performed with high efficiency. These features enabled new possibilities in model identification. For the active system, six lines were used (Figure 44). Since the tension at the fairlead was feedback-controlled, the hydrodynamic loads on

this limited portion of the line were compensated by the tension controller. Tie-back tests were performed and demonstrated that the active system can replicate results obtained with a passive mooring system.

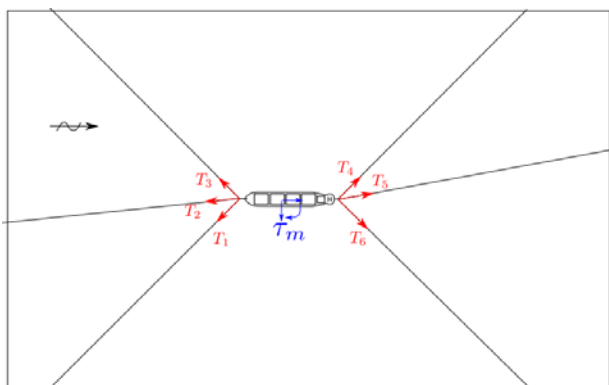


Figure 44: Sketch of active positioning system for seakeeping model test (Sauder and Tahchiev, 2020)

2.4 New technological developments

The hybrid foundation proposed by Cheng et al. (2019) is a novel and interesting development for bottom-founded OWTs, however further studies and validation at full-scale are still necessary. The topology optimization design method for jackets and other fixed structures proposed by Tian et al. (2019) is another development that deserves further studies and validation. W. Liu et al. (2017) have described the new concept of a Spar Drilling Production Storage Offloading Platform (SDPSO) for ultra-deep waters. Ren et al. (2018) have presented a new concept, the ‘MWWC’ (Monopile-WT-WEC- Combination) system that combines a 5 MW monopile type wind turbine and a heave-type wave energy converter. Fu et al. (2020) have proposed a new concept to remove large and heavy structures with a single lift, utilizing three semi-submerged DP vessels.

2.5 New experimental techniques and extrapolation methods

A creative method for the equivalent design of an oil offloading line for model tests was proposed by Kang et al. (2017). Park et al. (2021) have proposed a new experimental method for

the assessment of towing- and course-stability of a FPSO towed by a tug-boat.

2.6 Practical applications of computational methods for prediction and scaling

Lyu et al. (2019) have developed a novel multi-body dynamic mathematical modelling for the Soft Yoke Mooring System (SYMS) of FPSOs. Koop (2020) have used CFD simulations to address Reynolds scale effects and shielding effects on current loads of offshore vessels in side-by-side configuration. Wang and Zhou (2020) carried out numerical simulations and experiments about the scale effect of internal solitary wave loads on spar platforms.

2.7 Need for R&D for model experiments, numerical modelling and full-scale measurements

Model tests and additional numerical simulations are necessary to investigate collision scenarios, loads on structures and foundations and performance of repaired/upgraded and life-extended structures for bottom-founded structures. Recent studies have also shown a concern with semisubmersibles and DP operations under ice conditions. Although, in the present ITTC period, some model tests results and field measurements have been reported on that topic, further investigation and validations are still required.

3. REVIEW OF THE EXISTING PROCEDURES

The Committee reviewed and updated the following procedures and guidelines:

- 7.5-02-07-03.1 Floating Offshore Platform Experiments;
- 7.5-02-07-03.2 Analysis Procedure for Model Tests in Regular Waves;

- 7.5-02-07-03.4 Active Hybrid Model Tests of Floating Offshore Structures with Mooring Lines;
- 7.5-02-07-03.5 Passive Hybrid Model Tests of Floating Offshore Structures with Mooring Lines;
- 7.5-02-07-03.6 Dynamic Positioning System Model Test Experiments;
- 7.5-02-07-03.10 Guideline for VIV Testing;
- 7.5-02-07-03.11 Model Tests of Multibodies in Close Proximity;
- 7.5-02-07-03.13 Guideline for VIM Testing;
- 7.5-02-07-03.14 Analysis Procedure of Model Tests in Irregular Waves;

The objective of the review was to update the procedures/guidelines according to the current practices, and to provide references to understand and implement the techniques.

4. STATE-OF-THE-ART REVIEW IN OFFSHORE AQUACULTURE SYSTEMS

Offshore aquaculture may be defined as the rearing of marine organisms in ocean waters beyond significant coastal influence, primarily in federal waters of exclusive economic zones. According to C. M. Wang et al. (2019), for a fish farming site to be considered offshore, the following characteristics should be met:

- (i) unsheltered waters, defined by the sea space outside a straight line joining two major capes/promontories or within 25 nautical miles from the shoreline for economic feasibility;
- (ii) water depth greater than 3 times the cage height and at least 15 m between the cage bottom and the seabed for better dispersion of fish wastes and

- (iii) current speed ranging from 0.5 m/s to 1 m/s.

In the recent years, fish farming worldwide is moving offshore due to lack of available nearshore production sites (where conflicts with shipping, fishing, tourism, conservation, and recreation are frequent), much larger sea space availability and better water quality (essential to produce healthy fishes). However, going offshore poses many challenges due to the high energy environment, inaccessibility of power supply and supporting services (C. M. Wang et al., 2019).

Recent reviews concerning offshore aquaculture systems and their classification can be found in Chu et al. (2020) and Xu and Qin (2020). There is a variety of designs that include open and semi-closed systems, floating and submersible options, as well as fixed. In the following various types of offshore aquaculture systems are presented with examples of relevant structures.

4.1 Open net cage system

4.1.1 Floating flexible cages

Flexible collar cages were first invented in the 1970s and are now widely used in Japan, Western Europe, North America, South America, New Zealand, Australia. High-density polyethylene (HDPE) is commonly used for the material in modern industrial fish farming. The main structural elements of these cages are the floatable pipes, which can be assembled in various ways to produce the floating collar. The pipes are held together by a series of brackets with stanchions and distributed throughout the entire boundaries to suspend the fish net. This type of structures is flexible and typically follow the shape of waves as indicated in Figure 45. The material tolerates relatively large elongation without major fatigue. The structures are also relatively cheap and have been a popular solution in confined environment. In harsh environment conditions, the floating flexible cages have problems with deformation of the net due strong waves and currents,

stanchions that may cause twisting and turning problems. However, some plastic circular cages have been given an offshore designation and have survived storms with significant wave height H_s of 4.5 m (Turner, 2000). Examples of flexible circular cages are the Aqualine concept with PE pipes with circumference from 20 m to 100 m and PolarCirkel concept with HDPE pipes circumference of 60 m to 240 m (Figure 45).

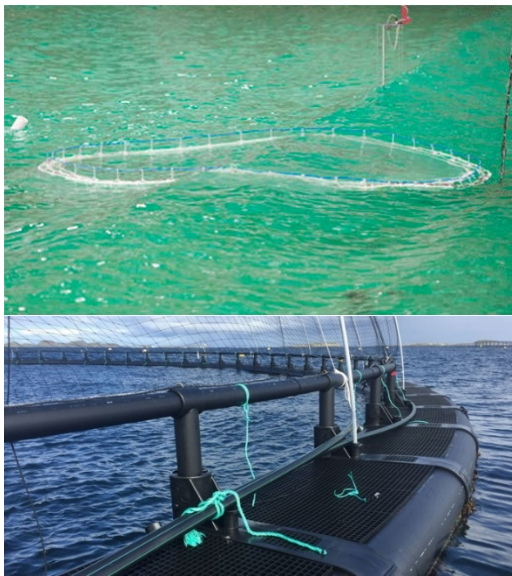


Figure 45: Floating flexible cages: (a) Model test in ocean waves (Picture courtesy of SINTEF Ocean) and (b) PolarCirkel HDPE Circular cage <https://www.akvagroup.com/merdbasert-oppdrett/r%C3%B8r-og-r%C3%B8rsystem>

4.1.2 Floating rigid cages

Floating rigid cages with robust frame structures (for strength, stiffness, stability, and buoyancy) are designed to withstand large wave actions. They are generally large structures, constructed from steel or concrete, and incorporate a variety of management-related features. Their susceptibility to structural failure in extreme conditions and the requirement for heavier mooring systems due to their large masses are the main disadvantages.

Examples of floating rigid cages are: Pisbarca (Figure 46), Seacon (Figure 47) and Havfarm (Figure 48).

The Pisbarca was built by a Spanish company. It is a hexagonal steel structure with 7 cages, with a total volume of 10000 m³ and a production capacity of 200 tons of fish per annum (Scott and Muir, 2000).



Figure 46: Pisbarca <https://www.pinterest.co.uk/pin/57772807700395421/?p=true>

Seacon, built also in Spain in 1987, consists of a hexagonal submerged pontoon construction and a deck construction in light-weight aggregate concrete. It has separated steel tube columns and pretensioned diagonal and vertical struts between top and bottom columns (Bjerke, 1990).



Figure 47: SEACON <https://www.lightcem.co.uk/fish-farm-c1gnk>

Havfarm has 385 m in length and 59.5 m wide and a capacity to contain 10000 tons of salmon (over 2 million fish). Havfarm was constructed as a steel-frame for 6 cages measuring 50 m × 50 m on the surface, with open nets at 60 m depth. The facilities were designed to withstand 10 m of significant wave

height. It was installed in Hadsel, northern part of Norway, in June 2020.



Figure 48: Havfarm. (a) concept (<https://www.nskshipdesign.com/designs/aquaculture/fishfarm-2/fish-farm/>) (b) Model tests (Picture courtesy of SINTEF Ocean).

4.1.3 Semi-submersible flexible cages

Semi-submersible cages can be characterized by their capability to be submerged from surface waters during a storm to avoid the higher energy regimes. Depending on mechanical types, semi-submersible cages may be divided into two structural classes: flexible and rigid. Tension Leg Cage (TLC) is the one of the representative types of semi-submersible flexible cage. In the TLC-submersible design, a buoyancy plastic-supporting frame is held in place by vertical mooring ropes attached to concrete blocks on the seabed and to sub-surface buoys. In storms or strong currents, the cage responds naturally, i.e., the net is being pulled under the water, thus escaping the worst wave action (Beveridge, 2008; Scott and Muir, 2000). Mooring strength is critical and the heavy block anchors used are difficult to install. Cage volume reduction due to

submergence of cage for a long period of time may affect fish's welfare (Beveridge, 2008).

Tension leg mooring system will behave more like a fixed structure and wave forces can be directly countered by the tendon stiffness forces, thereby, a large volume with high mass cage may not be suitable due to vulnerability of mooring lines (DNV, 2010). An example is the Refa tension leg cage design concept (Figure 49). The cage is available in a variety of sizes up to 12000 m³. The maximum harvest biomass is about 300 ton based on 25 kg/ m³ of stock density. The cages have been deployed in Italy, Spain, Portugal, and Brazil.

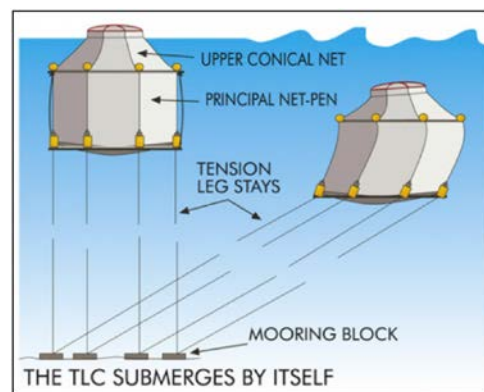


Figure 49: Refa tension leg cage concept design (http://refamed.com/gabbie_mare/tlc_system.html)

4.1.4 Semi-submersible rigid cages

Semi-submersible rigid cages are designed with rigid framework elements restricting movement or volume change in response to external wave and current forces. Normally having steel frame structures, the cages have adjustable ballast tanks to raise or lower the system. With a more rigid structure, it allows to have service facilities such as self-contained feeder systems (Scott and Muir, 2000). They are large and complex steel structures that require rigorous engineering analyses, design, and high-quality control in construction to ensure safety in offshore operation.

Examples of semi-submersible rigid cages are Ocean Farm 1, Shenlan 1, Shenlan 2,

Viewpoint Seafarm, Spider Cage, SSFF150 Pen, and Keppel offshore rig fish farm.

Ocean Farm 1 was developed in Norway and built in China. Ocean Farm 1 is a result of robust technology and principles used in submersible offshore units. With diameter of 110 m and volume of 250000 m³, the cage can accommodate 1.5 million salmon. It is intended for offshore installation in water at 100 to 300 m in depth with 25-year lifespan. It has more than 20000 sensors and over 100 monitors and control units.



Figure 50: Ocean Farm 1: (a) model tests (Picture courtesy of SINTEF Ocean); (b) <https://www.fishfarmingexpert.com/article/world-s-first-offshore-fish-farm-arrives-in-norway/>

Shenlan 1 and Shenlan 2 were developed for salmon farming about 130 nautical miles off the shore of Rizhao in east China's Shandong province. Shenlan 1 has already been deployed at the site, has a diameter of 60 m, a height of 35 m, and is able to culture 300000 salmon (Figure 51a). Shenlan 2 has 60 m diameter and a height of 80 m and can accommodate about 1 million salmon (Figure 51b).

Nova Sea AS, a Norwegian company, designed two innovative concepts: Viewpoint Seafarm (Figure 52) and Spider Cage (Figure 53) for offshore fish farm solutions based on semisubmersible technology. Viewpoint Seafarm comprises a hub, which supports four floating net cages interconnected through a dedicated hinge system. Each floater has a projected area of 50 m × 35 m. Model scale tests have been conducted with 11 m significant wave height and the system showed stable motion response (Hill, 2018). The Spider Cage has a dedicated barrier, with a diameter of 100 m having an outer steel ring with another ring inside with heave compensation. It is designed to shield the actual fish cage from heavy sea conditions and sea lice. The design has been tested up to sea states of 11 m with and without current, where general motions, accelerations, loads and sloshing have been assessed.



(a)



(b)

Figure 51: (a) Shenlan 1 (<http://www.cccisc.com/en/haiyanggongchengxiangguan/70.html>), (b) Shenlan 2

(<http://www.cccisc.com/en/haiyanggongchengxiangguan/72.html>)

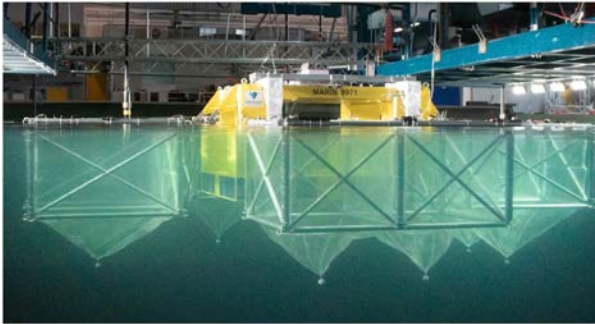


Figure 52: Viewpoint seafarm

(<https://www.youtube.com/embed/WWiU0dm-iKQ?autoplay=1&modestbranding=1&rel=0&showinfo=0&vd=hd1080>)



Figure 53: Spider cage

(<https://www.youtube.com/embed/gpPfUwD0te0?autoplay=1&modestbranding=1&rel=0&showinfo=0&vd=hd1080>)

4.1.5 Submerged cages

Normal operating condition of submerged cages would be at a suitable water depth below from the hazardous upper water column. The systems could be raised temporarily to the surface for necessary maintenance requirements and for fish harvesting. Various designs have been proposed and some pilot scale or commercial systems have been built.

Submerged cages have the best features to avoid surface debris and effects of storms (Scott and Muir, 2000). The latter supports the fact that their structural strength does not need to be as great as surface structures. Examples of submerged rigid cage designs are Sadco (see

Fig. 10), AquaPod (see Fig. 11a) and NSENGI sinking fish cages (see Fig. 11b).

Sadco is a Russian design that has been evolving since the early 1980s (Bugrov, 2006). A ballasted upper steel hexagonal superstructure carries the net kept in shape by a lower sinker tube. The cage volumes are available up to 2000 m³.

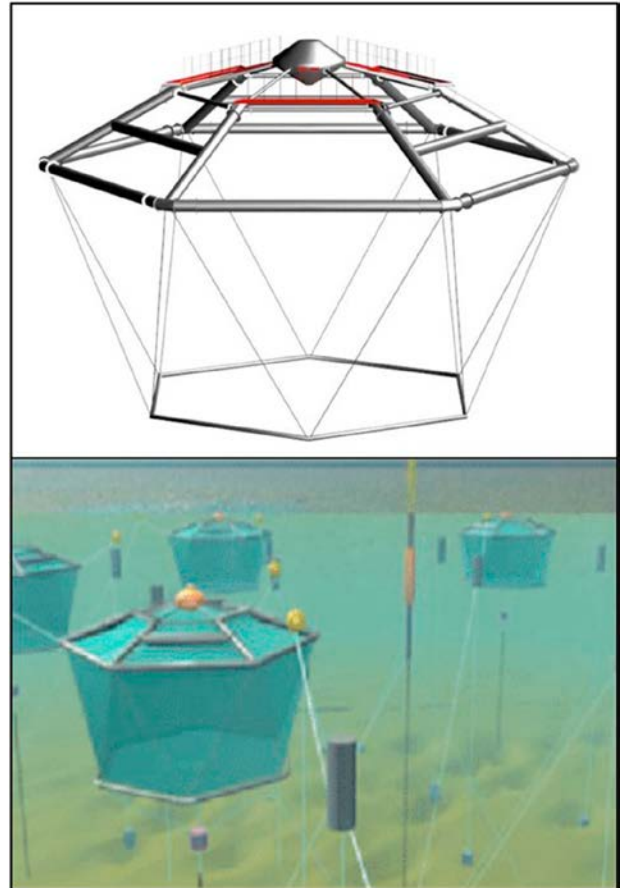
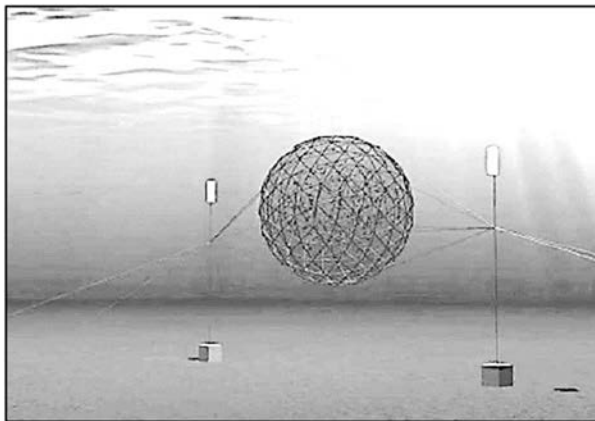


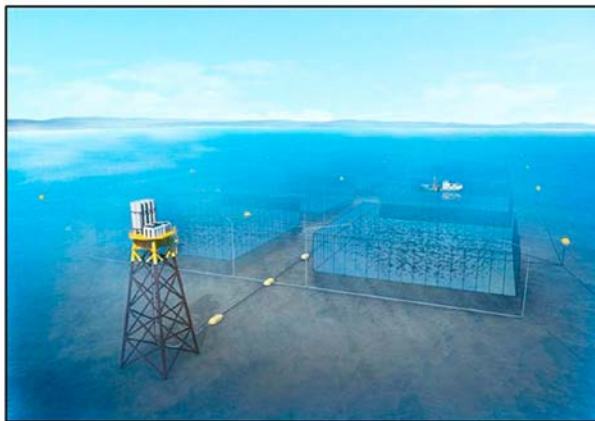
Figure 54: Sadco submerged rigid cage
(<http://www.sadco-shelf.com/>)

AquaPod was developed by Ocean Farm Technologies in the United States. It has a two-point anchor for mooring and some operational advances such as net cleaning and removal of mortalities. NSENGI (Nippon Steel & Sumikin Engineering Co., Ltd) had carried out offshore verification testing of large-scale sinking cages at a salmon farm which is 3 km from shoreline of Sakaiminato, Tottori Prefecture, Japan. Each cage has a volume of 50000 m³ with wave of 7 m height and current speed of 2 knots. The cages are serviced by a jack-up platform that houses

the equipment and feedstock storage facility for automated feeding of the fish.



(a)



(b)

Figure 55: (a) Submerged AquaPod cage from Ocean Farm Technologies (Tidwell, 2012), (b) NSENGI sinking fish cage (<https://www.eng.nipponsteel.com/english/news/2016/20161003.html>)

4.2 Closed containment tank system

Floating closed containment tanks for offshore fish farming are very recent developments prompted by the need to protect the fish from sea lice and other parasites. Floating closed containment tanks contain water that is constantly refreshed by a flow through system which also helps to provide proper temperature, sufficient oxygen, and waste removal.

By having control over water replacement, the water can be constantly disinfected to remove pathogenic organisms. External

environmental events like algae bloom are no longer a problem (Chadwick et al., 2010). Organic wastes can be removed by biofiltration system before discharging the water back to the sea. The threat of predators (such as sharks and seals) is eliminated. It also can achieve a higher production rate when compared to the open cage system (Tidwell, 2012). This is due to the greater control and inputs into these systems and the fact that their physical parameters can be optimized for maximum productivity. On the other hand, the main disadvantage of floating closed containment tanks is that they may lead to effects associated to the behaviour of the contained water, to both structure and fish.

An example of floating closed containment type is the fish farm egg (Figure 56), developed by “Hauge Aqua” using a fully enclosed egg-shaped structure. The water flow enables the system to draw inlet water segregated from where outlet water is released. Water enters using two main pumps that suck water from 20 m below the water surface. The water quality and volume can be controlled, ensuring steady oxygen levels. It is estimated to cost about NOK 600 million (about USD 60 million).



Figure 56: Closed fish farm concept “fish farm egg” (<http://sysla.no/fisk/skalbruke-600-mill-pa-lukkedeoppdrettsegg/>)

Neptun was developed by Aquafarm Equipment (Figure 57a). The tank has an internal diameter of 40 m, a depth of 22 m and the gross volume is 21000 m³. Figure 57b shows an underwater view of the tank with inlet and outlet holes for water circulation. The tank is made from Glass Fibre Reinforced Polymers (GFRP) elements and reinforced with steel in areas that bear the most stress. The design also includes a pump system to extract large volumes of water from a depth of 25 m or more. As the concept of the containment tank is to collect the waste from the fish and uneaten fish feed from the sloped bottom, there is a flexible pipeline that connects the low point to the waste separator.



Figure 57: Neptun closed containment fish tank (a) As installed, (b) Overview of the structure
<http://aquafarm.no>

Dr. Techn. Olav Olsen, Norway based marine technology consulting company, proposed a closed containment tank for offshore farming, built in concrete material (Figure 58).

The cylindrical concrete tank has 14.8 m of inner diameter, 16.5 m of outer diameter and 6 m height. Its bottom has a sloping bottom for easy collection of organic waste (Chu et al., 2020).



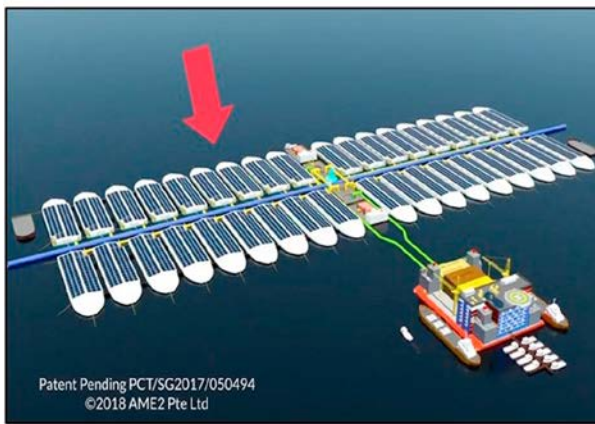
Figure 58: Concrete containment fish tank (Picture courtesy of Tor Ole Olsen).

AME2 Pte Ltd., Singapore based company, has developed a closed containment flow through floating fish farm called Eco-Ark (Figure 59a). It has several containment tanks with flow through water supply system. It has a roof equipped with solar panels to supply electricity for the fish farm. The Eco-Ark allows augmentation and integration by forming a fleet connected to a lift dock facility that enables to cultivate and process massive amount of fish on site (Figure 59b). The Eco-Ark was constructed in Batam Island, Indonesia, and was deployed in Singapore waters in August 2019.

The Norwegian salmon farmer, Marine harvest, developed a closed containment tank design named marine donut (Figure 60). The marine donut can accommodate 200000 fish in each unit. In 2019, Norway's directorate of fisheries granted permission for 1100 tonnes of biomass to be used to test the design.



(a)



(b)

Figure 59: (a) Eco-Ark closed containment system, (b) Eco-Ark fleet connected to lift-dock (Picture courtesy of Mr. Ban Tat Leow, the inventor of Eco-Ark).

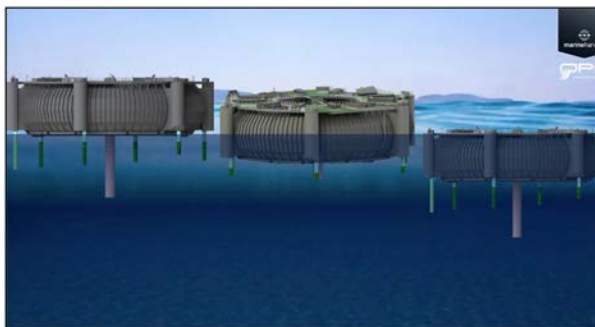


Figure 60: Marine donut – Close containment concept design of marine harvest (<http://marin.bergen-chamber.no/en/teknologi/Growth-through-innovation/>)

4.3 Recent challenges & developments

The preliminary study of the vessel-shaped offshore fish farm concept (that gave origin to Havfarm - Figure 48a) for open sea applications was reported in the work of (Li et al., 2017). The

structure included the vessel-shaped hull, a mooring system, and fish cages. The shape of the hull minimizes the wave loads coming from the bow, and the single-point mooring system is connected to the turret at the vessel bow. Such a system allows the whole fish farm to rotate freely about the turret, reduces the environmental loads on the structure, and increases the spread area of fish wastes. A basic geometry of the vessel hull was considered, and the hydrodynamic properties were obtained from frequency domain analysis. The preliminary mooring system was designed to avoid possible interactions with the fish cages. Time domain simulations coupling the hull with the mooring system were also performed. Fish cages were simplified by considering a rigid model. The global responses of the system and the mooring line loads were assessed in various waves and current conditions and the effects due to the misalignment of waves and current directions on the responses were also studied. Further studies on this system has been conducted and reported in (L. Li et al., 2019a, 2019b, 2018a, 2018b). For instance, L. Li et al. (2018a) conducted a numerical study to investigate the vessel’s responses using flexible and rigid net models under steady current conditions; L. Li et al. (2019a) proposed an integrated optimization methodology for the design of mooring systems. The methodology integrates the design of experiments, screening analysis, time-domain simulations, and a meta-model-based optimization procedure; L. Li et al.(2019b) proposed an integrated method for the numerical prediction of the heading misalignment between the vessel-shaped fish farm and the currents under combined waves and currents. The probability distribution of the misalignment angle was calculated using the Kriging metamodel for a reference site and based on the prediction, the requirement for the dynamic positioning system to improve the flow condition in the fish cages was discussed.

Kristiansen et al. (2017) addressed the description of exposure from waves and currents in coastal regions for design of marine fish farms. Dedicated field measurements at two

exposed aquaculture sites from February to December 2016 were presented. Results from statistical analyses of the measurement data demonstrated that common practice for characterization of exposure in design of fish farms has several deficiencies that should be improved to reduce uncertainties in design. Later, Kristiansen et al. (2018) investigated the seakeeping behaviour of a rigid type of floating closed fish cages, with focus on the effects of sloshing on the coupled motions and mooring loads. Scaled model tests of closed cages in waves revealed that the influence of sloshing on the rigid body motion is significant. Therefore, coupled motions with sloshing are important to consider in the design of this type of fish farming floating system.

Turner et al. (2017) have developed a net wake shielding and self-shielding model to accurately estimate the hydrodynamic loading on fin-fish aquaculture installation. The effect of containment net hydrodynamic wake shielding is important to avoid overly conservative estimation of loads on fish farm installations. The reduction in fluid velocity through a net can be significant in many cases, leading to decreased loading and changes in motion on downstream nets and mooring components. In as subsequent work, Turner et al. (2018) presented a comparative study of taut and catenary mooring systems for the fin-fish aquaculture installation. The results showed that a reduced footprint taut mooring configuration with integrated elastomeric mooring components can substitute a typical chain catenary mooring with no significant increase in peak mooring line loads at extreme sea states and significant reduction in peak loading at moderate and calm sea states.

Kitazawa et al. (2017) have performed water tank and field tests on the performance of a submersible fish cage for farming silver salmon. A submersible cage using flexible tubes was proposed to farm silver salmon in deeper and cooler waters to overcome the limitation of cultivation during August. The cage was submerged and floated up by ejecting air from

and injecting air into the flexible tubes, respectively. Water tank test using the 1/3.64 scaled model and field tests have been performed to assess the behaviour of the cage during floating up and submersion.

Lader et al. (2017) conducted a classification study of aquaculture locations in Norway with respect to wind wave exposure. The method was called fetch analysis and used long term wind data connected with the fetch length to estimate wind wave conditions. The method was divided into four steps: 1) Fetch analysis, 2) Wind data, 3) Estimating wave parameters H_s and T_p and 4) Wave statistics. Significant wave height H_s with return period 1 year and 50 years were estimated for each site. H_s 50 year is often used for design, and the analysis showed that for 38% of the sites H_s 50 year exceeds 1 meter, for 17% of the sites H_s 50 year exceeds 1.5 meter, while 1.4% of the sites have H_s 50 year larger than 2.5 meter. The most exposed site has a H_s 50 year of 2.9 meter. Thus, large differences in H_s 50 year in the various coastal regions of Norway exist.

Gansel et al. (2017) investigated the effects of different amount and sizes of fouling organisms (blue mussel and kelp) in Norwegian aquaculture on the drag on net panels. Drag forces on several clean and fouled nets were measured in a flume tank at a flow speed of 0.1 m/s. Drag on fouled nets largely depended on the distribution of fouling rather than on the wet weight. Knowledge about the effect of a given type of fouling on the drag on nets allows the use of drag as a proxy to find transfer functions between fouled and clean net solidity.

Føre et al. (2018) experimentally investigated traditional netting materials subjected to disinfecting chemicals during fish farming and treatment of net cages. A series of tests were performed to study the effect of various concentrations of disinfecting chemicals on the tensile strength of Raschel knitted Nylon netting materials. Simulated spill of diluted hydrogen peroxide to the jump fence during delousing did not affect the strength of the applied new and used knotless nylon netting samples.

Hydrogen peroxide reacted with biofouling forming gas bubbles, but this did not result in reduced netting strength. The performed tests did not indicate any effect on netting strength from a simulated single, traditional bath disinfection as performed at service stations applying the disinfectant Aqua Des containing peracetic acid. However, increasing the Aqua Des concentration from 1 to 10 % resulted in a strength reduction of 3–6 %. Simulated spill of concentrated Aqua Des on the jump fence of a net with copper coating residuals resulted in a severe reduction in strength of 45 %.

Fredriksen et al. (2018) carried out simulations on response characteristics of a fish farm system when subjected to combined irregular waves and current conditions. The studied fish farm system had a large horizontal extension with variable environmental conditions across the entire structure and the drag loads on the fish nets are thought to be the governing environmental force. The results showed that, in most cases, using the maximum expected wave height in an irregular sea state as criteria for selecting an equivalent regular wave give realistic design values.

Zhou et al. (2018) experimentally examined the feasibility of the net-hauling system for set net fishery using water tank tests. A flexible hose net is proposed to harvest fish in the box chamber net of set net fishery (Figure 61). The flexible hose net is installed on the water bottom below the box chamber net. Compressed air is injected from one edge of the hose net to haul the box chamber net gradually, resulting in cornering fish in the other edge. The variation in the formation of the hose net and the time for sinking and floating were examined, changing the parameters such as air pressure and buoyancy balance. The hose net sank automatically if the weight attached to the hose net was 39% of the total buoyancy of the hose net with full of air. To reduce the sinking time, the initial inner pressure of the hose net must be the atmospheric pressure before the beginning of the sinking operation. Motion analysis of flexible hoses revealed that the inside structure

of the hoses may have to be improved to secure the air flow in any condition.

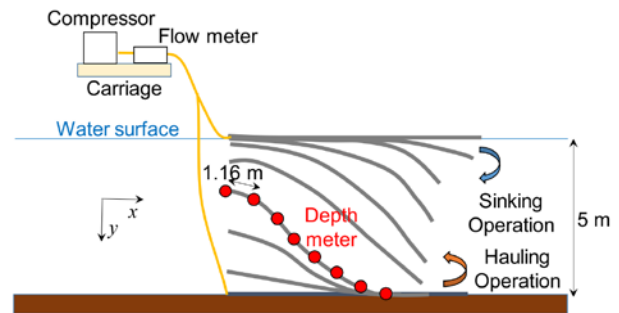


Figure 61: Two-dimensional schematic representation of the sinking and hauling experiments of the hose net (Zhou et al., 2018)

Yu et al. (2018) experimentally tested a controllable depth cage (CDC) with its mooring system (Figure 62). CDC consists of a cage, floats, and anchors, which are connected by ropes in this order. The vertical position of the cage is controllable by adjusting the buoyancy of floats. The effects of waves on the motions of the CDC were tested in smaller (1/100 scale model) and larger water tanks (1/25 scale model). The range of motion and the tension on the mooring ropes of CDC increased with increasing wave height. Close to the water surface, when the wavelength was around two times the size of the CDC, the tension of the mooring ropes increased. Under the same wave condition, the displacement and the inclination of the cage, and the tension of the mooring ropes decreased by about half when the cage was installed at 0.7 m below the water surface.



Figure 62: Controllable depth cage model test when the cage was at water surface (left) and at the submerged depth (right) (Yu et al., 2018)

Weiss et al. (2018) presented a new tool to identify potential zones for offshore aquaculture. A global case study for greater amberjack was reported highlighting

unexploited offshore zones in South and North America, Oceania, and Africa. The tool aims to identify optimal conditions for the growth of fish species and for cage resistance, a methodology developed in the framework of the TEN-SHORES project. The first step was based on the Delphi method and consists of the selection of variables according to their relevance to fish species and to the cage location. The selected variables were acquired from reanalysis models and remote sensing data (time series of 20–30 years). In the second step, an evaluation system was developed to estimate the percentage of time (on a 0-1 scale) that the selected variables remain in optimum conditions, for the fish and the cage, in the whole data series (grid of 0.25°). Suitability maps were generated according to the conditions for the fish species growth and to house a generic cage.

Zhao et al. (2019) carried out a series of physical model experiments to investigate the hydrodynamic responses in regular waves of a semi-submersible offshore fish farm, whose structural configuration refers to Ocean Farm 1 (Figure 63). Mooring line tension and motion response of the fish farm at three draughts were analysed. The consideration of net resulted in approximately 42% reduction in mooring line tension and approximately 51% reduction in surge motion. However, the heave and pitch of the fish farm increased slightly with the existence of net.



Figure 63: Primary frame of the fish farm (Zhao et al., 2019)

Xu and Qin (2020) examined the fluid-structure interactions between fluid, aquaculture cages and fish. A comparison between the traditional methods used to assess the interactions between environmental loads and aquaculture cages was presented. This

comparison included analytical studies, numerical implementations, field tests, and laboratory experiments. Reviews on topics such as mooring and grid systems, drag coefficients of the net panel, hydrodynamic behaviours of cage components, velocity reduction of cage array, and volume reduction caused by cage deformation are also provided. Conclusive data shows that the Morison equation-based empirical formulae underestimated the drag force on the net, while the screen-based empirical formulae overestimated the drag force. The most reliable methods to use are validated physical models and numerical implementations.

Qin et al. (2020) investigated the effects of extreme wave conditions by leveraging a physical model approach on aquaculture structures. Physical model tests have been conducted with the purpose of investigating the nonlinear vertical accelerations and mooring loads of a scaled aquaculture cage (Figure 64). For the floating collar model, regular waves with wave steepness of $1/60$, $1/30$ and $1/15$ were tested. For the floating cage model, the same regular waves combined with current 0.1 m/s and 0.2 m/s were examined. It was assumed that the wavelength was much larger than the size of the floating collar and that the wave frequency was much lower than the natural period of heave. For the floating collar model without netting, under wave-only conditions, the first- and second-harmonic components of the vertical acceleration are proportional to the wave amplitude and square of the wave amplitude, respectively. For the floating cage model under combined waves and current conditions, the first-harmonic component is more likely proportional to the wave amplitude, while the second-harmonic component shows erratic behaviour.

Huang et al. (2020) have developed a semi-submersible offshore fish farm with steel truss structure and single-point mooring system. The mooring forces and motion responses including heave, pitch, and roll for the fish farm exposed to waves and currents have been analysed

through a series of laboratory experiments for the offshore fish farm with the scale of 1:30 (Figure 65). Their results indicate that the dynamic response of the fish farm in combined conditions of wave-current is lower than that of the pure waves, since the current velocity is helpful to decrease the impact of the pulse owing to the high stiffness of the anchor chain of the farm that is exposed to water loads. Increasing the draught of the fish farm can lead to both the mooring force and roll becoming larger, besides reducing the heave. However, the tentative variation for the pitch is not obvious. The current velocity inside the fish farm is significantly lower than the outside of the fish farm. The resulting total reduction falls within 32.25%–63.00%.

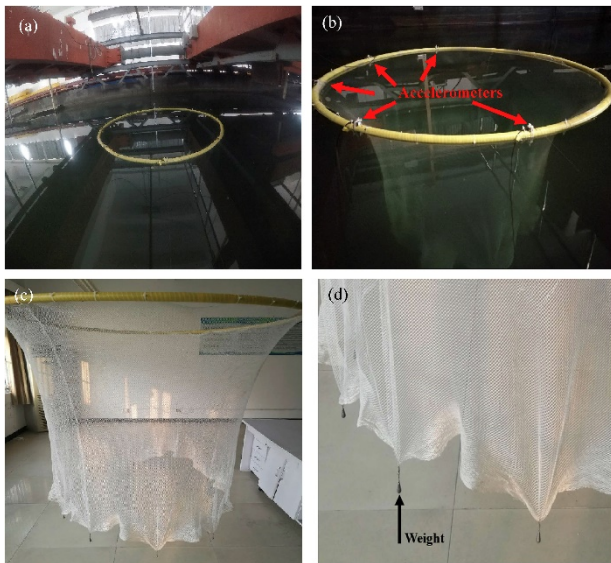


Figure 64: The physical model of the aquaculture cage: (a) model of the floating collar without netting from the top view; (b) installation of accelerometers along the floating collar model with netting; (c) floating cage model in the air and (d) details of the netting and weights (Qin et al., 2020)

Martin et al. (2020) derived a Lagrangian approach for the coupled numerical simulation of fixed net structures and fluid flow. The model was based on solving the Reynolds-averaged Navier-Stokes equations in a Eulerian fluid domain. The equations included disturbances to account for the presence of the net. Forces on the net were calculated using a screen force model and were distributed on Lagrangian points to

represent the geometry of the net. Different solidities, inflow velocities and angles of attack were considered. The comparison of loads on and velocity reductions behind the net with available measurements indicates superior performance of the proposed model over existing approaches for a wide range of applications. The numerical model is extensively validated against existing experiments for fixed net panels, multiple panels and cages with varying geometries and solidities in current and regular waves.

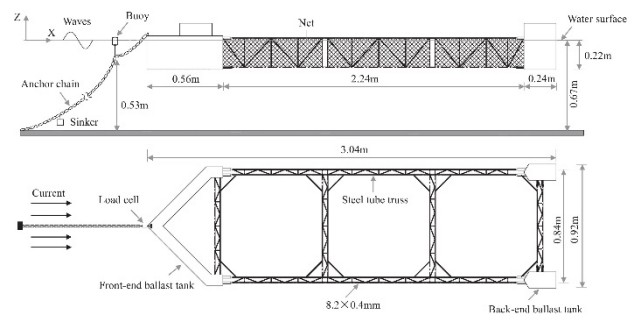


Figure 65: Physical model configuration of the offshore farm (Huang et al., 2020)

A concept of a floating wind-solar-aquaculture (WSA) system, combining multiple megawatt (MW) vertical-axis wind turbines (VAWTs) and solar arrays with a floating steel fish-farming cage, was presented in Zheng et al. (2020). An aerodynamic source code based on the double multi-streamtube theory is developed. It can be exported into the commercial software Orcaflex to achieve fully coupled analysis of the WSA system. Using the developed tool, turbine aerodynamic performance, tower base bending moments, global WSA motions, and tension of mooring lines were investigated. The results affirm that WSA is technically safe and feasible. It is a promising concept to deploy in intermediate and deep waters.

The study presented by Wang et al. (2020) aims to develop a fixed horizontal cylindrical fish cage which can rotate around the central axis. In this way, the biofouling on the main structure could be easy to be cleaned. For offshore engineering structures, the strong earthquake is one of the main loads leading to structural failure. Especially, some offshore fish

farms may be located on the edge of the continental plate where strong seismic activity often occur. Therefore, it is necessary to study the dynamic characteristics of the fish cage under earthquake load. A finite element model of the fixed horizontal cylindrical fish cage was established to calculate the dynamic characteristics based on the ABAQUS software (Figure 66). The natural frequency and vibration mode of the fish cage are obtained by modal analysis.

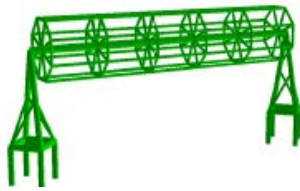
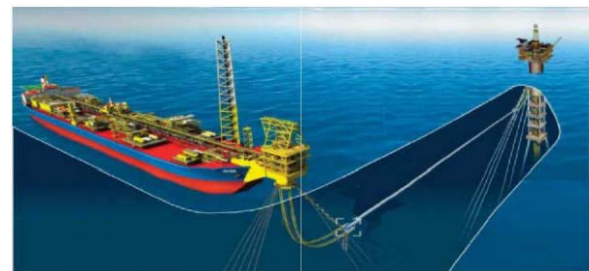


Figure 66: The finite element model of the fixed horizontal cylindrical fish cage structure (Wang et al., 2020)

5. STATE-OF-THE-ART REVIEW IN MODEL TESTS OF CABLE/PIPE DYNAMICS CLOSE TO THE SEA SURFACE

With the development of deep-sea oil production technology, a composite deep sea oil production system has emerged, namely the combination of spar & FPSO or other platform forms of compound oil production. The biggest advantage of this composite system is that as many facilities other than the production unit on the spar or semi oil production platform can be transferred and installed on the FPSO to reduce costs. This type of operation plan needs to connect the two platforms with FTL (Fluid Transfer Lines), as seen in Figure 67. Compared to the seabed pipelines, the suspended FTLs are well known to be an attractive alternative solution. The main advantages of the suspended FTL compared to the subsea pipeline are (a) improved flow assurance due to higher seawater temperature leading to reduced risk of blockage by formation of wax and hydrates; (b) avoidance of seabed constraints, such as ground instability, irregular sea-bed profile, and subsea hardware congestion.

However, the free-hanging flow lines with single or multiple wave configuration or with bonded hose are much longer than the distance between the DTU and FPSO to have less local curvature. The long transfer line requires higher discharge pressure to withstand the pressure drop due to the friction loss along the long pipe inner wall. In the case the distance is too large (i.e., larger than 1000 m), the flow line motion may also significantly influence the FPSO and DTU motions in extreme environments, which results in the increase of the motion and load of the flow line itself.



Artist impression of the suspended FTL connected to the Spar and FPSO

Figure 67: Suspended FTL connected to a spar and a FPSO

In summary, the disadvantages of the conventional suspended flow-transfer pipelines are limitation in the sizes of the FTLs, strength and fatigue problems, flow-assurance concerns due to the long line length with possible temperature drop, and the high cost of materials and installation.

5.1 Fluid Transfer Lines (FTL)

The FTL is one of the core equipment of the composite deep-sea oil production system, which is affected by ocean currents and waves near the water surface and produces complex hydrodynamic responses such as vortex-induced vibration (VIV). When the vortex frequency is close to the natural frequency of the FTL, resonance locking will occur, leading to fatigue damage. For offshore risers with similar structure and offshore pipelines with large slender ratio, the VIV responses of these flexible structures have sustained a lot of theoretical and experimental research. Carmo et al. (2013), Wu et al. (2012) and Chen et al. (2013) presented

studies on VIV of long slender cylinders and circular cylinders. All of these can be used as the basis for the research of VIV problem for special FTL structures.

Chang and Isherwood (2003) considered the effect of the platform heave motions on the VIV of steel catenary risers and steel offloading lines. The uniqueness of the FTL used in the composite production system lies in that both ends of the FTL are connected to the floating platform, which is bound to be coupled by the multi-degree of freedom movement of the platform, resulting in complex unsteady motion and oscillating inlet flow, which also significantly affects the hydrodynamic response of the FTL.

As part of the design process of deep-water marine risers to minimize top tensioning requirements, mitigate flow-induced vibrations, and to increase the expected fatigue life of these slender structural members, Fang et al. (2014) have employed external buoyancy modules and strakes in an experimental study. A horizontal cylinder with a length to diameter ratio of 263 was fitted with a variety of strake and buoyancy element configurations and towed at uniform speeds ranging from 0.4 to 2.0 m/s. Fibre optic strain gages were used to measure both in-line and crossflow strain response. The resulting time series information was processed to resolve the modal strain information that included frequency, mode shape, and critical damping ratio information. The test data for the 100% coverage by helical stakes demonstrated the effectiveness of that suppression device over the range of current velocities investigated.

Gao et al. (2016) investigated the VIM's influence for the spar-FPSO to mooring line tension by using API simple summation method. The results show that VIM phenomenon leads to a more complex mooring tension distribution, higher offset motion and more serious mooring line fatigue problem.

Yang and Kim (2018) used a fully coupled multi-body-mooring-riser time domain analysis program to model the pipeline bundle with finite

elements as one line member with the equivalent diameter and structural properties. The axial friction forces as well as the transverse drags on the pipeline bundle are considered because their accumulated effects along the very long FTL can be significant. The coupled relative motions of the spar and FPSO can significantly affect the dynamics and tensions of the FTL. The dynamics of the FTL can also affect the relative motions of the two platforms two. The complex coupled system is also significantly affected by the headings of environmental loadings.

Cheng et al. (2018) performed a comprehensive test on straked riser buoyancy modules in a wave basin. The objective of the model test is to obtain hydrodynamic coefficients for the straked pipe and to better understand the global dynamic behaviour of pipe with distributed buoyancy modules due to vessel induced motion and vortex-induced-vibration (VIV). The response of the riser under floater motions including VIV were measured. The model test setup included a fully instrumented pipe, a planar motion mechanism (PMM) which simulates the vessel motion as shown in Figure 68. The riser was instrumented with Fibre Bragg Grating (FBG) strain gauges along the pipe length and circumference. Both in-plane and out-of-plane signals were recorded. The drag and inertia coefficients for the straked pipe are calculated using the modal reconstruction method. The response for different pipe and buoyancy modules were also discussed.

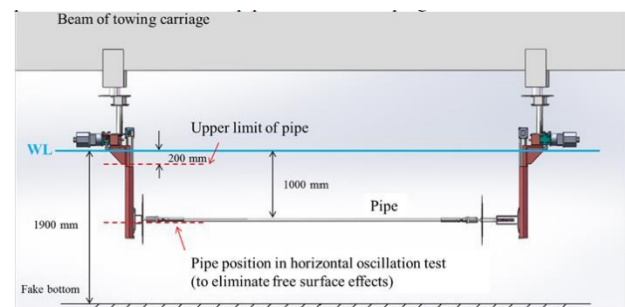


Figure 68: Sketch of horizontal oscillation test for the pipe with buoyancy modules (Cheng et al., 2018)

L. Zhao et al. (2018) studied the VIV response characteristics of flexible catenary

riser model with the slenderness ratio of 578 by means of scale physical model experiments. In the experiment shown in Figure 69, the riser model was installed on a towing carriage, which might move horizontally above a wave basin with constant speed to simulate the working condition of the riser model under uniform current. The tension sensor was used to measure the time-history variation of the top tension. The acceleration sensor was used to measure the accelerations of the riser model in crossflow (CF) and in-line (IL) directions. The top tension, vibration spectrum, amplitude and vibration locus of the riser were analysed in accordance with the flexible riser model experiment, and the VIV law of the model experiment working condition was analysed. The hydrodynamic software Orcaflex was used to verify the finite element analysis (FEA) of the experiment. The experimental results showed that the physical model experimental results well matched those of Orcaflex numerical model. The physical model experimental results reflected the vibration law of flexible risers under actual working conditions. Through the analysis of the tension of the riser, it was evident that the top tension of the riser increases with the increase of the flow velocity due to the flexibility and the catenary shapes of the flexible catenary risers, and the faster the flow velocity increases, the faster the growth rate is. According to the displacement and spectrum analysis, the dominant frequency of the riser in IL direction was twice that in CF direction.

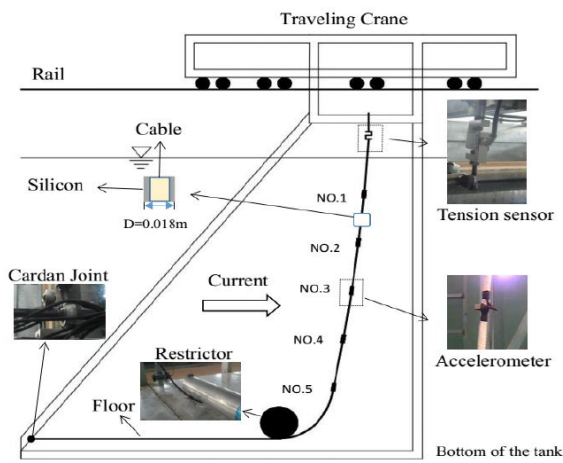


Figure 69: Experiment setup for VIV measurement of flexible catenary riser (L. Zhao et al., 2018)

Ren et al. (2019b) investigated the hydrodynamic forces on stationary partially submerged cylinder through towing test with Reynolds number ranging from 5×10^4 to 9×10^5 . Three test groups of partially submerged cylinders with submerged depths of $0.25 D$, $0.50 D$, and $0.75 D$ and one validation group of fully submerged cylinders were conducted. The test results showed a considerable difference in the hydrodynamic coefficients for the partially submerged cylinders versus the fully submerged cylinders. A significant mean downward lift force is first observed for the partially submerged cylinders in a steady flow. The maximum of the mean lift coefficients can reach 1.5. Two distinct features are observed due to the effects of overtopping: random distributions in the mean drag coefficients and a clear quadratic relationship between the mean lift coefficients and the Froude number appear in the non-overtopping region. However, the novel phenomenon of a good linear relationship with the Froude number for the mean hydrodynamic coefficients was clearly shown in the overtopping region. In addition, fluctuating hydrodynamic coefficients were proposed and investigated.

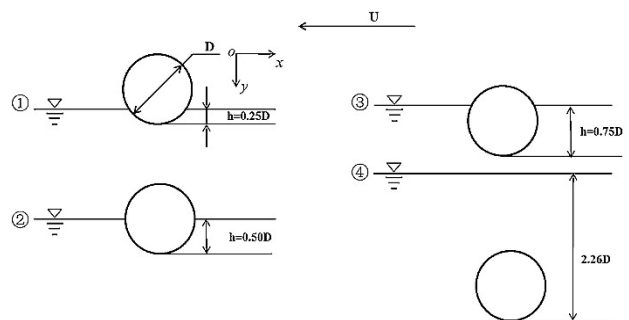


Figure 70: Sketch of the experimental cases (Ren et al., 2019b)

In another experimental study, Ren et al. (2019a) have investigated the oscillatory flow around a flexible pipe fitted with helical strakes for Keulegan-Carpenter (KC) number varying from 21 to 165 and maximum reduced velocities ranging from 4 to 12. The effects of the helical strakes on the VIV response, Strouhal number,

suppression efficiency and fatigue damage were assessed. The results showed that the suppression efficiency and fatigue damage reduction ratio are not as ideal in oscillatory flow as those in steady flow. Moreover, under a lower reduced velocity ($V_R = 4$), the helical strakes significantly increased the VIV dominant frequency and the Strouhal number reached 0.439. Under a higher reduced velocity, two distinct branches in the variation of the St number against the KC number were observed.



Figure 71: Overview of the whole experimental setup (Ren et al., 2019a)

Tumen Ozdil and Akilli (2019) compared the flow characteristics around horizontal single and tandem cylinders at different immersion elevations in shallow water. Particle Image Velocimetry (PIV) was used to evaluate the time-averaged and instantaneous velocity vector area in the wake zone at Reynolds number; $Re_D = 5000$ based on the diameter (D) of cylinder. The gap (L) between the tandem cylinders was enhanced from 0 until 90 mm through 15 mm enhancements to observe effect of the gap on flow characteristics. Five hundred instantaneous images were used to obtain the mean velocity vector field, the streamline topology, and the Reynolds stress correlation. For instance, Figure 72 presents the results for the gap configuration $L/D = 1$ and different immersion distances. The investigation showed that the wake zone happens between tandem cylinders at the starting of $L/D=1$ location. Furthermore, when the space between tandem cylinders deepens, the dimension of the wake zone rises.

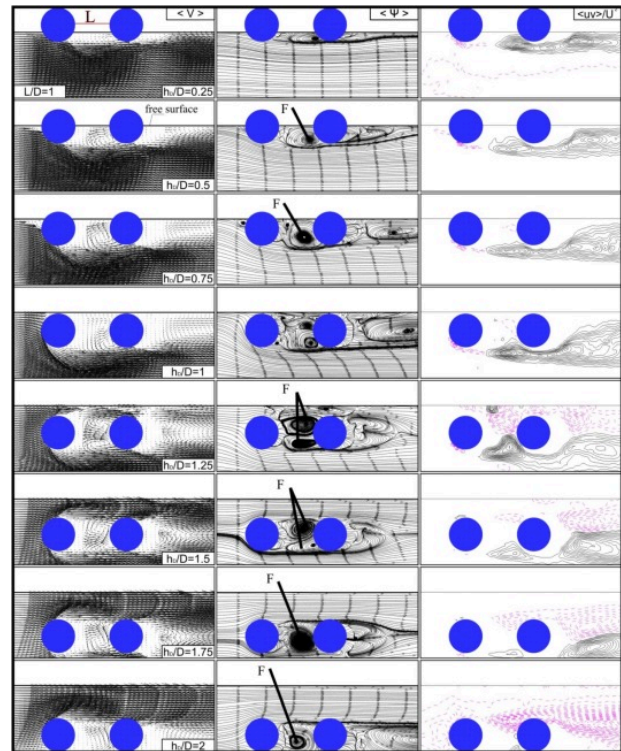


Figure 72: Flow structure around tandem horizontal cylinders for $L/D = 1$ situation.

Gao et al. (2020) presented some recommendations for the prediction of hydrodynamic damping in WIR (Water Intake Riser) design based on experiments. In this study, the hydrodynamic damping of a smooth WIR oscillating in still water or in steady currents is measured with a series of experiments at $KC < 5$ and the Reynolds number (Re) in the range of 103 ~ 105. The effect of in-line or cross steady currents on the in-line hydrodynamic damping is investigated and the performance of the relative velocity Morison model for predicting the hydrodynamic damping at low KC is examined. Experiments are also conducted for a WIR with helical strakes in in-line or cross currents. The model test setup, as illustrated in Figure 73, includes a hexapod that generates the forced oscillation, a mass-spring system that simulates the dynamic behaviour for the WIR and a smooth/straked rigid WIR model. The mass-spring system consists of a trolley with four rollers, a rigid support beam along which the trolley can move and two springs that connect the trolley with both ends of the support beam. For the smooth

WIR, the measured drag coefficients agree reasonably well with the published data and the theoretical Stokes-Wang's solution when it is applicable. The hydrodynamic damping is found to increase with the velocity of the in-line steady current, and the relative velocity with a constant drag coefficient is still applicable in the low KC flow regime when the in-line steady current is considered. For the WIR with helical strakes, a good correlation between the drag coefficient and the velocity ratio r is found, based on which the empirical formulae for drag coefficients are proposed.

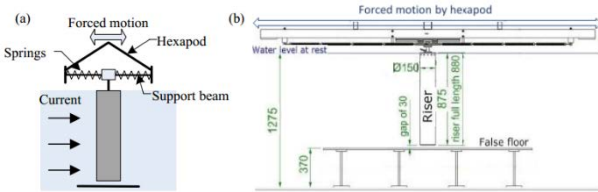


Figure 73: Experiment setup for drag coefficient (Gao et al., 2020)

5.2 Other types of pipes/cables

Besides the applications related to fluid transfer pipes/lines for the oil and gas industry, the dynamics of cables close to the sea surface is also of concern for other types of applications such as power cables for wave energy converters, cable net barriers, and towing cables. However, in the literature review only few numerical studies have been found. For instance, Yang et al. (2017) and (S.-H. Yang et al. (2018) numerically investigated a wave energy converter (WEC) system consisting of a buoy, a mooring system, and a power cable connected to a hub. The study assessed the characteristics of the entire system regarding the energy performance and fatigue life of the mooring lines and power cable. In the former study, the effects of marine biofouling and its growth on the system's components was considered. Hydrodynamic and structural response simulations were conducted in a coupled response analysis using the DNV-GL software SESAM. Energy performance analyses and stress-based rain flow counting fatigue calculations were performed separately using an in-house code. In the latter study, the WEC

system formed an array, with several WECs located around a central hub to which they were each connected by a short, free-hanging power cable. The study is analysed the dynamic characteristics and estimate the fatigue life of the power cable which is not yet in use or available on the commercial market. A novel approach was adopted considering that the power cable's length was restricted by several factors (e.g., the clearances between the service vessel and seabed and the cable), and the cable was subjected to motion and loading from the WEC and to environmental loads from waves and currents (i.e., dynamic cable). The results of the numerical simulations were discussed regarding the responses of the power cables, including dynamic motion, curvature, cross-sectional forces, and accumulated fatigue damage. The effects of environmental conditions on the long-term mechanical life spans of the power cables are also investigated. Important cable design parameters that resulted in a long power cable (fatigue) service life are identified, and the cable service life was predicted.

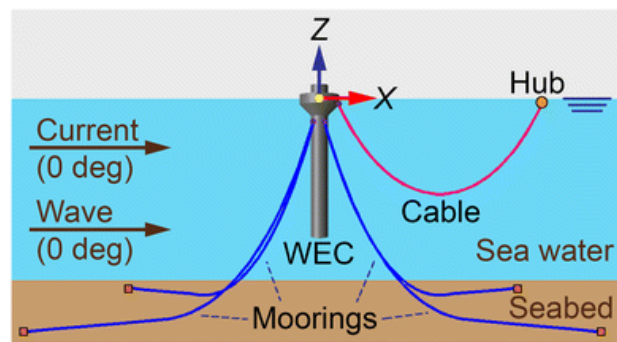


Figure 74: WEC system, including the WEC and its moorings, the hub and the cable (S.-H. Yang et al., 2018)

Da Silva Gomes and Pinheiro Gomes (2021) have proposed a new formalism for the dynamic modelling of a cable towing system, in which both the tugboat and the towed vessel were subject to forces from waves on the sea surface. The continuous flexibility of the cable was approximated by a discrete equivalent, formed by rigid links connected by fictitious elastic joints that allow elevation movements, since the dynamics are restricted to the vertical plane. The Euler-Lagrange formalism was used to

determine the dynamic models considering two, three and four links. Vertical forces obtained from proportional and derivative control were applied to the tugboat and the towed vessel, thus simulating the wave motion of the sea surface. Simultaneously, a motor thrust is applied to the tugboat. An algorithmic procedure was also proposed to determine the dynamic tension in the cable.

Finally, motivated by the design of a protective anti-shark cable net enclosure located in heavy surf on La Réunion, France, Niewiarowski et al. (2018) presented a modelling technique for underwater cable structures subject to breaking wave action. In the presented work, the Morison equation was coupled with a high-resolution breaking wave simulation obtained by solving the full air-water Navier-Stokes equations, creating a time-domain analysis approach suitable for studying underwater cable structures subject to breaking waves. The hydrodynamic model was validated using the software package ProteusDS, and the presented model was used to characterize the mechanical response of a moored cable net.

6. STATE-OF-THE-ART REVIEW IN HYBRID TESTING – SOFTWARE-IN-THE-LOOP TESTS FOR MODELLING WIND FORCES

The Software-in-the-Loop (SIL) approach in the floating wind turbine model testing is to include a realistic force to represent the aerodynamic thrust in combination with wind and wave scaled tests. It is based on the use of a ducted fan substituting the wind turbine scaled rotor. The fan thrust is controlled by the fan rotational speed set by the controller, which again depends on a computer real time simulation of the full-scale rotor in the wind field. The real time simulation considers the platform motions measured in real time in the wave tank test. Therefore, the aerodynamic damping is modelled by the fan force (Müller et al., 2014). In those tests, a brushless motor was integrated with the ducted fan. The motor power electronics was regulated by an Electronic

Speed Controller (ESC) card that was powered by an industrial AC/DC power supply. The rotational speed of the motor was controlled by a Pulse Width Modulation (PWM) signal that was generated with a LabVIEW control software, using servo libraries for Arduino. The demanded force for the fan was provided by the full-scale simulation of the rotor’s aerodynamic thrust. Figure 75 shows the layout of the system hardware. The selection of the power of the fan system is based on the range of required thrust during the test. This depends on the nominal power of the wind turbine and the scale factor. In addition, the thermal stability of the fan system must be considered, in order to run at the required power during the requested time of the test and avoid using a cooling down phase (Azcona et al., 2014).

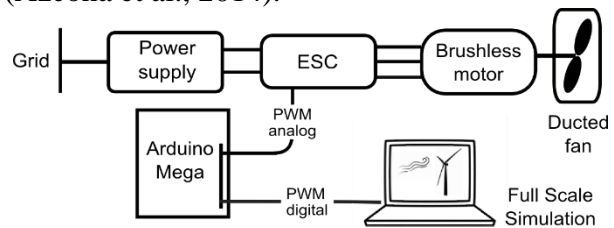


Figure 75: Fan control system layout (Azcona et al., 2014)

A typical SIL system can be found from the research of Azcona et al. (2014) and displayed in Figure 76. The left side describes the simulation part of the system, which works in full scale, and the right side represents the wave tank scaled test.

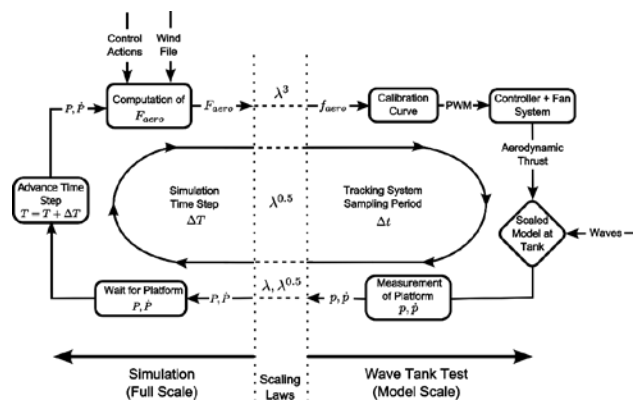


Figure 76: Software-in-the-Loop method diagram (Azcona et al., 2014)

The SIL approach required a communication protocol between the simulation and the tank hardware. Azcona et al. (2014) have used the LabVIEW software to acquire the data from the wave tank motion capture system at ECN (Qualisys) and to communicate with the wind turbine simulation software during the test execution. A TCP/IP network protocol was selected for the communication between LabVIEW and Qualisys and between LabVIEW and the simulation code.

SIL approach could overcome the limit of applying the actuating the forces through direct physical simulation such as lack of ability to simulate part of the physical environment (e.g. lack of wind generation in a test tank), issues of the size of the facility (e.g. simulation of spread moorings), or issues of the similarity between model and full-scale prototype.

6.1 Impact of the SIL approach

The SIL approach can provide a realistic aerodynamic thrust on the scaled model. As the computation of the force takes into consideration the motion of the platform, the effect of the aerodynamic damping is included. In addition, the control actions, the different types of wind (turbulent, constant, gusts) and the operating condition (idling, power production, etc.) are considered for the calculation of the thrust. Conditions where the waves and wind are misaligned are sometimes not easy to be reproduced in wave tanks with wind generation systems. With this method, it can be easily achieved by changing the fan orientation at the tower top. Furthermore, the SIL system allows performing test cases including wind at wave basins where the wind generation system is not available. In addition, the simplicity of the method makes it cost effective and flexible because the material is not specific for a certain wind turbine model and it could be used in different tests for different models (Müller et al., 2014). Some more key benefits are listed below (Day et al., 2017):

- the tests could take place without the need for deployment of a wind generation system;
- there is no requirement to construct a scale-model (or distorted-scale-model) rotor and drive;
- the scale of the tests is dictated only by the hydrodynamics of the floater, which in this case allows a test at relatively large scale;
- the test procedure can replicate the forces generated by turbulent or steady wind in a variety of directions relative to the wave heading;
- the impact of the turbine control system and blade elasticity may be modelled in the tests;
- correct simulation of the aerodynamic drag load on the tower and parked turbine in extreme conditions is possible;
- Some special cases, such as emergency stop tests can be simulated with correct full-scale behaviour.

Effects that are not scaled correctly with this procedure are the aerodynamic torque and the gyroscopic momentum. Alternatively, the use of a rotating scaled mass to represent the rotor inertia can be used to match the gyroscopic effects. Active research on the response of different fan units depending on the size of the wind turbine, scale factor, etc. is being conducted with the aim to explore the limits of the methodology.

6.2 SIL applications

In recent years, many research papers have been published by using the SIL approaches in different research area. SIL was used in wind tunnel testing to model behaviour of a floating wind turbine by mounting a Reynolds-scaled working turbine model on a hexapod (Bayati et al., 2014) and utilizing the hexapod to simulate the impact of the platform motions on the turbine performance.

A 6-Degrees-of-Freedom PKM-Hexaglide robot for simulating the dynamics of Floating Offshore Wind Turbines in wind tunnel scale tests is used in their experiments, as shown in Figure 77. They validate the sophisticated aero-hydro-elastic simulation tools as well as control strategies through the scale test experiments and to provide a complementary approach with respect to water basin scale tests, with a greater attention to the influence of the floating motion on the aerodynamics.

In addition, they define the requirements due to extreme sea-state and the related dynamics of three different platform concepts combined with the 5-MW reference floating turbine. A rigid multibody model is developed for assessing the dynamics of the robot due specific motion-tasks and for sizing the actuation system. The scaled motions of a 5-MW spar buoy floating turbine were analysed as reference case to verify the reliability of the robot to reproduce the dynamics of nominal operating conditions, in terms of slider displacements, forces and power within the design ranges.



Figure 77: 6-DoF Robotic platform “HexaFloat” for wind tunnel tests (Bayati et al., 2014)

In ship model testing, Tsukada et al. (2013) used a ducted fan as an auxiliary thruster mounted on a free-running ship model in order to correct for Reynolds scaling effects on the ship resistance in manoeuvring tests.

Azcona et al. (2014) implemented and performed a first validation of the SIL approach coupling in real time of rotor simulation that

controls the fan with the measured motions of a 6 MW semisubmersible scaled floating wind turbine. The scaled model of the turbine is shown in Figure 78 and the fan system is shown in Figure 79. The described methodology was applied during a test campaign of a floating semisubmersible platform performed during 2013 at the Ecole Centrale de Nantes (ECN) wave tank in France. The purpose of the test campaign was the verification of the platform design and the assessment of the performance of the SiL system. The experimental results have been compared with computations, in general, with good correspondence. The platform pitch displacements under different constant wind loading compare well between tests and computations, showing the correct static performance of the ducted fan system. The free decay test in pitch under a constant wind of 12.7 m/s illustrates the capability of the fan to capture the coupling of the aerodynamic thrust with the rotor's relative displacements within the wind field. Nevertheless, when the turbulent wind is included to the irregular wave cases, these differences disappear, and the experimental results match very well the computations. In particular, the effect of wind over the pitch motion is very accurately captured, which is important to calculate the correct rotor loads.

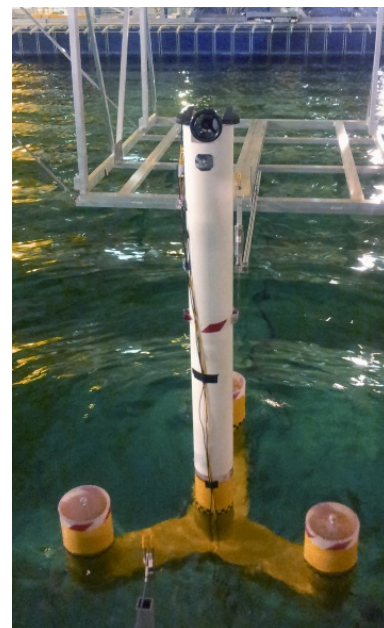


Figure 78: Scaled Model in the Wave Tank (Azcona et al., 2014)

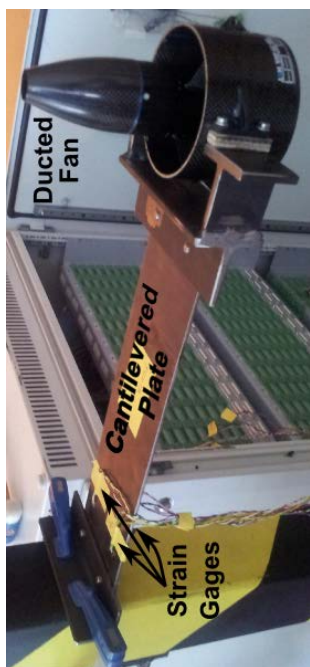


Figure 79: Fan Set Up for Calibration (Azcona et al., 2014)

Zamora-Rodriguez et al. (2014) generated the unsteady aerodynamic thrust force in a hydrodynamic test of a floating wind turbine using a speed-controlled fan. The Iberdrola TLPWT platform consists of a central cylindrical column with four square section pontoons (perpendicularly symmetrically distributed) attached at its bottom, each with two tendons as shown in Figure 80, aimed at supporting a 5 MW generator, positioned at a height of 89 m from MSL.

To consider the wind effect, a speed-controlled fan is positioned at the top of the tower. The fan produces thrust action only in the x direction. The fan thrust depends on the relative wind speed, which in turn, is mainly function of surge and sway velocities. Motion information is transferred in real time from OPTITRACK system to the fan control to adjust the thrust accordingly. Regular waves, operational, survival, failure and transport experiments have been conducted. They find that all motion RAOs are very small, except surge, consistently with the type of platform (TLP). A maximum motion RAO of 5 in surge in a period range between 20-25s is found. That value decays quadratic for lower periods leading

to operational sea states RAOs that is lower than one. Maximum accelerations values in nacelle are below 3 m/s^2 and tensions below 40% of MBL in survival conditions.

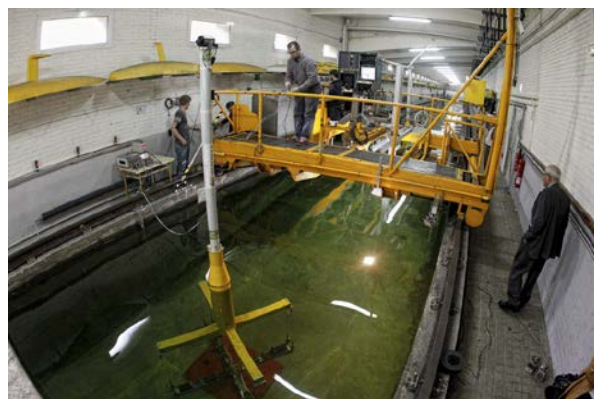


Figure 80: Floating wind turbine case study (Zamora-Rodriguez et al., 2014)

In the research work of Sauder et al. (2016) and Bachynski et al. (2016), all aerodynamic load components for the structure are identified and applied on the physical model, which is significantly different from other previous studies, where only the aerodynamic thrust force was applied on the physical model. The study is carried out at Real-Time Hybrid Model Testing with 5-MW-CSC design for a range of testing including turbine shutdown. The numerical substructure contains only the turbine while the floater and rigid tower are modelled physically.

Wave and current environment are modelled physically in the Ocean Basin, while the wind environment is modelled numerically. A detailed examination of the motions, mooring line forces, and tower and column bending moments in severe waves, aligned wind and waves, misaligned wind, and waves, wind-wave-current, and in several wind turbine fault conditions are thoroughly investigated. It is concluded that for the platform tested, the interaction between the aerodynamic and hydrodynamic loads was primarily at low frequencies.

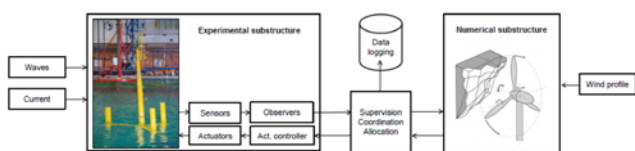


Figure 81: Sub-structuring strategy for the work of Sauder et al. (2016) and Bachynski et al. (2016)

The software in the loop approach was used by Day et al. (2017) and Oguz et al. (2018) to control a ducted fan to simulate the aerodynamic thrust load on a TLP floating wind turbine in the Kelvin Hydrodynamics Laboratory at the University of Strathclyde, as shown in Figure 82. The floater consists of a TLP designed for 70 m water depth with four pontoons in a cross arrangement each fitted with two tendons. The floater is designed to utilize the benchmark NREL 5 MW turbine. A ducted fan unit intended for use on a model aircraft was fitted at the correct vertical location for the drive train. This could develop up to 50 N of thrust. This was mounted on a load cell and extensively bench-tested to determine the relationship between steady speed and thrust. The SIL control system for the fan was developed by CENER. The 6-DOF rigid-body motions of the platform are computed from the measurements by the Qualisys motion capture system and output in real time to the control PC. The control PC runs a highly modified version of the well-known FAST aero-hydro-servo-elastic code, as shown in Figure 83, in which the standard hydrodynamic calculations to find instantaneous platform position, attitude and velocities are replaced by the values obtained from the tank measurements. The code then calculates the aerodynamic thrust expected with the instantaneous platform location and dynamics in the wind field (either steady or turbulent) and outputs the thrust demand to the fan controller. This in turn controls the fan to rotate at the speed associated with the target value of thrust. Results for free oscillation tests and regular wave responses for the TLP turbine show that the implementation of the SIL approach gives greater quadratic damping and can affect the RAO in surge by as much as 20% compared to

the case with no wind, and more than 10% compared to the case with a predefined thrust.

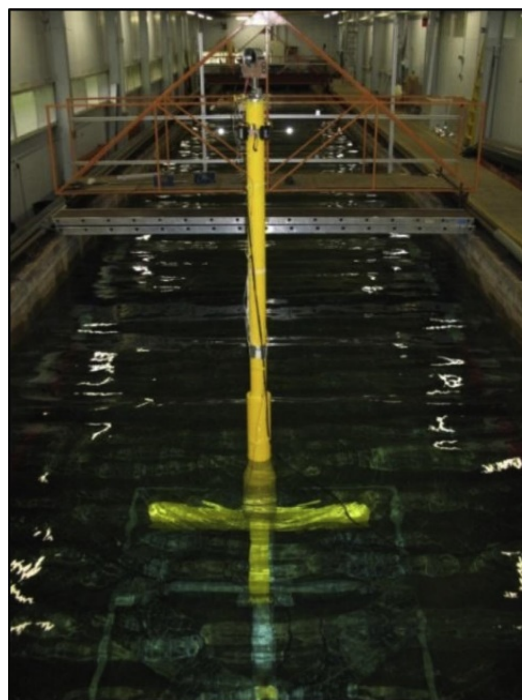


Figure 82: View of the model in KHL tank looking towards wave maker (Oguz et al., 2018)

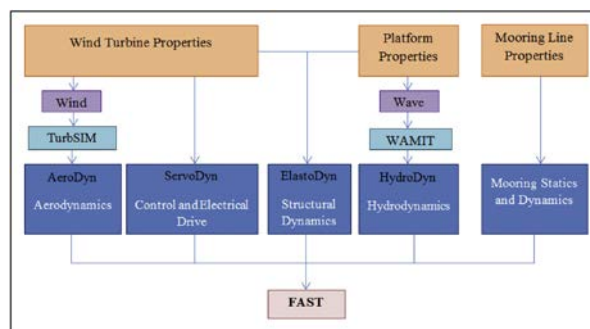


Figure 83: Fast structure (Oguz et al., 2018)

Vittori et al. (2018) at National Renewable Energy Center in Spain (CENER) has developed a hybrid testing method (SiP) to replace the rotor by a ducted fan at the model tower top. Like other SiL methods, the introduction of fan brought in a variable force representing the total wind thrust by the rotor. This load is obtained from an aerodynamic simulation that is performed in synchrony with the test and it is fed in real time with the displacements of the platform provided by the acquisition system. With the use of such method, the displacements

of the turbine and the relative wind speed on the rotor is considered.

A test campaign is taken at the Ecole Centrale de Nantes wave tank of the OC4 semisubmersible 5 MW wind turbine, with a scale factor of 1/45. The experimental results are compared with NREL FAST. Simple cases as only steady wind and free decays with constant wind showed a good agreement with computations, demonstrating that the SiL method can successfully introduce the rotor scaled thrust and the effect of the aerodynamic damping on the global dynamics. Cases with turbulent wind and irregular waves showed better agreement with the simulations when mooring line dynamics and second order effects were included in the numerical models.

Thys et al. (2018) presents Real-Time Hybrid Model (ReaTHM) tests that are performed on a 10-MW semisubmersible floating wind turbine in the Ocean Basin at SINTEF Ocean in March 2018, see Figure 84 and Figure 85 for experimental setup and control loop. For the tests in the ocean basin, the FOWT system is divided into two substructures. The physical substructure contains the Froude-scaled floating substructure, tower, and mooring system subject to physical waves and current. The wind turbine tower and rotor were modelled in a modified version of NREAL FAST and used to compute the aerodynamic loads on the tower, and the rotor loads, except for inertia and gravity, which were modelled physically. The simulation model takes the real-time floater motions as input and computes the rotor and tower loads, which were then applied on the model by use of a cable-driven parallel robot.

Different from the campaign reported in Sauder et al. (2016) and Bachynski et al. (2016), there are several improvements of the ReaTHM in the aspect of modelling capabilities. These included the testing of design load cases with varying wind direction; inclusion of loads on the turbine tower to allowing for the tests with the wind turbine in parked condition and increase the bandwidth to model the 3p frequency and the first tower bending frequency. Test results show

that the wind turbulence played an important role for the surge and pitch responses at low frequency. The surge and pitch response in the wave frequency zone is seen to be nearly unaffected by the wind. The pitch period varies depending on the wind conditions and the low frequency loads at base of tower are dominated by the gravity loads due to the pitch motions.

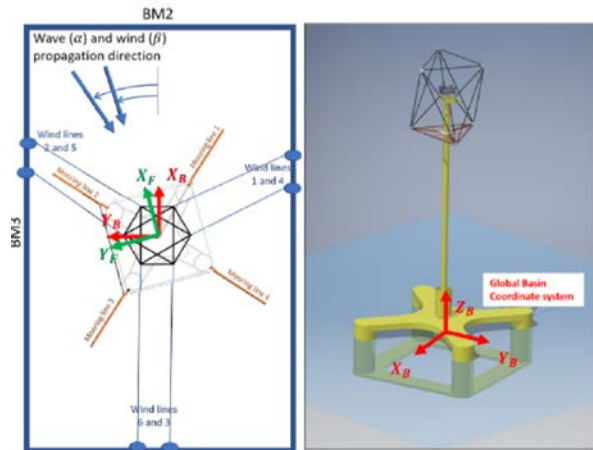


Figure 84: Experimental setup (Thys et al., 2018)

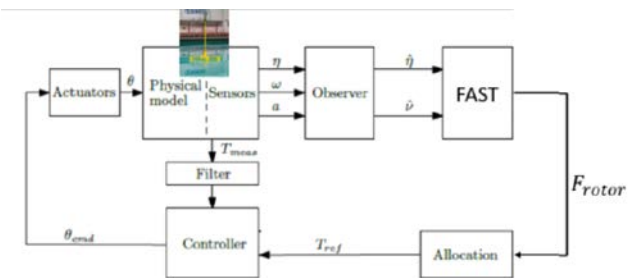


Figure 85: Control loop for REATHM tests (Thys et al., 2018)

A subsequent work led by Thys et al. (2019) for hybrid model tests performed in the EU H2020 LIFES50+ was published. LIFES50+ has two main test campaigns, where hybrid wind tunnel and ocean basin model tests with a FOWT were performed. Politecnico di Milano (POLIMI) developed a method for model tests in a wind tunnel and SINTEF Ocean developed a method for tests in an ocean basin. The setup of the hybrid model tests in the wind tunnel and ocean basin are shown in Figure 86 and Figure 87, respectively. In the wind tunnel, a physical wind turbine was connected to a 6-DOF parallel kinematic robot controlled by real-time

simulations of the floater subject to hydrodynamic loads. In the ocean basin, a physical model of the FOWT, without the rotor geometry, was placed in the basin and coupled to a force actuator controlled by the simulated aerodynamic loads.

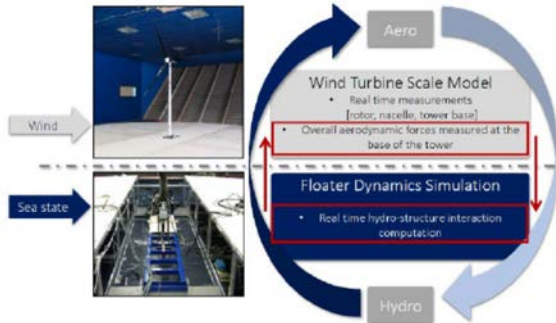


Figure 86: Setup of the hybrid model tests in the wind tunnel at POLIMI (Thys et al., 2019)

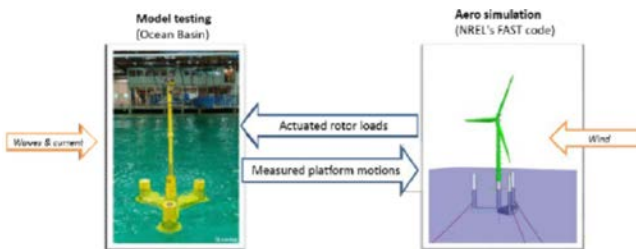


Figure 87: Setup of the hybrid model tests in the Ocean Basin at SINTEF OCEAN (Thys et al., 2019)

Comparison between wind tunnel and ocean basin results are made in terms of floater and mooring, rotor, and the characteristics of the complete system (mooring, floater, wind turbine subject to wind and waves). The wind tunnel test results indicated that the linear response to small to moderate wave excitation is accurately modelled, but calibration of the numerical model is needed for accurate modelling of the low frequency response. The comparison between wind tunnel and ocean basin tests on irregular waves and wind results show that both testing techniques were giving comparable statistical values.

In the recent work of Pires et al. (2020), the hybrid testing method developed by National Renewable Energy Center in Spain (CENER) for floating wind turbine scaled tests combining wind and waves (SiL) has been upgraded in

order to introduce not only the wind turbine rotor thrust, but also the out-of-plane rotor moments (aerodynamic and gyroscopic). To achieve this goal, the former ducted fan has been substituted by a multi-propellers actuator system. The new system has been completely developed, calibrated, and used on a test campaign carried out at MARIN’s Concept Basin. It was installed on a 1/50 scaled model of the DeepCwind 5-MW semisubmersible turbine built by MARIN within the EU MARINET2/Call No. 3 under ACTFLOW project framework. The control strategy of the floating turbine was developed by POLIMI and TU-DELFT and integrated into the SiL numerical model. The experiment has proved a good behaviour of the enhanced SiL method. It has revealed that the relative importance of gyroscopic moments is low in comparison with the aerodynamic rotor moments in the considered cases. The results also show how rotor moments are particularly important in FOWT dynamics in cases with large rotor load imbalances such as situations where one blade fails to pitch.

Matoug et al. (2020) reports the testing result for the WindQuest 10-MW turbine in comparison to the reference DTU 10-MW horizontal axis turbine (HAWT) developed for the Lifes50+ project. Figure 88 shows a schematic diagram representing the WindQuest and the DTU scale models. The Nautilus-semi-submersible floater is used with both turbines. The seakeeping of the two FOWT is studied experimentally at the Ifremer waves & wind tank, Brest, France (Figure 89 and Figure 90).

In the SiL loop, the hydrodynamics are scaled in the wave tank, the aerodynamics is simulated using an actuator. The thrust is computed and applied in real-time. The measurements from the motion capture system are streamed in real-time to account for platform motions. Thrust set points are computed with tabulated aerodynamic parameters extracted from simulations. The resulting set point is computed in real-time, thus allowing for a

feedback loop in between the aerodynamics and the hydrodynamics (plotted in Figure 91).

Test and post-processing results indicate the advantage of using a SiL for wind-driven cases. The SiL follows the FAST simulation trend by filtering the natural frequency and maximizing the power in the wave spectrum. Though the SiL configuration shows higher levels of energy around 0.5 – 0.7 Hz bandwidth when compared to OpenFAST.

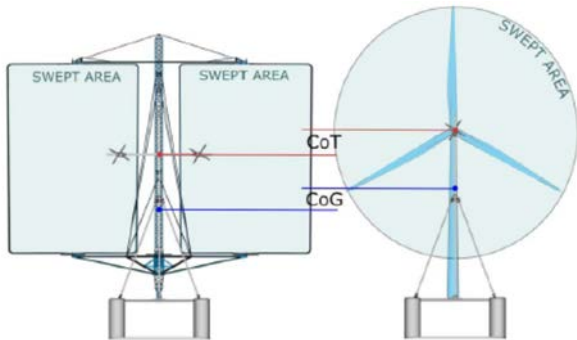


Figure 88: Comparison of the WindQuest (left) scale model with the DTU (right) (Matoug et al., 2020)



Figure 89: Scale model during wave tank tests (Matoug et al., 2020)

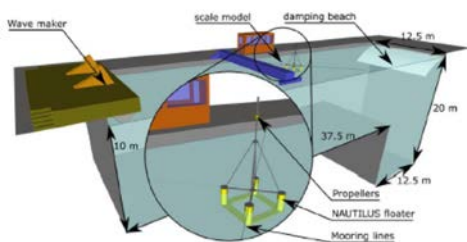


Figure 90: Representation of the Ifremer waves & wind tank with the scale model positioned for tests (Matoug et al., 2020)

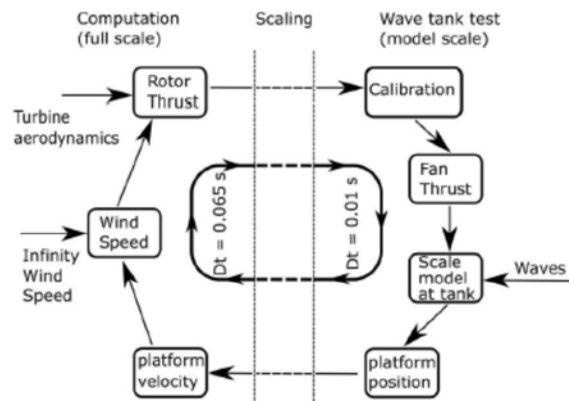


Figure 91: SiL retroaction loop: scaled part (right) and computations (left) - (Matoug et al., 2020)

7. EXPERIMENTAL BENCHMARK ON WAVE RUN-UP ON CYLINDERS

The Committee conducted benchmark studies of wave run-up heights on the fixed four-squared-cylinder system under regular and irregular waves and provided a set of benchmark results for analysing the influences of wave parameters and validating related numerical simulations. It extends the benchmark studies of wave run-ups on single and four truncated cylinders conducted in 2013.

The benchmark tests of wave run-ups on the fixed four-squared-cylinder system were carried out by State Key Laboratory of Ocean Engineering (SKLOE) at Shanghai Jiao Tong University. The benchmark test and data are summarized in the following sections.

7.1 Description of benchmark test

One configuration of fixed four-square-cylinder system is considered, as illustrated in Figure 92, in which the half column breadth $a=8$ m and the column spacing $b=34$ m, respectively. The fillet radius, the height, and the constant draft of all columns are 3 m, 40 m, and 20 m, respectively. The model scale is selected as 1:50.

The locations of wave probes and four cylinders as well as wave headings are shown in Figure 92. The coordinates of wave probes are

given in Table 1. Figure 2 shows the test setup of the model in the basin.

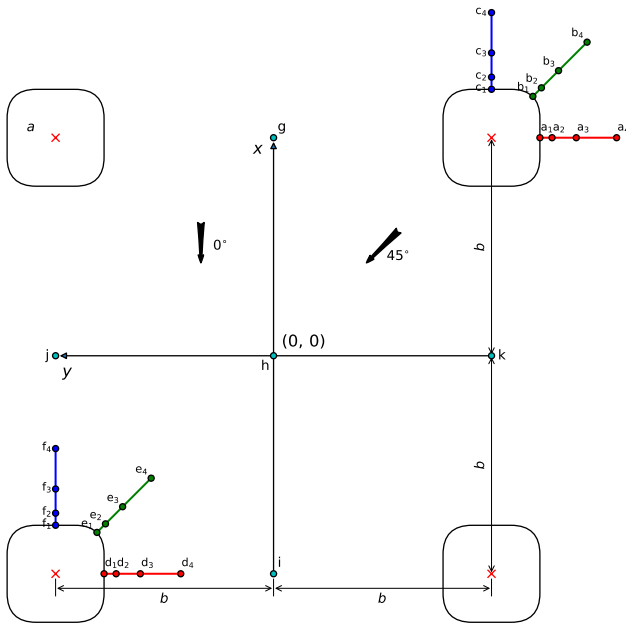


Figure 92: The fixed four-squared-cylinder system

Table 1: Locations of wave probes (in prototype)

	x (m)	y (m)
a ₁	34.0	-42.0
a ₂	34.0	-43.5
a ₃	34.0	-46.5
a ₄	34.0	-51.5
b ₁	41.12	-41.12
b ₂	42.18	-42.18
b ₃	44.30	-44.30
b ₄	47.84	-47.84
c ₁	42.0	-34.0
c ₂	43.5	-34.0
c ₃	46.5	-34.0
c ₄	51.5	-34.0
d ₁	-34.0	26.0
d ₂	-34.0	24.5
d ₃	-34.0	21.5
d ₄	-34.0	16.5
e ₁	-26.88	26.88
e ₂	-25.82	25.82
e ₃	-23.70	23.70
e ₄	-20.16	20.16
f ₁	-26.0	34.0
f ₂	-24.5	34.0
f ₃	-21.5	34.0
f ₄	-16.5	34.0
g	34.0	0

h	0	0
i	-34.0	0
j	0	34.0
k	0	-34.0

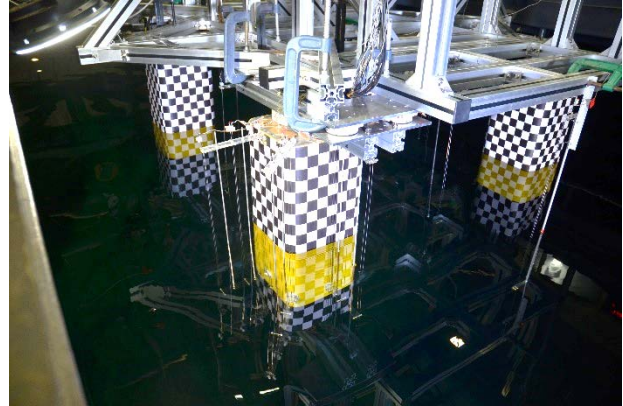


Figure 93: Test setup of the fixed four-squared-cylinder systems

Four (04) wave periods and three (03) wave steepness of regular waves were considered, as shown in Table 2. In addition, Table 3 presents parameters of the irregular waves.

Table 2: Parameters of regular waves

Full scale					
Wave No.	H/λ	kA	T (s)	ka	A (m)
1	1/30	0.105	7	0.657	1.275
2		0.105	9	0.398	2.107
3		0.105	12	0.224	3.746
4		0.105	15	0.143	5.853
5	1/16	0.196	7	0.657	2.390
6		0.196	9	0.398	3.951
7		0.196	12	0.224	7.024
8		0.196	15	0.143	10.975
9	0.07	0.220	7	0.657	2.677
10		0.220	9	0.398	4.425
11		0.220	12	0.224	7.867
12		0.220	15	0.143	12.292

Table 3: Parameters of irregular waves

Wave No.	H_s (m)	T_p (s)	γ	Realization
13	12.0	12.0	5	Seed 1
14	12.0	12.0	5	Seed 2
15	12.0	12.0	5	Seed 3

In the benchmark studies, the max values of following measured items were compared at various wave periods and wave steepness in terms of H/λ (H is wave elevation and λ is wavelength) and kA (k is wave number and A is wave amplitude):

- 1) Horizontal force, F_x, F_y
- 2) Vertical force, F_z ,
- 3) Wave elevations at 29 locations.

The sampling rate is 100 Hz. The wave calibrations were performed prior to placing the model in the basin. The effective duration of each regular wave test was approximately 1 minute in model scale, and that of each irregular wave test was no less than 3 hours in full scale after the wave profile reaches steady state.

7.2 Wave run-ups around the fixed four squared cylinders

7.2.1 Regular waves, 0° wave direction

Figure 94 and Figure 95 show the max values of wave run-ups at 6 locations ($a_1, b_1, c_1, d_1, e_1, f_1$) for fixed four-squared-cylinder system at various wave steepness ($H/L=1/30, 1/16$ and 0.07) and periods ($T=0.99$ s, 1.27 s, 1.69 s and 2.12 s) along the centre plane in terms of wave probes location (x/D). The max values are normalized by incident wave amplitude (A).

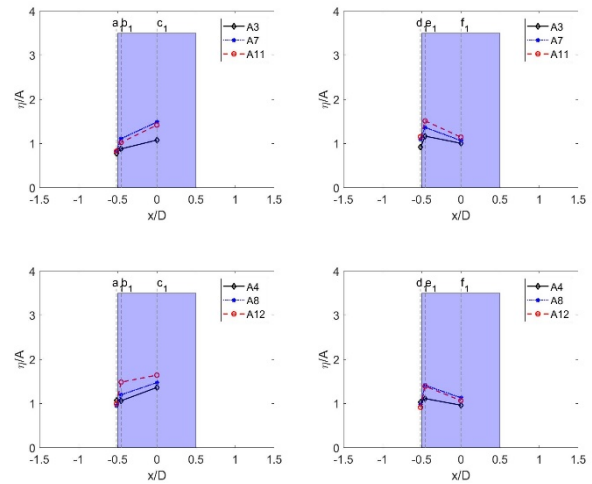
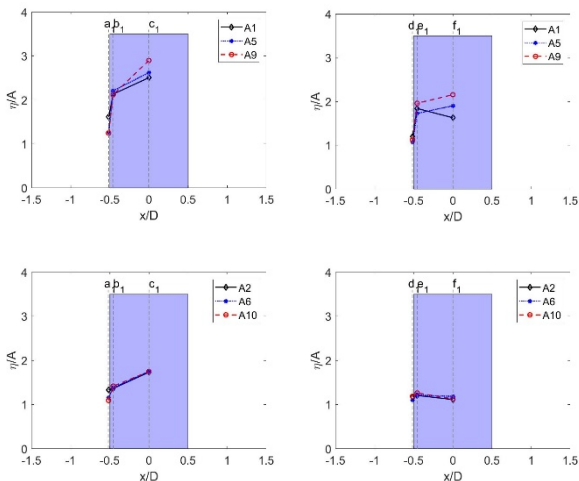


Figure 94: Max values of wave run-up heights at various wave steepness (heading 0°)

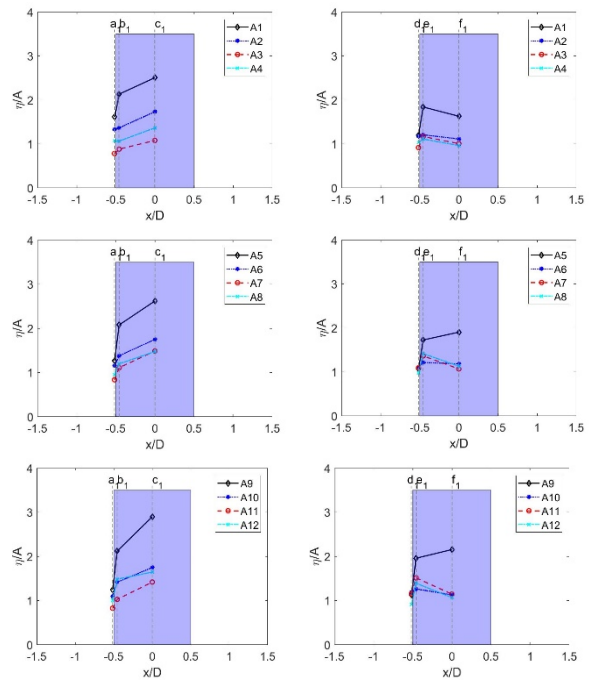


Figure 95: Max values of wave run-up heights at various wave periods (heading 0°)

7.2.2 Regular waves, 45° wave direction

Figure 96 and Figure 97 show the max values of wave run-ups at 6 locations ($a_1, b_1, c_1, d_1, e_1, f_1$) for fixed four-squared-cylinder system at various wave steepness ($H/L=1/30, 1/16$ and 0.07) and periods ($T=0.99$ s, 1.27 s, 1.69 s and 2.12 s).

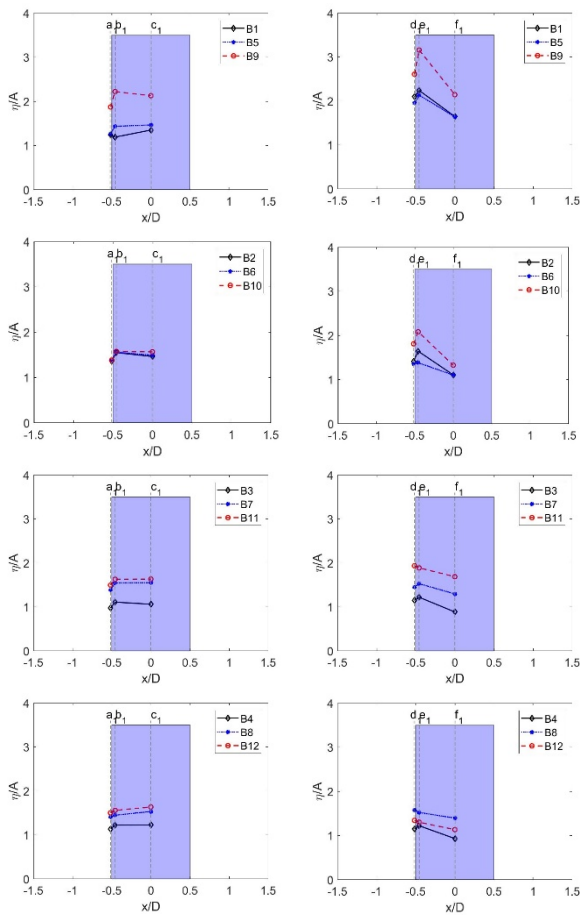


Figure 96: Max values of wave run-up heights at various wave steepness (heading 45°)

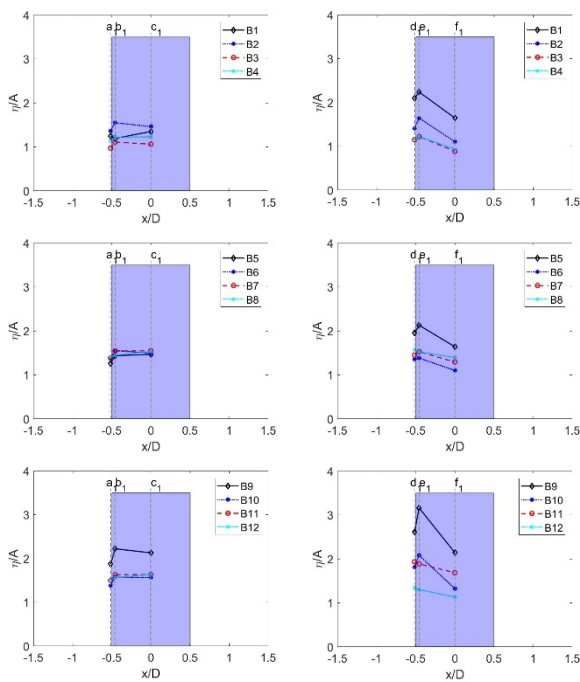


Figure 97: Max values of wave run-up heights at various wave periods (heading 45°)

Figure 98 shows the max values of wave run-ups at 24 locations (a₁-a₄, b₁-b₄, c₁-c₄, d₁-d₄, e₁-e₄, f₁-f₄) for fixed four-squared-cylinder system of each case with 0° wave direction. In the figure, D₁ means the distance from wave probe to the column surface, and D means the half column breadth. Figure 99 shows the max values for each case with 45° wave direction.

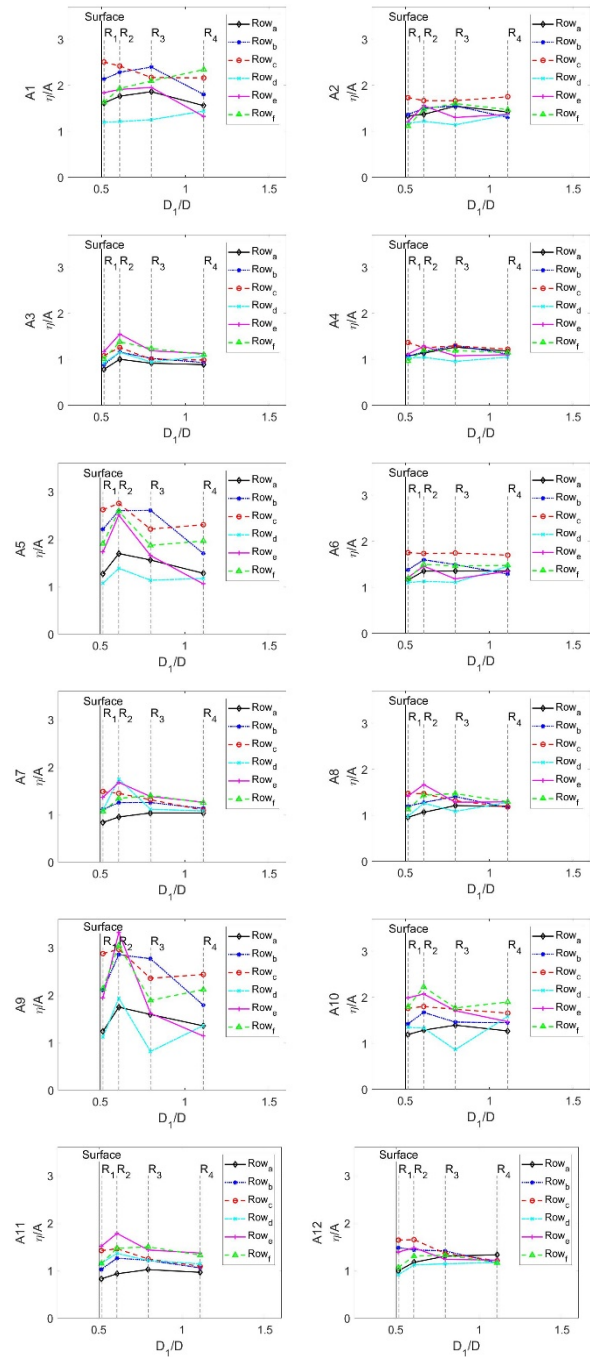


Figure 98: Max values of wave run-ups around the front and rear columns (heading 0°)

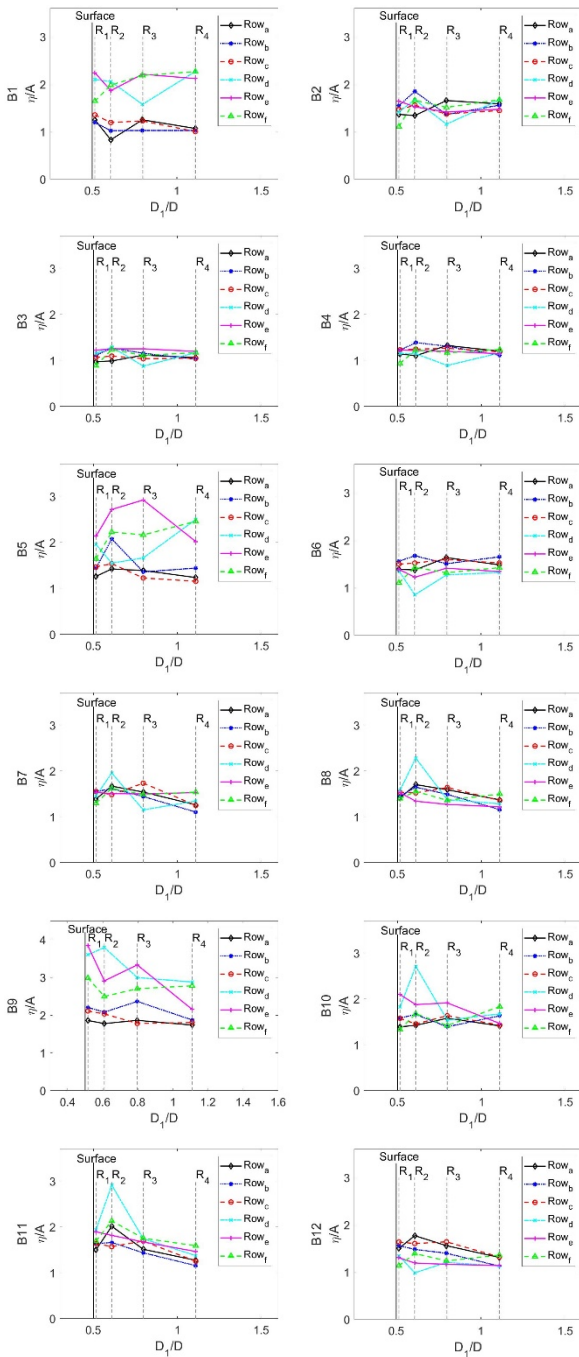


Figure 99: Max values of wave run-ups around the front and rear columns (heading 45°)

7.2.3 Irregular waves

Figure 100 and Figure 101 show the max values of wave run-ups at 24 locations (a1-a4, b1-b4, c1-c4, d1-d4, e1-e4, f1-f4) for fixed four-squared-cylinder system of each case with 0° and 45° wave directions, respectively.

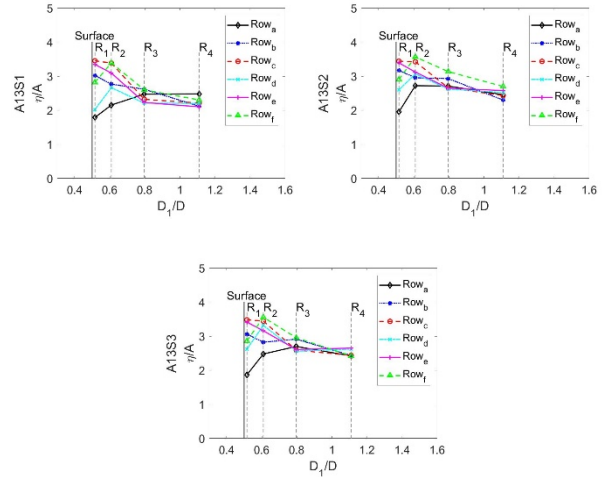


Figure 100: Max values of wave run-ups around the front and rear columns in irregular waves (heading 0°)

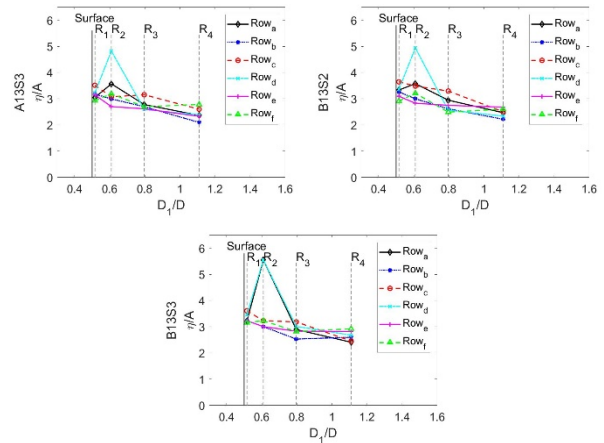
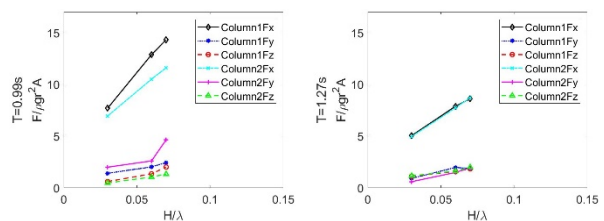


Figure 101: Max values of wave run-ups around the front and rear columns in irregular waves (heading 45°)

7.3 Effects of wave period and steepness on wave forces

The max and mean values of wave forces of the front and rear columns at various wave steepness and periods were shown in Figures Figure 102-Figure 105 (0° wave direction) and Figure 106-Figure 109 (45° wave direction).



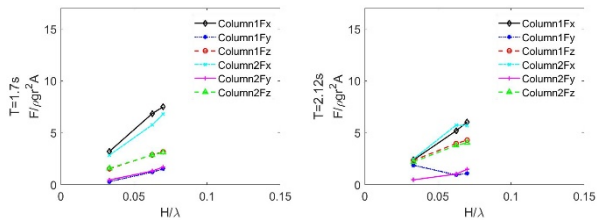


Figure 102: Max values of wave forces on the front and rear columns at various wave steepness (heading 0°)

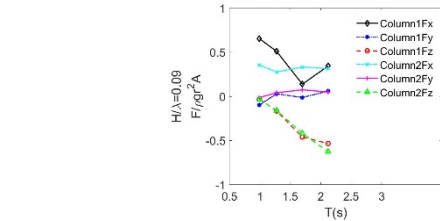


Figure 105: Mean values of wave forces on the front and rear columns at various wave periods (heading 0°)

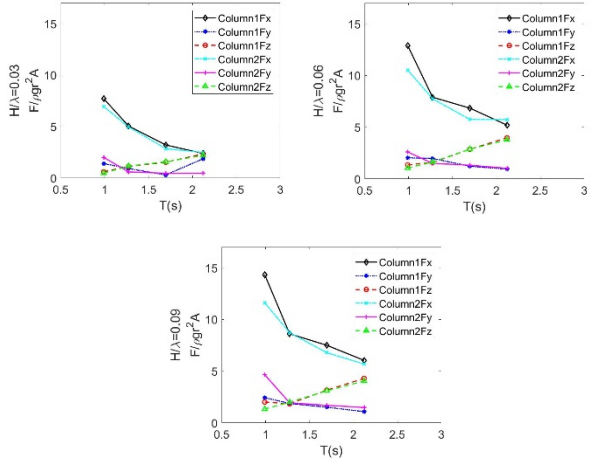


Figure 103: Max values of wave forces on the front and rear columns at various wave periods (heading 0°)

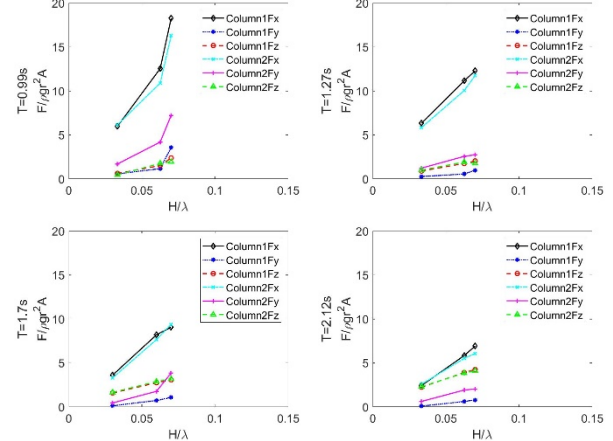


Figure 106: Max values of wave forces on the front and rear columns at various wave steepness (heading 45°)

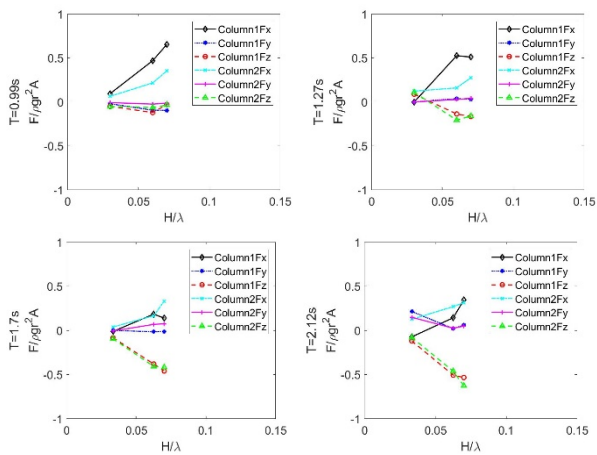


Figure 104: Mean values of wave forces on the front and rear columns at various wave steepness (heading 0°)

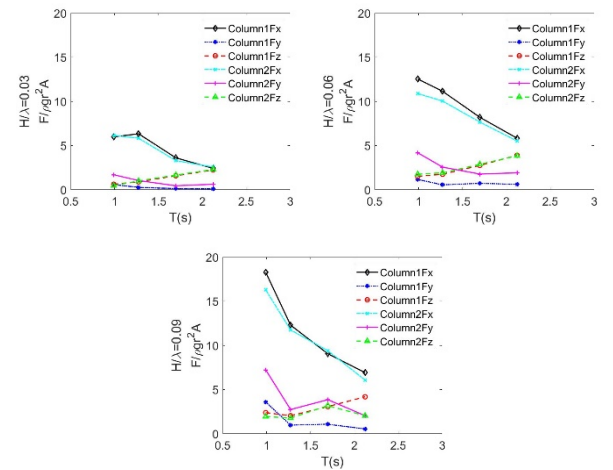
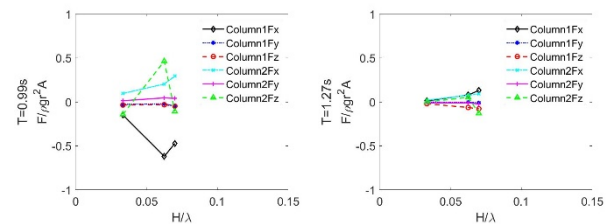
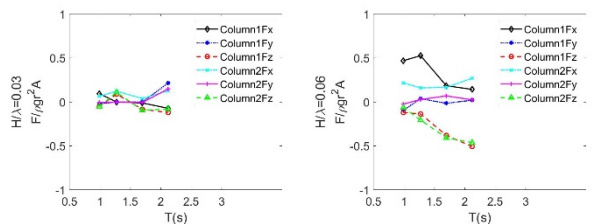


Figure 107: Max values of wave forces on the front and rear columns at various wave periods (heading 45°)



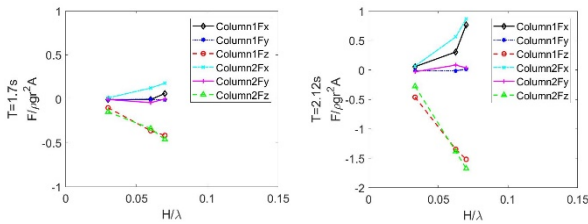


Figure 108: Mean values of wave forces on the front and rear columns at various wave steepness (heading 45°)

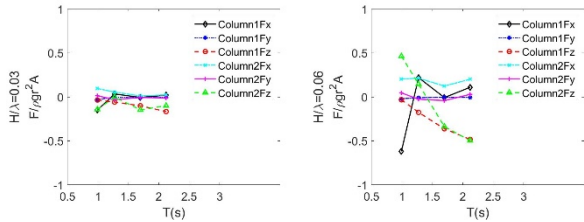


Figure 109: Mean values of wave forces on the front and rear columns at various wave periods (heading 45°)

7.4 Wave forces in irregular waves

Figure 110-Figure 113 show the maxima and mean values of wave forces on the front and rear columns in irregular waves with 0° and 45° wave directions for three random seeds.

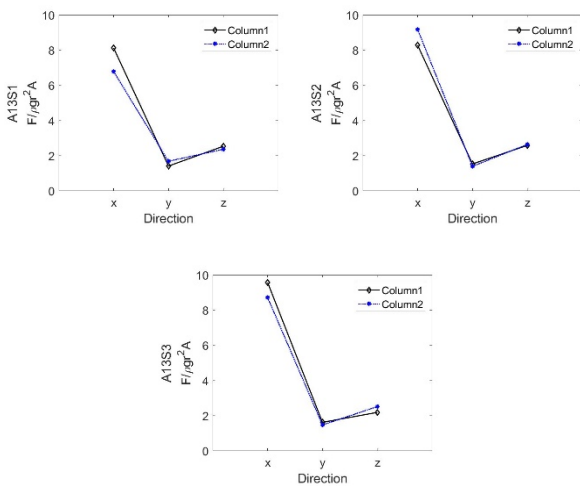


Figure 110: Max values of wave forces on the front and rear columns in irregular waves (heading 0°)

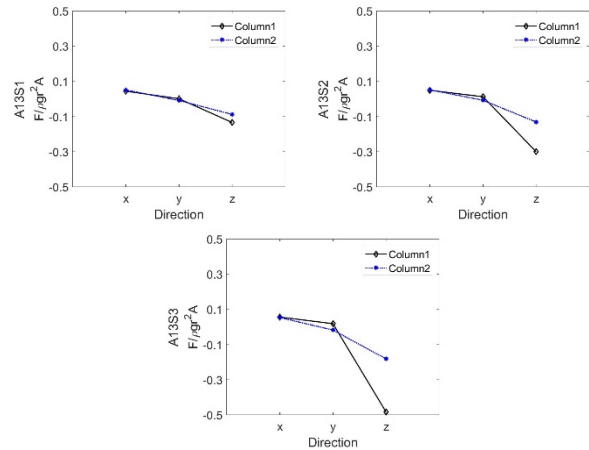


Figure 111: Mean values of wave forces on the front and rear columns in irregular waves (heading 0°)

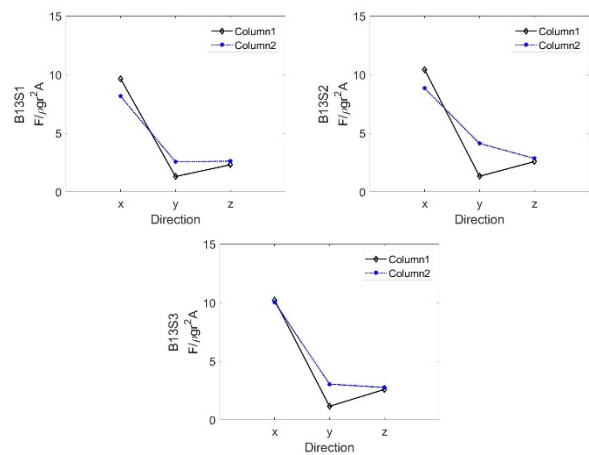


Figure 112: Max values of wave forces on the front and rear columns in irregular waves (heading 45°)

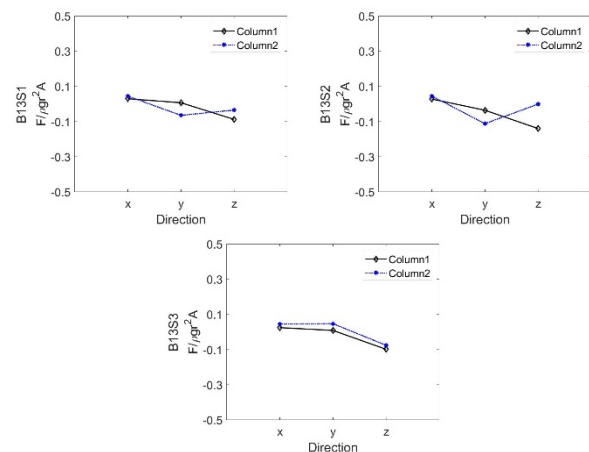


Figure 113: Mean values of wave forces on the front and rear columns in irregular waves (heading 45°)

8. CFD BENCHMARK ON TWO-BODY INTERACTIONS

8.1 Objective

The primary objective of this CFD program is to carry out benchmark studies on multiple-body interactions in regular waves, model test of two identical floaters in close proximity. The motions of two bodies, wave elevations in the gap and drift forces will be calculated and compared with the experimental data which were measured at the tests performed as a part of the test campaign of 27th and 28th ITTC Ocean Engineering Committee (OEC). The organizations participated in the benchmark studies can use the various CFD software and methodologies such as a turbulence modelling, free-surface tracking method, wave absorption, solvers and so on in model scale to produce the best solution for the two-body interactions.

8.2 System Modelling

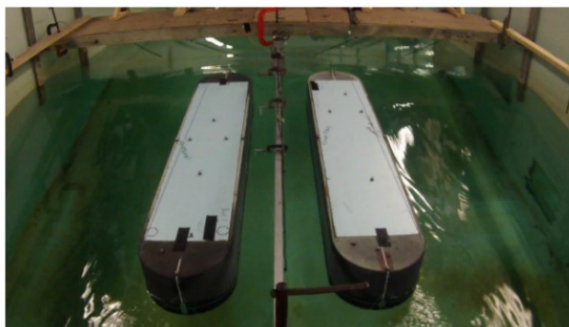
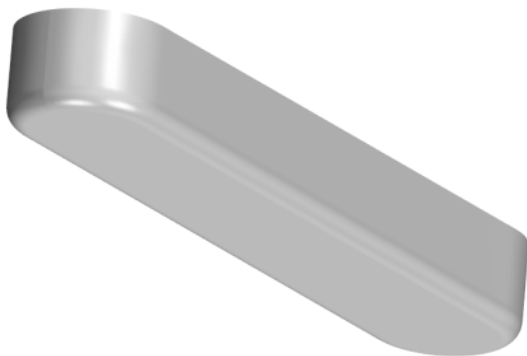


Figure 114: Ship modelling

8.2.1 Target model

- Two identical box-like models, as shown in Figure 114, are considered. Their main dimensions are given in Table 1.
- The model scale is 1:60.

Table 4 Main dimensions of ship models

	Ship 1		Ship 2	
	Full scale	Model	Full scale	Model
<i>Length(m)</i>	120.0	1.997	120.0	1.998
<i>Breadth(m)</i>	24.0	0.397	24.0	0.397
<i>Depth (m)</i>	18.0	0.301	18.0	0.301
<i>Draft (m)</i>	6.0	0.103	6.0	0.104
$\Delta (m)$	1.64 $\times 10^7$	76.6	1.64 $\times 10^7$	76.6
<i>KG (m)</i>	7.68	0.128	7.56	0.126
<i>R_{xx} (m)</i>	7.02	0.117	7.08	0.118
<i>R_{yy} (m)</i>	28.02	0.467	28.92	0.482
<i>GM_T (m)</i>	3.24	0.054	3.18	0.053

8.2.2 Test basin

Three different basins: the towing tank of the Memorial University (MUN) - Canada, the wave basin of Ecole Centrale de Nantes (ECN) - France and the ocean basin of LabOceano – Brazil were considered to investigate the wall effect. The principal dimensions of basins are summarized in Table 2.

Table 5 Principal dimensions of test basins

	<i>Towing tank (MUN)</i>	<i>Wave basin (ECN)</i>	<i>Ocean basin (LabOceano)</i>
<i>Length (m)</i>	58.0	50.0	40.0
<i>Width (m)</i>	4.5	30.0	30.0
<i>Depth (m)</i>	1.8	5.0	15.0

8.2.3 Mooring system

- The two models are positioned near the middle of the test basin and each model is restraint by four soft mooring lines, as shown in Figure 115 and Figure 116.
- The stiffness of each spring is 3.4 N/m, which was determined to meet the equation below.

$$\sqrt{\frac{K'}{M + M'}} \leq \frac{\omega_{min}}{10}$$

where,

K = stiffness of each spring;

K' = effective stiffness ($=4K$);

M = mass of the model;

M' = added mass of the model;

ω_{min} = minimum value between the lowest wave frequency and model's natural frequency.

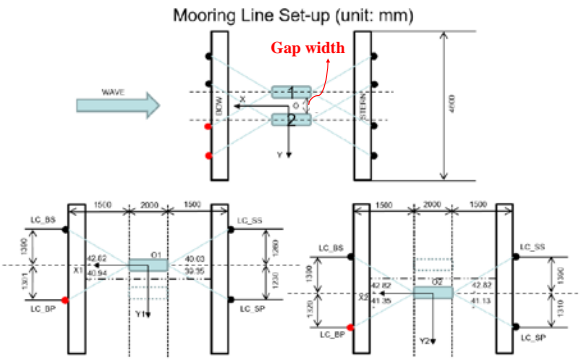


Figure 115: Set-up of the mooring system (at towing tank)

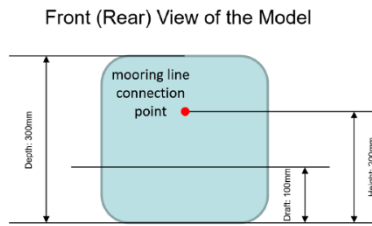


Figure 116: Mooring line connection point on a model

8.3 Test Case

8.3.1 Gap width

- The test cases are presented in Table 3.
- There is a little difference in 'Case 3' condition between MUN and ECN due to the installation constrains.

Table 6 Gap Width

Test case	Test basin	Full scale (m)	Model (m)
Case1	MUN	24.0	0.40
Case2	MUN	27.0	0.45
Case3	MUN	33.0	0.55
	ECN	31.2	0.52

8.3.2 Incident wave condition

- The test cases are presented in Table 4.
- The eighteen (18) wave period is considered with three different gap widths.
- The wave steepness is kept as 1/30.
- The tests are carried out in head seas (wave heading: 180°) only.

Table 7 Incident wave conditions

No.	ω (rad/s)	λ/L	No.	ω (rad/s)	λ/L
Case*-1	3.90	2.03	Case*-10	6.09	0.83
Case*-2	4.27	1.69	Case*-11	6.22	0.80
Case*-3	4.65	1.43	Case*-12	6.41	0.75
Case*-4	4.96	1.25	Case*-13	6.53	0.72
Case*-5	5.09	1.19	Case*-14	6.66	0.69
Case*-6	5.34	1.08	Case*-15	6.79	0.67
Case*-7	5.53	1.01	Case*-16	6.91	0.65
Case*-8	5.72	0.94	Case*-17	7.04	0.62
Case*-9	5.91	0.88	Case*-18	7.16	0.60

Case*: Test cases for gap width (1~3)

8.4 Calculation Item

Ship motions, wave elevation in the gap and mean drift forces are compared with the experimental results.

- 6-DOF (Surge, Sway, Heave, Roll, Pitch, Yaw) motions
- Wave elevation in the gap (WP 4,5,6)
- Mean drift forces (longitudinal and transverse)

Three wave probes (WP-4, 5 and 6) are positioned along the centre line of the gap, as shown in Figure 117. WP-5 is in line with the mid-ship sections of the two models. The spacing between these three wave probes is 0.5 m.

All items are calculated from average responses of at least ten (10) periods after truncating transient range and then nondimensionalized as shown below.

Translational motions: $X'_j = \frac{X_j}{\xi_0}$ ($j = 1,2,3$)

Rotational motions: $X'_j = \frac{X_j}{k\xi_0}$ ($j = 4,5,6$)

Wave elevation: $\xi' = \frac{\xi}{\xi_0}$

longitudinal drift force: $F'_x = \frac{F_x}{(1/4)\rho g \xi_0^2 L}$

Transverse drift force: $F'_y = \frac{F_y}{(1/4)\rho g \xi_0^2 L}$

Wave frequency: $\omega' = \omega \left(\frac{L}{g}\right)^{0.5}$

where,

X_j = 6-DOF body motion (j=1~6);

ξ_0 = amplitude of incident wave;

ξ_i = wave elevation at WP-i (i=4~6);

F_x = force in x-direction on model;

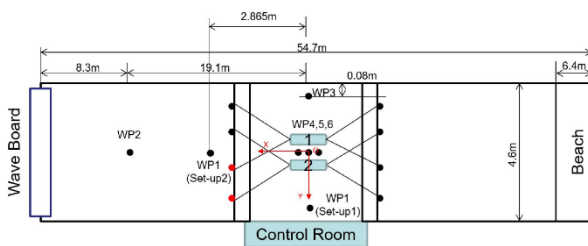
F_y = force in y-direction on model;

k = wave number;

L = model length;

ρ = fresh water density;

g = gravitational acceleration.



	X (from wave board)	Y
WP-4 (m)	26.9	0.0
WP-5 (m)	27.4	0.0
WP-6 (m)	27.9	0.0

Figure 117: Locations of wave probes

8.5 CFD methodologies

General information of CFD methodology such as grid system, numerical schemes,

turbulence modelling and boundary conditions, should be specified in appendix.

8.6 Participated Research

Several facilities under KTTC (Korea Towing Tank Conference) have performed the cooperated study with their own CFD methodologies. Five (05) facilities below are carrying out the CFD benchmark study:

- SHI (Samsung Heavy Industries);
- KRISO (Korea Research Institute of Ships and Offshore Engineering);
- PNU (Pusan National University): 2 labs;
- KSOE (Korea Shipbuilding and Offshore Engineering);
- KMOU (Korea Maritime and Ocean University);

8.7 Potential Analysis

Before starting full CFD analysis, the potential computation was performed and compared to the experimental results.

SHI used the commercial tool HydroStar (BV) by using the 3D panel model denoted in Figure 118. The damping of 2% is applied at the gap between two bodies to prevent the spurious spiky response which is normally happened in potential calculation for two body located in proximity. The control surface is also modelled to obtain the mean drift force by middle field method. Total number of mesh is 3640. The results will be shown together with the CFD results in next section.

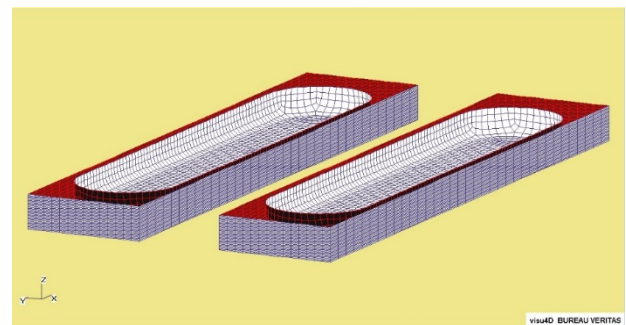


Figure 118: 3D Panel Model for Potential Calculation (HydroStar)

KRISO used the in-house code, AdFLOW, for the potential computation. The results will be shown in next section.

8.8 CFD Method Summary

The methodology used for CFD analysis is separately summarized in the appendix. It covers below:

- General Numerical Method (Software, Discretization scheme, Density definition, Pressure and velocity field, Treatment for unsteady characteristics)
- Grid System (Software, Coordinate, Dimension and type, Handling method for body motion, Number of grids, Non-dimensional length of first grid size)
- Numerical Scheme (Convection term, Order of accuracy of convection term, Temporal term, Order of accuracy of temporal term, Conserved quantities, Linearization scheme, Iterative scheme, Pre-conditioning, or acceleration techniques)
- Boundary Condition (Boundary type, Wave generation, Wave absorption)
- Turbulence Modelling (Viscous Regime, Type of turbulence model, Transition treatment, Wall treatment)
- Free-surface treatment (Treat method)
- Computation (Computer performance in simulation, Computer system, Parallel computing, Computation time / finest grid)
- Etc.

For example, the CFD method used in SHI is summarized below.

- Software: STAR-CCM+
- Numerical modelling

Item	scheme
Governing equation	RANS (Reynolds-averaged Navier-Stokes equations)
Multiphase model	Implicit VOF (Volume of Fluid method)
Temporal discretization	2nd-order implicit unsteady

Turbulence model	k-Omega SST with all y+ wall treatment
Body-Environment coupling	Linear spring
Body motion	Overset mesh w/ 3-DOFs (surge, heave, pitch)

- Boundary conditions (Figure 119)

Type	Surface, Region
Velocity inlet	Inlet/Outlet/Side (far from the model)/Bottom boundary
Symmetry	Side boundary
Pressure outlet	Top boundary
Forcing zone (Relaxation zone)	Forward, Backward, Side region

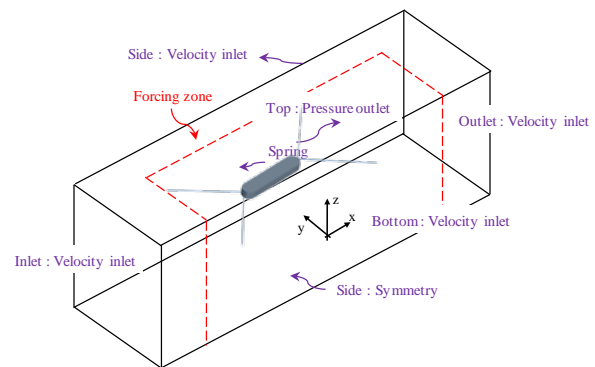


Figure 119: Boundary conditions for the numerical domain

- Computational Domain (Figure 120)

- Total volume mesh: 1.5~2.5 million
- Mesh refinement (x-dir: 70 or more per wavelength, z-dir: 15 or more per wave height)

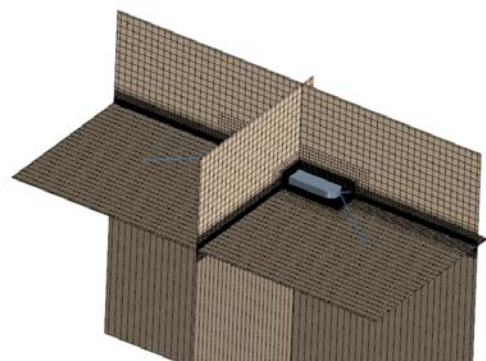


Figure 120: Mesh of the computational domain

8.9 CFD Results

8.9.1 SHI

The numerical wave test was performed without model in advance to the actual simulation. The result is depicted in Figure 121 with a wave period versus wave amplitude curve. The solid line means the theoretical target value.

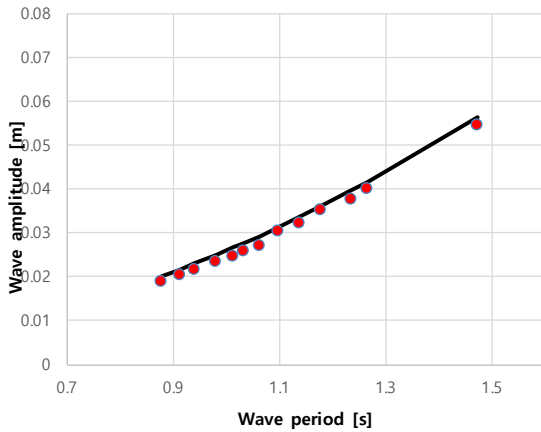


Figure 121: Numerical Wave Calibration Result by SHI

For simplicity, only the 3 DoF (Surge, heave, pitch) motion is considered in the simulation, the comparison of body motion for gap distance of 0.40 m is shown in Figure 122.

The potential and CFD calculation compare well with each other. The model test results show little bit larger value in low frequency range, but the accuracy of computation can be said quite good enough to simulate the model test. There is no effect from the viscosity on the motion at the gap distance of 0.4 m.

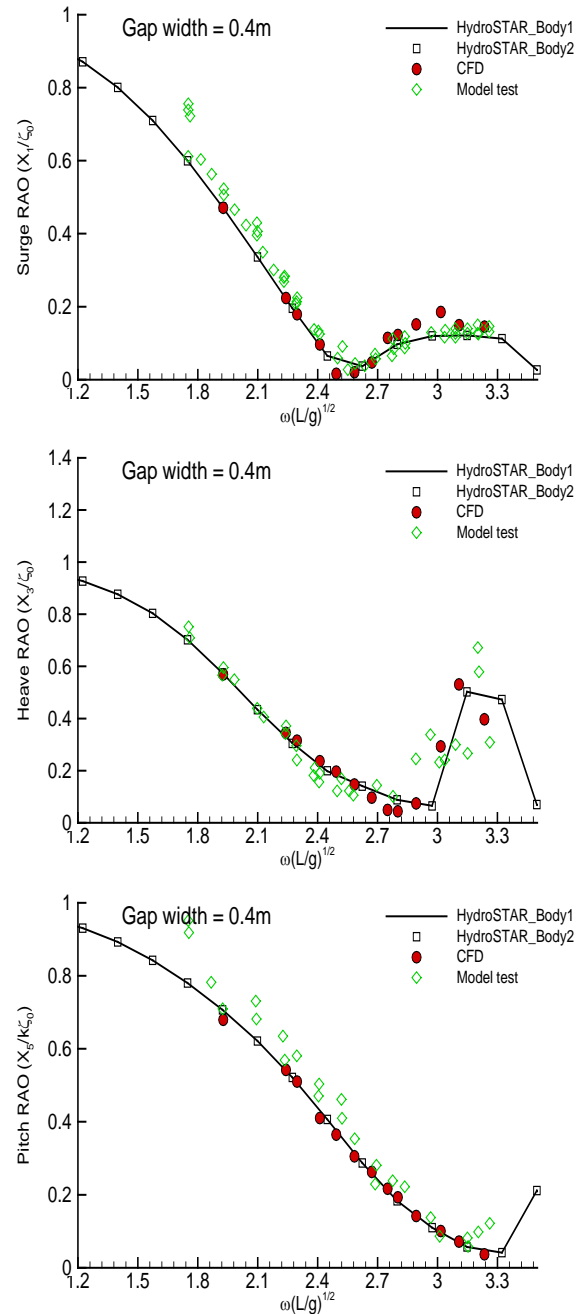


Figure 122: Motion Comparison of SHI (Gap=0.40 m)

The results of motion at the gap distance of 0.45 m are depicted in Figure 123.

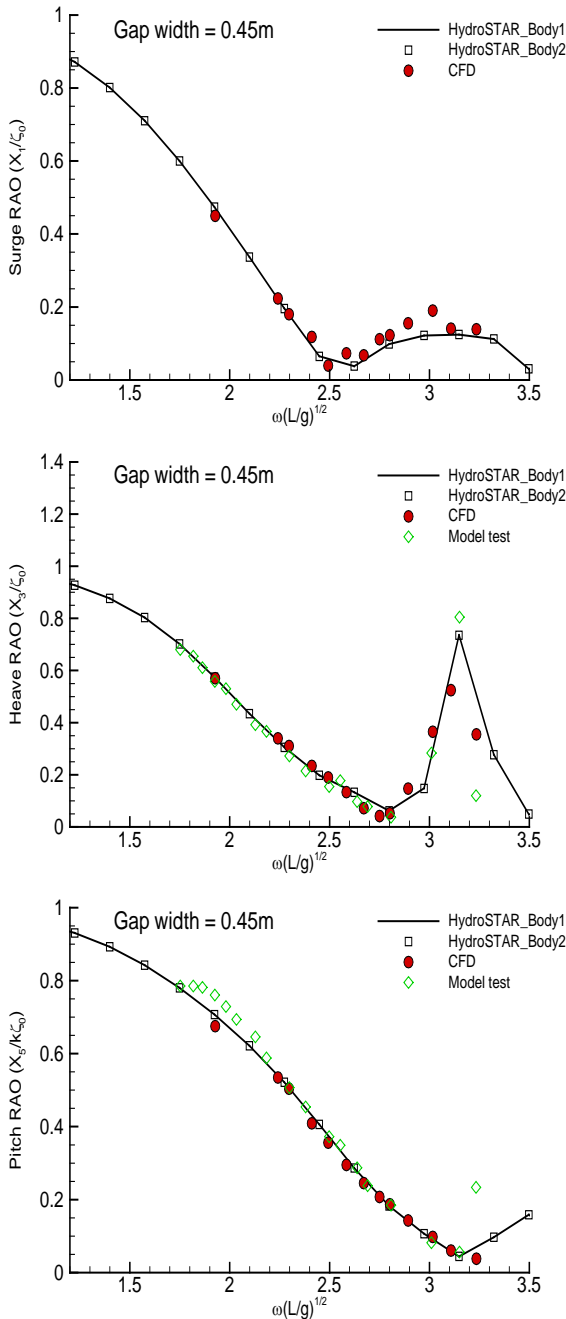


Figure 123: Motion Comparison of SHI (Gap=0.45 m)

The results among the potential, CFD calculation and the model test shows good correspondence. The 3 DoF motion calculation in CFD is comparable with that of 6 DoF in potential calculation and model test. It means that there is little effect from the gap between the bodies on the body motion under head sea condition at the gap distance of 0.45 m.

The motion comparison for the gap of 0.55 m is shown in Figure 9.

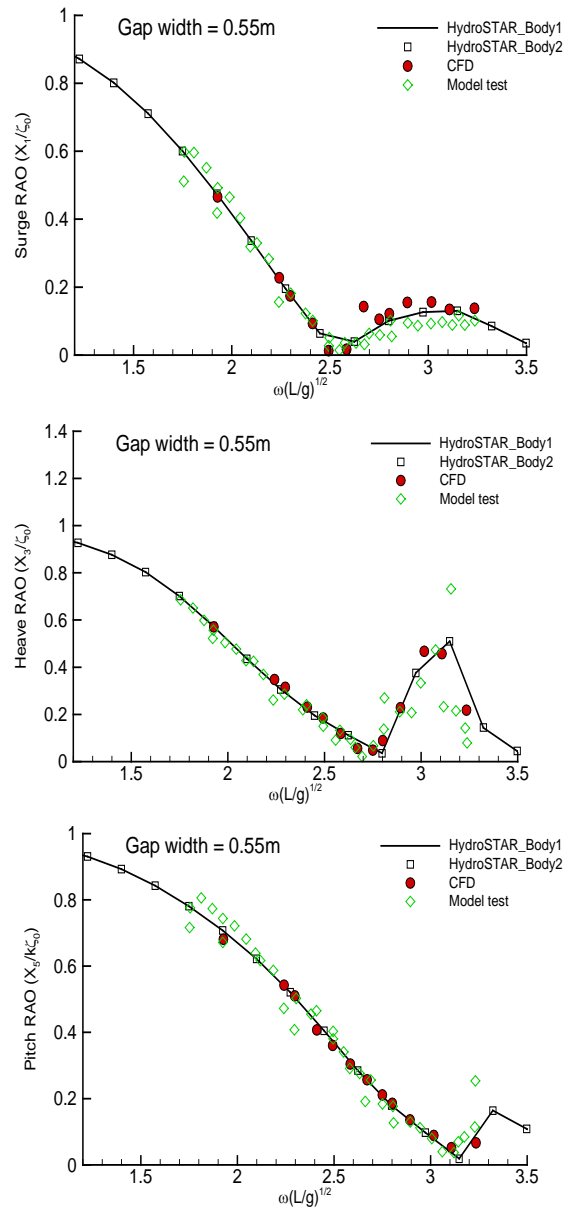


Figure 124: Motion Comparison of SHI (Gap=0.55 m)

The mean drift force is compared and depicted in Figure 10 for the gap of 0.40 m. The CFD (long) means longer the simulation duration (number of cyclic responses, i.e., short: 4~5 cycle, long: 15~20). For surge direction, the potential results correspond well with CFD calculation, but both shows little deviation in high frequency region. For sway direction, the CFD (long) results show good correspondence with the model test. The potential calculation shows the difference in very high frequency range. It is hard to quantify the viscous effect on the drift force, but the viscosity can make

difference in the drift force on the models moored in side by side.

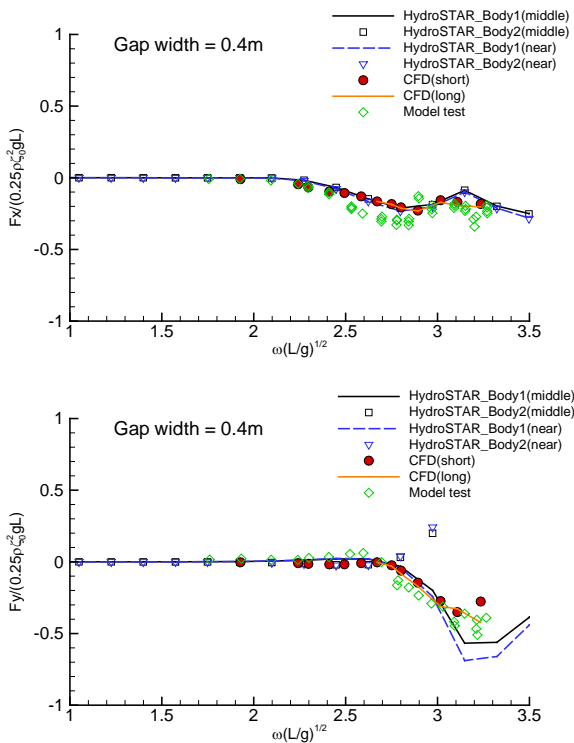


Figure 125: Mean Drift Force Comparison of SHI (Gap=0.40 m)

The mean drift force for the gap of 0.45 m is denoted in Figure 126. The potential results deviate more at the very high frequency region for the sway drift force.

The mean drift force for the gap of 0.55 m is also shown in Figure 127.

The wave elevation at the gap 0.40 m is compared in Figure 128. There is little deviation between CFD and model test, the trend of CFD results is closer to the model test than that of potential calculation. The potential calculation shows some deviation from the model test at a wide range of frequencies, and it means that viscosity affects the gap elevation.

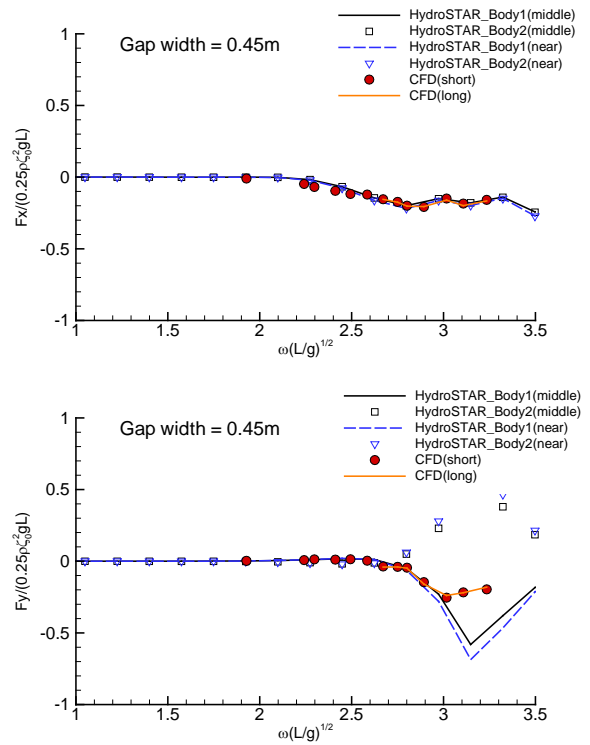


Figure 126: Mean Drift Force Comparison of SHI (Gap=0.45 m)

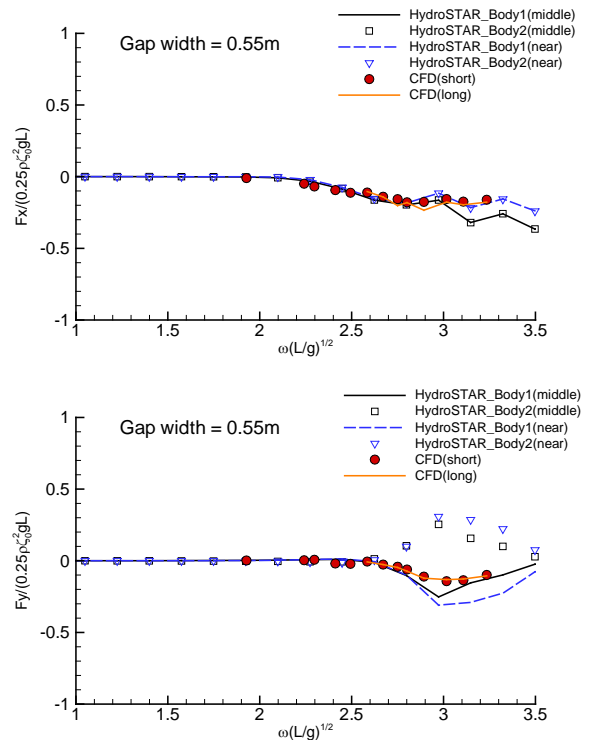


Figure 127: Mean Drift Force Comparison of SHI (Gap=0.55 m)

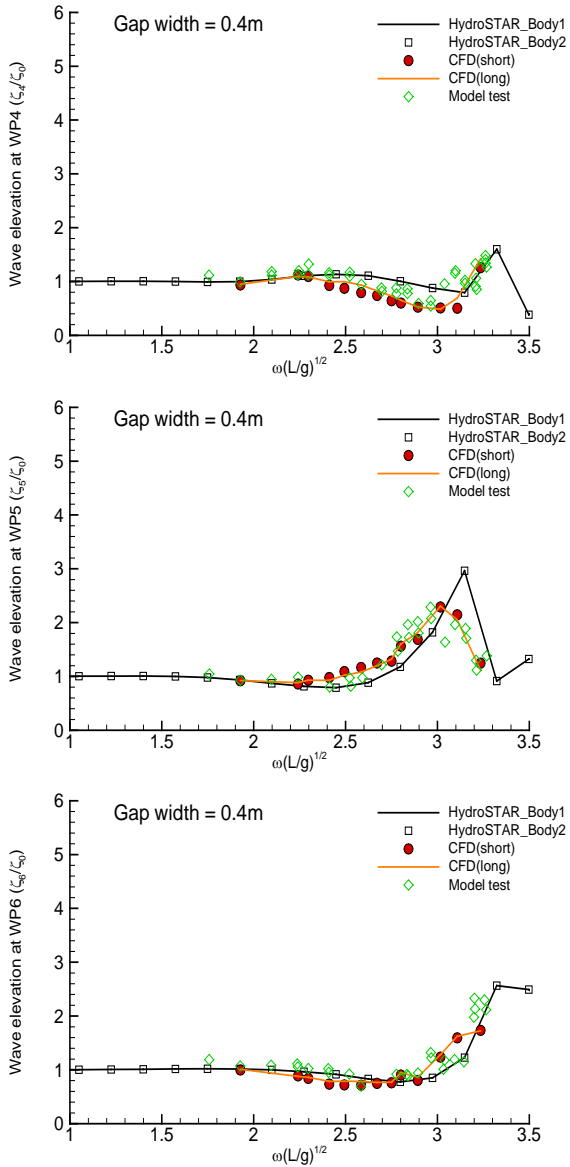


Figure 128: Gap Wave Elevation Comparison of SHI (Gap=0.40 m)

The comparison of gap wave elevation for the gap distance of 0.45 m is denoted in Figure 129. It shows the same trend compared to the case for the gap of 0.40 m. The CFD calculation shows different values compared to the potential calculation.

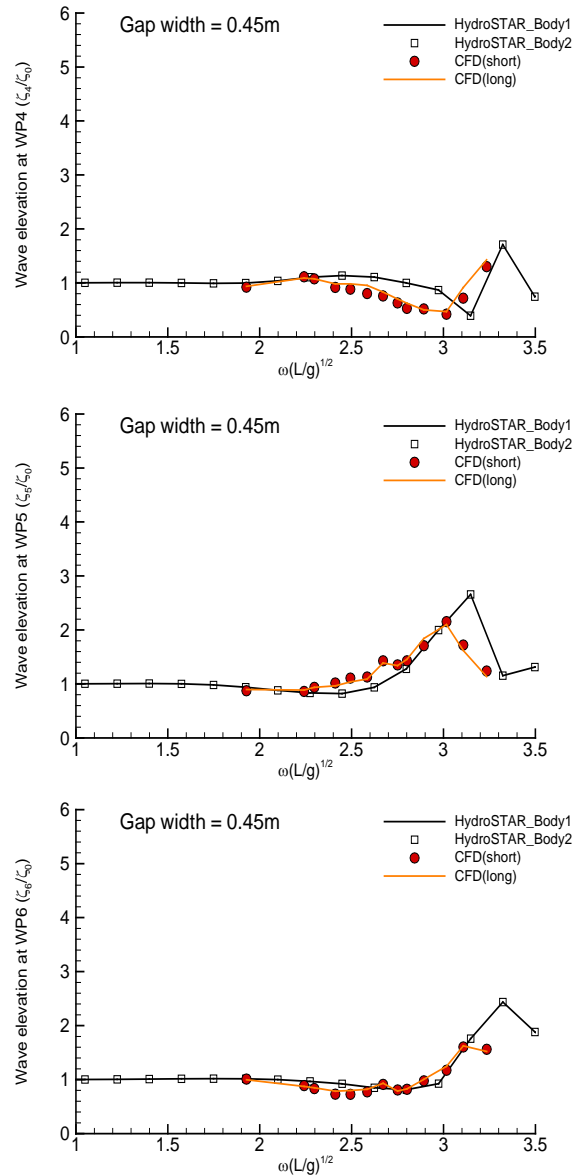


Figure 129: Gap Wave Elevation Comparison of SHI (Gap=0.45 m)

The gap wave elevation for the gap of 0.55 m is shown in Figure 130. The difference among the CFD, potential calculation and model test becomes smaller. It can be said that the viscous effect on the gap wave elevation is now negligible when the gap distance between the bodies is to be large enough.

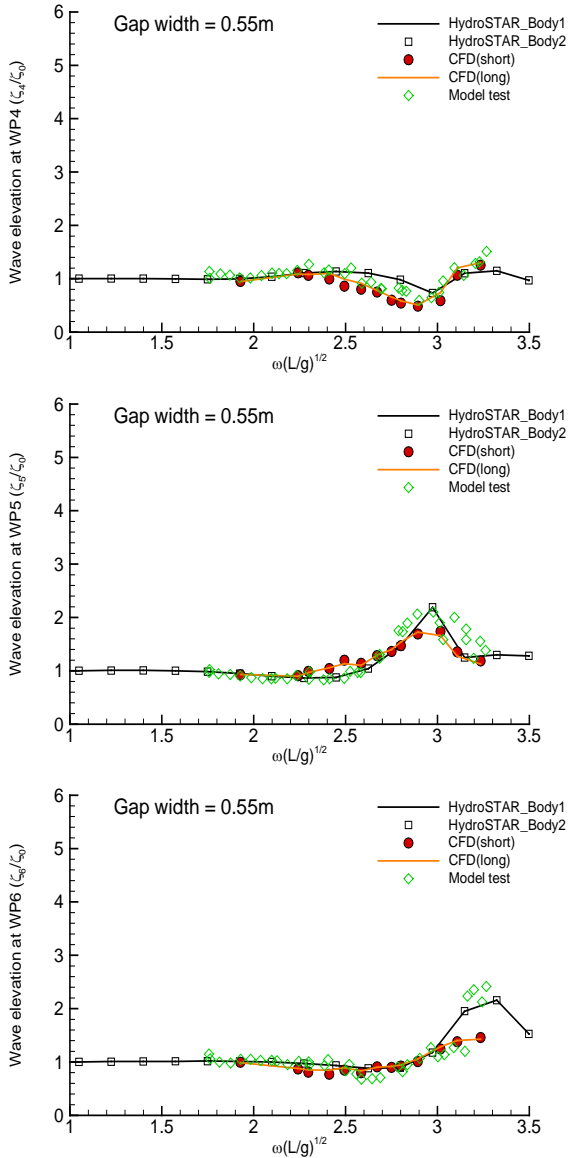


Figure 130: Gap Wave Elevation Comparison of SHI (Gap=0.55 m)

The raw time series of CFD results will be summarized and tabulated in a separated data sheet.

8.9.2 KRISO

The same calculation was performed by KRISO. In the analysis of KRISO, the 6 DoF motion is considered both the potential and CFD (Figure 131). KRISO used the StarCCM+ for CFD analysis and the detail method is summarized in the appendix. The calculation (wave frequency) points for CFD analysis are not many for now and will be updated in the future.

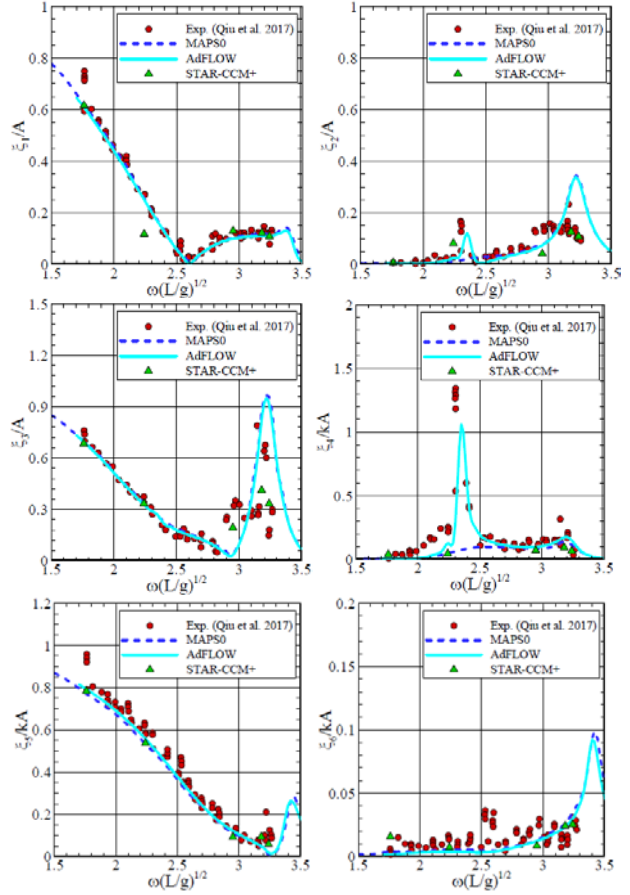


Figure 131: Motion Comparison of KRISO (Gap=0.40 m)

The potential calculation shows good correspondence with the model test in the motion. The sway and roll motion induced by two body interaction in head sea condition is well captured. The results of MAPS0 are also the potential calculation which was performed at the time of model test.

The mean drift force is compared and denoted in Figure 132. The potential calculation by AdFLOW shows the difference compared to the model test. There are five calculation points for CFD analysis. The sway drift force of CFD corresponds well with the model test. For the further discussion, more calculation will be needed in CFD analysis.

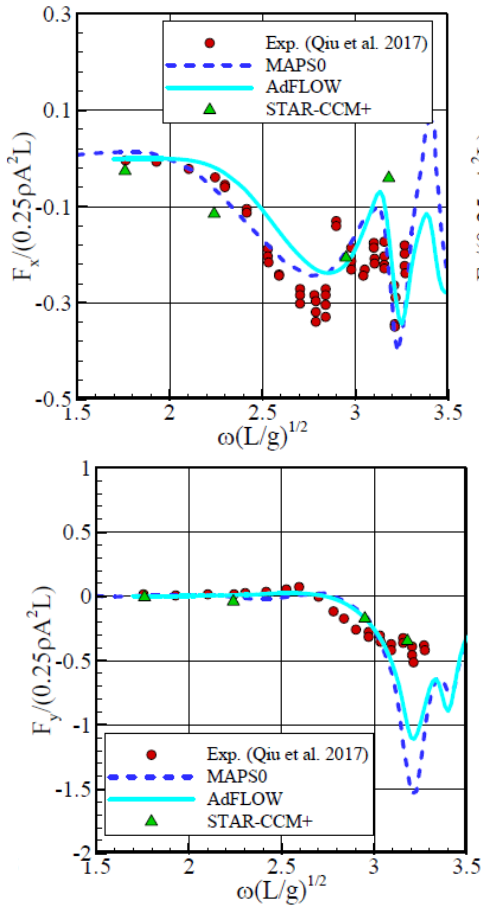


Figure 132: Mean Drift Force Comparison of KRISO (Gap=0.40 m)

For the gap wave elevation, the results are depicted in Figure 133. The CFD results at low frequency region show good correspondence with the model test, but those at high frequency region deviate from the model test at some probe location. More calculation points are needed for further discussion.

8.9.3 PNU

The actual simulation for this benchmark study is not started yet. Some verification works are now performing for the numerical modelling, wave generation and system identification.

In the CFD calculation, the same tool of StarCCM+ is used. The detail method is also summarized in the appendix. The grid system and boundary condition were checked and the so called the numerical wave tank is established for this benchmark test.

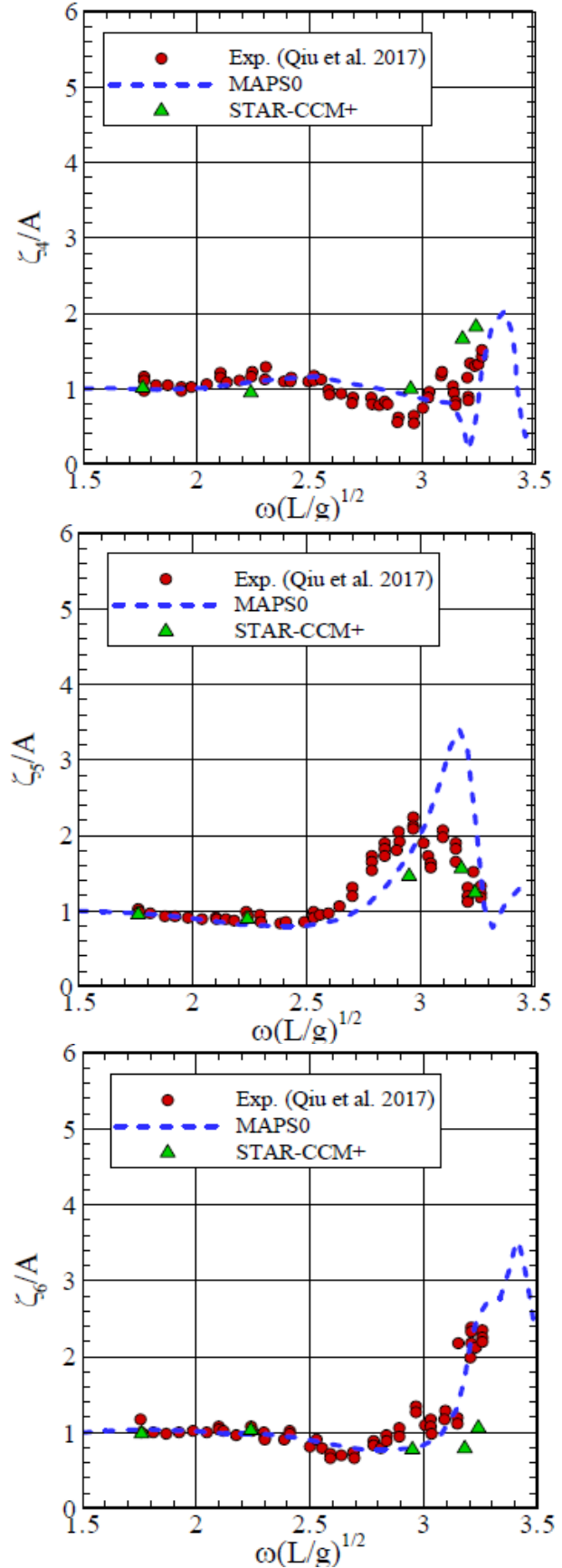


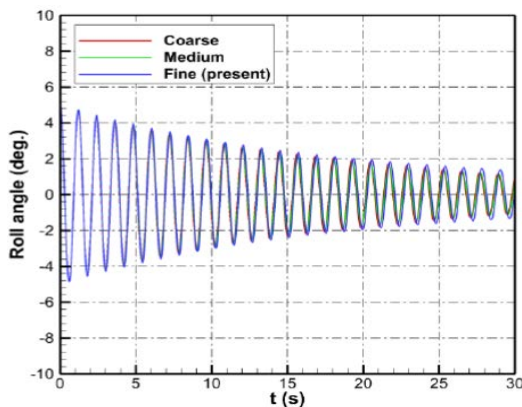
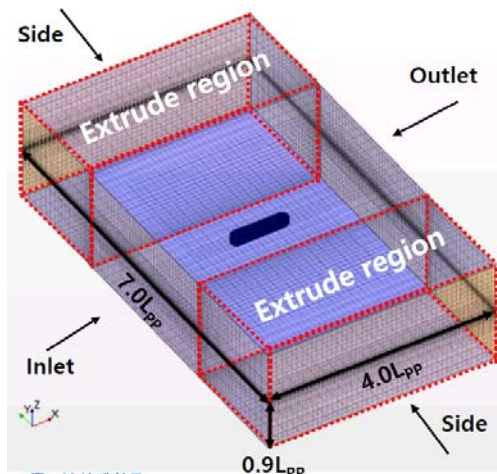
Figure 133: Gap wave elevation comparison of KRISO (Gap=0.40 m)

- Numerical Wave Calibration

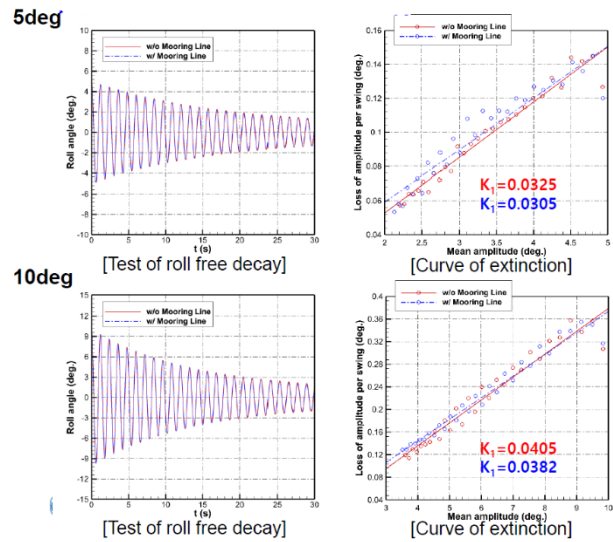
	T(s)			H(m)		
	Target wave period	CFD	%D	Target wave height	CFD	%D
RW-01	1.611	1.600	0.687	0.135	0.132	2.380
RW-02	1.471	1.447	1.637	0.113	0.110	2.521
RW-03	1.351	1.355	-0.267	0.095	0.092	3.342
RW-04	1.267	1.280	-1.064	0.083	0.080	3.480
RW-05	1.234	1.235	-0.074	0.079	0.077	3.403
RW-06	1.177	1.183	-0.555	0.072	0.070	3.068
RW-07	1.136	1.115	1.881	0.067	0.065	3.570
RW-08	1.098	1.086	1.176	0.063	0.061	3.104
RW-09	1.063	1.044	1.775	0.059	0.057	2.978
RW-10	1.032	1.037	-0.472	0.055	0.053	3.926
RW-11	1.010	1.024	-1.377	0.053	0.051	4.291
RW-12	0.980	0.988	-0.809	0.050	0.048	3.724
RW-13	0.962	0.966	-0.414	0.048	0.046	3.823
RW-14	0.943	0.961	-1.822	0.046	0.044	3.346
RW-15	0.925	0.943	-1.853	0.045	0.043	3.285
RW-16	0.909	0.917	-0.803	0.043	0.041	4.611
RW-17	0.892	0.910	-1.952	0.041	0.039	4.747
	0.878	0.872	0.650	0.040	0.038	4.222

- Roll Free Decay

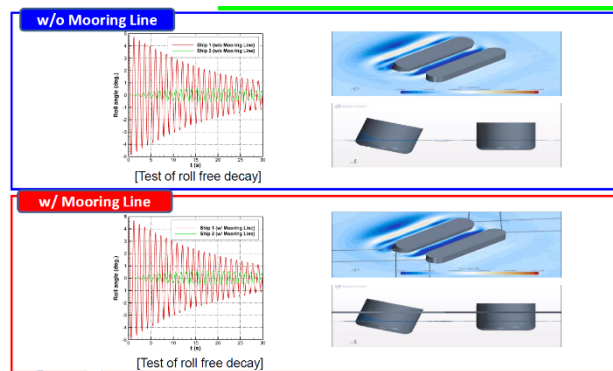
- Grid and boundary condition (Overset body, No. of grid: 2.0M)
- Convergence check for decay signal



- Result of Roll Free Decay (single body)



- Results of Roll Decay (two body)



8.9.4 Other facilities

The results of CFD analyses for other facilities are not summarized yet. The CFD tool and method being tried by other facilities are summarized in the appendix and denoted in short as below.

- PNU (2): Tool (ReFRESKO by MARIN)
- KMOU: Tool (OpenFoam)

9. STATE-OF-THE-ART REVIEW IN LARGE DIAMETER FLEXIBLE RISERS FOR DEEP WATER MINING

9.1 Introduction

Deepwater mining has been proposed since the 1960s to meet the increasing demands of the natural resources. The most feasible concept of deep-water mining system is divided into three categories: a seafloor mining vehicle, a vertical transporting system and a surface supporting vessel. Two typical applications of vertical transporting systems are utilized: (1) a vertical rigid pipe connecting the support vessel and the free hanging buffer, and a flexible riser connecting the buffer and the mining vehicle (see Figure 134(a)); (2) a single flexible riser connecting the mining vehicle and the support vessel (see Figure 134(b)). The former has been adopted in projects such as Blue Mining, Blue Nodules and the coming commercial project Solwara 1; the latter has been proposed by scholars in India and Germany, and a sea test was conducted in 2004 (Deepak et al., 2001; Handschuh et al., 2001).

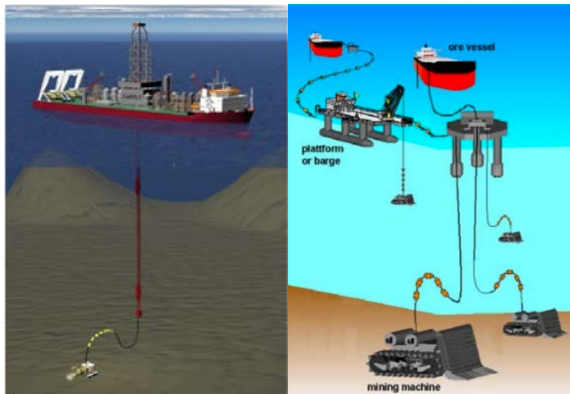


Figure 134: Typical vertical transporting systems: (a) Rigid pipe (Vercrujisse and Verichev, 2011); (b) Flexible riser (Deepak et al., 2007).

In vertical transporting systems, flexible risers/hoses are commonly used to cater the varying water depth, the seabed topography, and the movement of the mining vehicle. The material of flexible risers is usually composed of synthetic rubber, high strength-two stage cord, and synthetic rubber with enhanced tensile strength by using steel wires. The buoyant

material is mounted to compensate for the weight of flexible risers and to make the shape of flexible risers to ensure the movement of a mining vehicle, as shown in Figure 135. The studies on large diameter flexible risers for deep sea mining are mainly focused on three aspects: (1) pressure loss of the mixture; (2) dynamic responses and spatial configurations of the riser, and (3) flow assurance issues. Both full-scale and model tests have been carried out to provide guidance on the design of the flexible riser. In addition, various numerical methods have been developed to address these issues.



Figure 135: Flexible hoses with buoyancy materials (Yoon et al., 2011)

9.2 Pressure drop inside the flexible riser

One of the critical parameters during the flexible riser transportation is the pressure drop of the mixture, which determines the pump head and energy consumption. Owing to large ore particles in the slurry, the pressure drop of the mixture is entirely different from that of seawater and is affected by many factors such as particle size, particle density, solid volume fraction, flow rate and spatial configuration of the flexible risers. Both experiments and numerical simulations have been conducted in recent years. The previous works in the literature are summarized as follows:

Yoon et al. (2002, 2001) analysed the flow characteristics of the solid-liquid two-phase mixture in a flexible hose by experiments and summarized the effects of volume fraction, hose shape and mixture velocity on the pressure drop. The experimental results show that the increase of discharged volume fraction and particle diameter causes the increase of the minimum velocity for transporting the solid particles. The pressure drop increases as the solid volume

fraction increases irrespective of the shape of the flexible hose (also described in Yoon et al. (2006) and Yoon et al. (2009)). As for the mixture velocity and hose shape, the pressure drop increases when the superficial mixture velocity is more than a critical velocity (1.5 m/s in the experiments) and decreases as the more the pipe is curved in the case of low velocity below the critical velocity. Experiments conducted by Yoon et al. (2006) and Yoon et al. (2009) showed that the frictional hydraulic gradient becomes close to the hydraulic gradient of water as the mixture velocity increases. As the mixture velocity increases, the solid particles move at the centre of the pipe rather than at the wall side, and therefore the influence of the friction decreases.

The differences in flow characteristics between real and artificial manganese nodules-water mixture and synthetic nodules-water were experimentally studied by Yoon et al. (2009). The results show that the hydraulic gradients of the mixtures are almost identical in the case of both the real and synthetic nodules. However, when the solid volume fraction is high, the hydraulic gradient of the flow containing the real manganese nodules is a little lower than that of the artificial ones, because the drag effect is not so apparent.

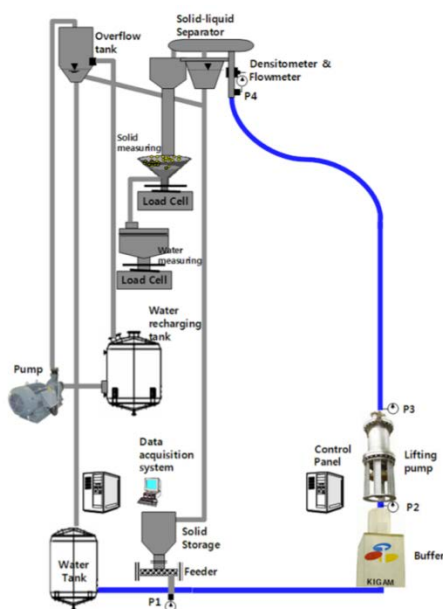


Figure 136: Flow experiment system for flexible riser by (Yoon et al., 2009).

Yu et al. (2010) developed a numerical method for computing the hydraulic power and pressure loss for the “S” shape jumper (flexible hose) in deep sea mining application based on Computational Fluid Dynamics (CFD). The CFD results were then used for calibrating a simplified equation for estimating pressure loss. Using specific energy consumption (SEC) numbers, it was found that if the delivered volumetric concentration (C_{vd}) is above 8%, SEC is relatively insensitive to the C_{vd} for the example system for deep sea mining. One of the key elements to ensure a successful hydraulic lifting design is to keep the ratio between the average slurry flow velocity and the largest particle settling velocity for the vertical riser section above 4 to 1. For the horizontal and jumper sections, a minimum ratio of 5 to 1 is needed based on CFD simulation and reference.

The methods of estimating the pressure drop and the solid-liquid two-phase flow regimes were reviewed by Parenteau (2010). The CFD method was then conducted for understanding transient behaviour and pressure and power prediction for the wave-shaped riser. Further, coupling of CFD and discrete element method (DEM) was proposed to improve the computational efficiency and accuracy of computational results.

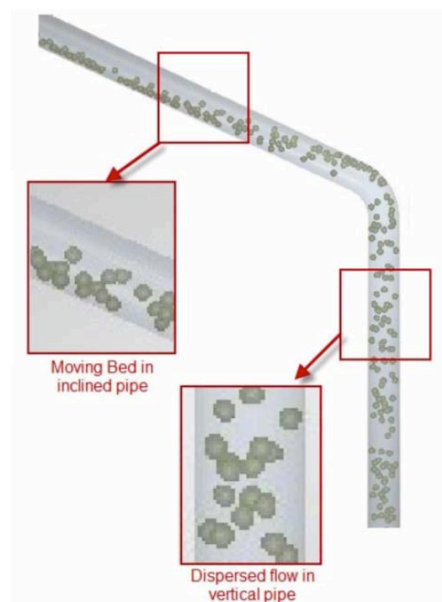


Figure 137: An example of CFD-DEM simulation of ore particles (Parenteau, 2010)

Parenteau and Lemaire (2011) summarized the flow tests made in a subsea mining experimental flow loop including horizontal and “S” shape sections. These tests allowed to identify the main flow characteristics of the slurry in subsea mining condition transporting large particles (5 mm to 20 mm) in reduced diameter “S” shape flexible riser (4”). Light glass beads and heavy alumina beads were demonstrated valid to represent the real solid flow and to simulate the impacts of the particle diameter and density on the pressure drop. “S” shape pipe has first shown higher pressure drop than the horizontal pipe in the tests. Pressure drop curves are influenced by two main slurry flow regimes: stratified below critical velocity, and homogeneous above critical velocity. The operating velocity should be well into developed homogeneous regime to avoid any potential solid deposit at the pipe bottom. Solid volume fraction clearly defined the level of pressure drop of the subsea mining system. The density has a significant impact on the pressure drop curves. The system needs to be designed for the maximum density observed on the field. Pressure drop follows the average density of the mixture. The particle size distribution also has a significant impact on the pressure drop. Increasing particle size reduces horizontal pressure drop but increases vertical pressure drop.

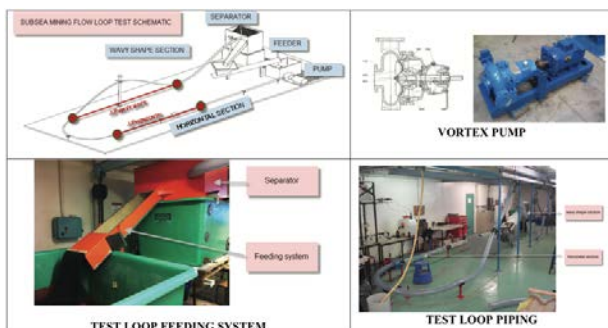


Figure 138: Subsea Mining small-scale flow loop test description (Parenteau and Lemaire, 2011)

Wang et al. (2012) investigated the resistance loss of transportation and the influences of buoyancy layout, solid volume fraction and elastic modulus of flexible hose using Finite Element Method (FEM). The numerical results show that the resistance loss

increases with the increase of solid volume fraction and internal fluid velocity and decreases with the increase of elastic modulus of flexible hose. The buoyancy layout and the internal flow velocity have greater impacts on the resistance loss than the elastic modulus of flexible hose. To reduce the resistance loss and improve the efficiency of deep-sea mining, solid volume fraction and flow velocity must be restricted in a suitable range (e.g., 10%~25% and 2.5 ~ 4 m/s, respectively). Effective buoyancy layout should be adopted, and the suitable material of moderate elastic modulus should be used for the flexible hose.

Ramesh et al. (2013) studied the pressure drop in flexible hoses of varied bend angles and various bend radii containing a pulsating flow. The studies were conducted for the most likely occurring bend angle of 70°, 20° and 60° with a bend radius of 5 times the hose diameter for various flow rates. The head losses in terms of differential pressure amplitude for clean water and slurry with solids of 10 mm size for various volume fraction were obtained experimentally. The authors concluded from the experimental results that the pressure drop of the mixture flow increased by 1.5 to 1.8 times for slurry flow when compared to the clear water.

Rhee et al. (2013) simulated the slurry behaviour in spooled hoses by using CFD (Figure 139). They described the phenomena that occur in elbows and in the spooled hoses at the entrance of the spool, the development of the slurry to a new stratification regime along the first part of the spooled hoses and the phenomena which occurred thereafter. The envelope of slurry conditions (concentration, particle size distribution, and velocity) has an impact on the dynamic pressure losses in the spooled hoses. When a stratified flow enters the spool, two vortices are identified, of which one is clearly stronger and dominates the other. For a stratified flow in the vertical spool, the pressure is approximately the same as that in a straight pipe. However, the pressure in a horizontal orientation of the spool is smaller than that in a straight pipe.



Figure 139: Spooled riser applied on a vessel (Rhee et al., 2013)

Beauchesne et al. (2015) developed a new transient flow assurance model named FASST: Flow Assurance Simulation for Slurry Transportation, to correctly assess the pressure drop in deep sea mining riser. The model was validated against both small-scale and large-scale tests. Theoretical results proved to agree with experimental results allowing a very good confidence in the FASST prediction of transient flow regimes.

Peng et al. (2015) analysed critical flow velocity of solid-liquid two-phase mixture and total pressure drop of flexible hose by existing formulas under conditions of different spatial configurations of hose, different particle sizes, and different solid volume fraction. The results show that the critical flow velocity and pressure drop regularly increase with the increase of particle size and volume fraction. Considering transmission efficiency and transportation safety, 10% to 15% is the optimal volume fraction, and critical flow velocity is about 2.8 m/s ~3.6 m/s. The results are close to those of Wang et al. (2012). To avoid clogging and reduce energy consumption, the critical flow velocity should be controlled according to the different relative distance between buffer and mining vehicle.

Nijun et al. (2017) investigated the flow characteristics in flexible hoses based on the experimental system shown in Figure 140. The hydraulic gradient of coarse particle slurry in flexible hoses increases with the increase of particle volume fraction and mixture velocity, and it decreases with the increase of particle size. This change rule is similar to hydraulic transportation research results in inclined pipelines. In addition, with hose curvature

increasing, the particle easily moves in turbulence, and the hydraulic gradient increases. Comparing hydraulic gradient in inclined pipelines and flexible hoses, the hydraulic gradient computational equations of coarse particles in flexible hoses were proposed.

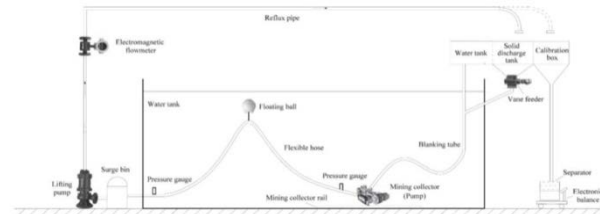


Figure 140: Experimental system of Nijun et al. (2017)

9.3 Dynamic responses and spatial configurations

During deep sea mining, one of the main tasks is to estimate the dynamic responses and spatial configurations of flexible risers under complicated sea states and operating conditions of the mining vehicle. Reliable experimental and numerical methods are required to predict the nonlinear geometric deformation and tension of the flexible risers. In recent years, both experiments and numerical simulations have been conducted. The main works are listed as follows.

Wang and Liu (2005) and Wang et al. (2007) established a 3D dynamic analysis model of 1000 m deep sea mining pipeline by FEM. The effect of concentrated buoyancy provided by buoyancy balls was analysed by simulating the configuration of a 400 m flexible hose. The results show that, to form the configuration of a saddle shape, the total concentrated suspension buoyancy of flexible hose should be 95% ~ 105% of the gravity of flexible hose in water, the first suspension point occupies 1/3 of the total buoyancy, and the second suspension point occupies 2/3 of the total buoyancy (Figure 141).

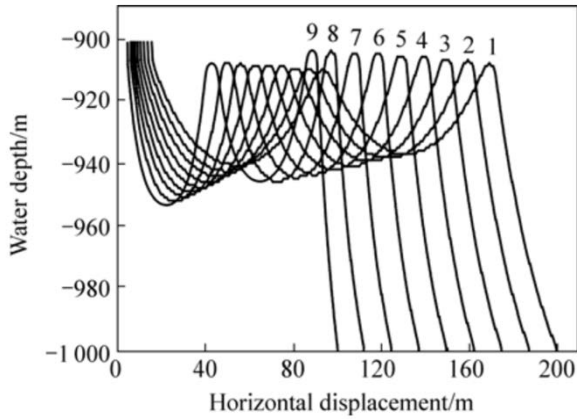


Figure 141: Shape of flexible hose due to movement of mining vehicle (Wang et al., 2007)

Wang and Liu (2005) and Li et al. (2007) analysed the deep sea mining pipe system using DEM. The results were validated and compared to the simulations based on FEM. The dynamic responses of the entire mining pipe system in different work conditions were discussed. Some suggestions were made for the actual operation of deep-sea mining systems.

Rao et al. (2009) studied the interaction of fluid-solid coupled flexible hose and mining vehicle in a 1000 m deep sea mining system based on nonlinear FEM with fluid-solid coupling model. Effects of the walking paths (e.g., line, circle, and square), walking velocities of the mining vehicle on the spatial configuration, support restrained force and maximum tensile stress of the flexible hose were investigated. Results show that the line walking of the mining vehicle is better for small lateral displacement, maximum tensile stress and support constrained force of the flexible hose than the circle and square walking. The walking velocities of the mining vehicle should be limited to an appropriate range (about 0.2 ~ 0.4 m/s when flow velocity in flexible hose is 4 m/s) for the safety and efficiency of the mining operation.

Wang et al. (2011) carried out a short 10 s simulation of the interactions between the dynamics of the mining vehicle on seabed and the flexible hose. The calculation results show that the hose has a relatively large vibration in the vertical direction and the maximum

amplitude reached 1.5 m which may result in low efficiency of inner fluid transportation or poor safety and stability of the flexible hose.

Chen et al. (2014) developed a quasi-static analysis method that succeeded in finding equilibrium configurations of flexible marine hoses dragged by mining vehicles based on FEM. In addition, an experiment of the flexible hose has been conducted to validate the proposed numerical method. The numerical method was used in modelling a typical mining procedure in which the mining vehicle was moving counter clockwise in a circle. Simulation results show variations of configurations of the pipe and constraint forces/torques.



(a) A photograph of the experiment

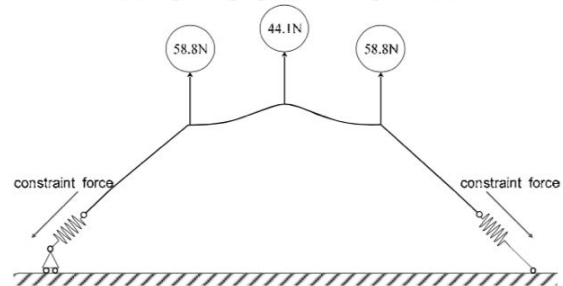


Figure 142: Photograph and schematic diagram of the experiment by Chen et al. (2014)

9.4 Flow assurance issues

Flow assurance issues of flexible risers, such as erosion and clogging, are of great importance in deep sea mining applications. The investigations on these issues have been conducted by means of full-scale experiments, model tests and numerical simulations recently.

Parenteau (2012) conducted the large-scale experiments for flow correlation validation and abrasion test to have an in-depth understanding of the flow assurance issues in deep-sea mining. This large-scale test used an innovative method to allow the reproduction of realistic erosion rate in the pipe by preventing the solid particle to be eroded when looping through the pump. The author assessed pressure drop and erosion rate close to real flow conditions and summarized the findings and results from this large-scale experimental set-up, testing concentration from 10% to 45%, velocities from 2.5 m/s to 5.5 m/s in an 8" flexible pipe with equivalent rocks particles.

Rongau and Viale (2017) built a large-scale bench test to reproduce realistic flow in a piping system and compare wear on different materials. A complete analysis of the wear patterns was conducted with the expertise of a laboratory. A statistical comparison between materials was presented. The response to wear, depending on material, geometry, and position, was better known. One of the materials showed much better wear resistance than the others and was selected for further development.



Figure 143: Large-scale rig test overview (Rongau and Viale, 2017)

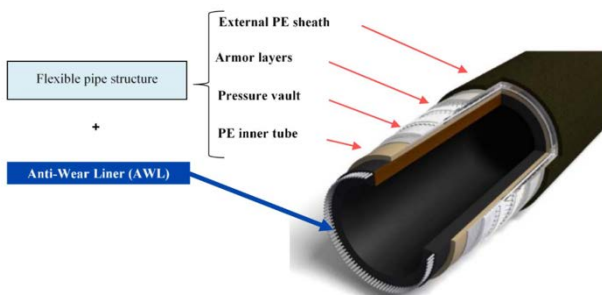


Figure 144: Design for flexible cross-section containing anti-abrasion layer (Rongau and Viale, 2017)

Neale et al. (2017) conducted a long-term abrasion test on 10" hoses and compared the results to those of abrasion calculations based on

flow simulations. Three different lining materials were applied in the full-scale test. The abrasion rate increases in the following order: armoured liner, rubber, and plastic, although the plastic has better Schopper abrasion than rubber. The results indicate the superiority of rubber liner over plastic liner in high impact wear regime. Parameterized erosion model and a discrete phase model (DPM) combined in a CFD simulation proved to be an effective tool to predict erosion rate. The simulation proved to be very sensitive to the dependence of the impact angle on the abrasion rate, particularly at low impact angles. Breakdown of the abrading particles has a high influence on the results. Natural material, granite with wide size distribution (32 ~ 60 mm) was used in the full-scale abrasion test. In addition, there was significant batch to batch variation in the granite properties.



Figure 145: Rotating full-scale abrasion tester (Neale et al., 2017)

Takano et al. (2015) conducted a small-scale test for a fundamental understanding of pipe wear under hydraulic transportation of deep-sea mining. The small-scale test apparatus was set up using the pipes of about 80 mm in diameter and the rocks of which maximum particle diameters were about 20 mm. In the test, the pipe materials and the pipe inclination were changed to evaluate the differential of the amount of pipe material loss. Furthermore, the amount of the pipe material loss in full scale was estimated based on the small-scale test results. From the research on the wear of the riser with

different inclinations, the authors concluded that the configuration of the flexible hose to connect the seafloor mining vehicle and the buffer should be considered carefully in designing of the mining system and preparing the operating procedure.

A novel framework for coupled analysis of risers with internal flow utilized to study the VIV of a mining riser was presented in Thorsen et al. (2019). Focus was on the effect of time-varying internal slurry flows, and the associated density waves traveling along the riser. Simulated VIV response and fatigue damage were reported in detail, to illuminate the effect of the period/wavelength of the internal flow. It was found that the internal flow produces significant changes to the VIV fatigue damage, if the wavelength of the internal density wave is close to $\lambda_{cr} = L/n$, where L is the riser length, and n is the dominating VIV mode. The results suggest that careful analysis is necessary when designing a mining riser where internal density waves are expected to occur with a wavelength near or above the critical value. In such cases, the presented numerical method may be a useful tool.

10. PROCEDURE/GUIDELINE FOR MODEL CONSTRUCTION

The 28th Ocean Engineering Committee developed a preliminary procedure for model construction of floating offshore platforms; however, its Advisory Committee (AC) made a series of comments/recommendations and suggested to develop a guideline instead of a procedure. As indicated by the 28th AC, a procedure should provide specific details and criteria.

Since the nature of tests and models covered by the Ocean Engineering Committee is quite diverse and specific at the same time, to develop generic standards/procedures/criteria to attend all the possible scenarios is not feasible. So, after consulting the present AC, a new guideline was developed: 7.5-02-07-03.15 Model Construction of Offshore Systems.

The new guideline is based on the version submitted to the 28th Conference and incorporated the 28th AC's comments and suggestions. Focus on model construction issues regarding materials, tolerances, production methods, quality control, acceptance testing, etc. were also included as required by the current Terms of Reference.

The design, manufacture, and pre-tests in water of offshore systems models have been addressed. An offshore system can be composed of bottom-founded or stationary floating structures, mooring lines/risers and umbilicals, dynamic positioning systems, and/or any other auxiliary structure or equipment involved in offshore operations. Those structures may be subjected to environmental loads such as wind, water waves and current (excluding ice). The guideline may also be applied to subsea and coastal structures such as floating breakwaters and fish farms.

The purpose of this guideline is to ensure the correct design and manufacture of the model of the offshore system for its testing in towing tanks, wave/current basins, and/or wind tunnels (excluding field tests). In typical tests of offshore systems, hull platform models are assumed to be rigid bodies, so the focus of this guideline is on this type of structure. Additional considerations should be done when the elasticity of the platform must be modelled.

11. CONCLUSIONS & RECOMMENDATIONS

11.1 State-of-the-art reviews in offshore structures

In the present ITTC period (2017-2021), the review has allowed to identify some issues associated to bottom founded and stationary floating structures. For bottom-founded structures, life extension of existing fixed platforms has attracted attention. Fatigue and vessel impact loads are of concern. For (fixed) offshore wind turbines, besides waves, wind and current loads, earthquake loads have become an

item of concern. Model and full-scale tests are needed for validation studies.

In the case of FPSO and/or FLNGs, several experimental and numerical studies have been devoted to green water and water impacts associated to extreme waves. Hydrodynamic behaviour associated to side-by-side configurations and viscous damping are also issues that have attracted much attention in the recent years. In the case of TLPs and semisubmersibles, several works have been devoted to applications related to the investigation of the occurrence and mitigation of VIM as well as applications for floating offshore wind turbines. Operations under ice conditions have also attracted attention and deserve further experimental and numerical research.

11.2 Review of the Existing Procedures

The Committee has reviewed and updated nine (09) procedures and guidelines. In general, minor revisions have been made. The detailed comments from the Advisory Committee have been also incorporated.

Concerning the existing procedures and guidelines, the Ocean Engineering Committee would like to make the following recommendations to the 29th ITTC:

- Adopt the updated procedure: 7.5-02-07-03.1 Floating Offshore Platform Experiments;
- Adopt the updated procedure: 7.5-02-07-03.2 Analysis Procedure for Model Tests in Regular Waves;
- Adopt the updated procedure: 7.5-02-07-03.4 Active Hybrid Model Tests of Floating Offshore Structures with Mooring Lines;
- Adopt the updated procedure: 7.5-02-07-03.5 Passive Hybrid Model Tests of Floating Offshore Structures with Mooring Lines;

- Adopt the updated procedure: 7.5-02-07-03.6 Dynamic Positioning System Model Test Experiments;
- Adopt the updated guideline: 7.5-02-07-03.10 Guideline for VIV Testing;
- Adopt the updated guideline: 7.5-02-07-03.11 Model Tests of Multibodies in Close Proximity;
- Adopt the updated guideline: 7.5-02-07-03.13 Guideline for VIM Testing;
- Adopt the updated procedure: 7.5-02-07-03.14 Analysis Procedure of Model Tests in Irregular Waves.

Since, in the period 2017-2021, several works and developments on side-by-side configuration and VIM tests have been reported, it is recommended that Procedure 7.5-02-07-03.11 Model Tests of Multibodies in Close Proximity and Guideline 7.5-02-07-03.13 Guideline for VIM Testing should be continuously reviewed and updated accordingly, by the next committees.

11.3 State-of-the-art review in offshore aquaculture systems

Offshore aquaculture systems continue to attract attention, with particular focus on larger floating structures. Close containment tank systems have been proposed to avoid the effects of sea lice on fish. Hydrodynamic interaction among the main floating structure, mooring system, and the fishing nets continues to be a concern, especially under harsh environmental conditions.

According to Xu and Qin (2020), still several issues need to be addressed. More physical model tests and numerical simulations are required to study the fast-swimming behaviour and swimming efficiency of fish to select appropriate farming sites and improve the

designs of offshore aquaculture cage systems. Fluid-ice-aquaculture structure interactions must be studied for aquaculture cages deployed in North Atlantic where drift ice could damage the cage structures. Some new elements have been introduced together with aquaculture technology such as the integration of aquaculture farming and ocean renewable energy system. A vast array of applications is ready for the evolution of aquaculture engineering and technology.

11.4 State-of-the-art review in cable/pipe dynamics close to sea-surface

Although the number of applications of cable/pipes close to the sea surface is growing, there are still few experimental studies on this topic. Most of these works are concerned with fluid transfer lines (FTL) such as risers or offloading hoses. However, for other applications such as power cables for wave energy converters, cable net barriers or towing cables, only numerical studies have been found. Thus, it is suggested that model tests should be performed for the latter applications to validate the numerical results and gain more insight on the observed phenomena.

11.5 State-of-the-art review in Software-in-the-Loop (SiL) tests

A software in the loop (SiL) system for the use in experimental tests has been reviewed in this report. The SiL approach offers several advantages over conventional full-coupled modelling utilizing a working rotor in a wind field, including the ability to deploy in a wide range of facilities, reduced cost, greater flexibility of scale, and ability to simulate the impact of some features such as control systems and blade elasticity which may prove challenging with a working rotor. At present, the system is still under development and there are some issues regarding repeatability and experiment methodology which require further refinement.

11.6 Experimental benchmark on wave run-up on cylinders

As an extension of the benchmark studies of wave run-ups on single and four truncated circular cylinders conducted in 2013 during the 27th ITTC, the present benchmark tests were conducted to measure the wave run-ups and global wave loads on fixed four squared cylinders under regular and irregular waves. A set of benchmark data and results were provided for validating related numerical simulations. Owing to the complicated wave-column interactions, more experimental and CFD studies are recommended in consideration of four-column cases with different configurations and more extreme waves such as focused waves. In addition, local wave impact loads on the columns are also critical and deserve further in-depth studies.

11.7 CFD benchmark on two-body interactions

The CFD benchmark study for two-body interaction is now on going and the interim conclusion can be summarized as below:

- The model test and CFD results show the viscous effect on the motion and drift force on bodies and the gap wave elevation when comparing the potential calculation;
- The viscous effect on body motion is the smallest and it shows larger influence on the gap wave elevation;
- The viscous effect is more pronounced at the higher wave frequency region;
- The smallest gap distance of 0.40 m shows the largest viscous effect and the distance of 0.55 m shows negligible viscous effect on the body motion, drift force and gap wave elevation.

Further CFD studies are needed by the various participants to establish the CFD procedure for 2 body interaction problem and resultantly to update the procedure for 2 body model test based on this CFD benchmark study. The conclusion will be made when the CFD

study proposed as the cooperative work in this task is completed. It would be good if the model test and CFD study between the smaller gap are carried out. list.

11.8 State-of-the-art review in large diameter flexible risers for deep water mining

In general, many experimental and numerical investigations on flexible risers used in deep sea mining applications have been conducted. However, the technologies for the design of flexible risers are not firmly established yet. It is difficult to arrive to general conclusions or formulae to measure the parameters such as the pressure drop of the mixture, the spatial configurations of the risers and the erosion rate.

Owing to the complicated interaction of the flexible riser, the inner flow and the environmental loads, the coupled analysis of the inner flow regime and the external loads are rare. Additionally, the aggregation and clogging of the ores in the flexible riser should be investigated in detail due to the complex flow regimes and particle motion when the mixture flow is passing the crest and trough of the curved risers.

As the vertical ore transporting system consists of the rigid pipe, the pumps, the buffer and the flexible hoses, the integrated system should be experimental and numerical investigated to predict the dynamic responses of all the components, the continuous flow regimes and to address the flow assurance issues of the whole transporting system in the next step.

11.9 New Guideline for Model Construction

The Ocean Engineering Committee would like to make the following recommendation to the 29th ITTC:

- Adopt the new guideline: 7.5-02-07-03.15 Model Construction of Offshore Systems

12. REFERENCES

- Abdussamie, N., Drobyshevski, Y., Ojeda, R., Thomas, G., Amin, W., 2017. "Experimental investigation of wave-in-deck impact events on a TLP model". *Ocean Eng.* 142, 541–562. <https://doi.org/https://doi.org/10.1016/j.oceaneng.2017.07.037>
- An, S., Chen, D., Bai, Y., 2019. "Dynamic Positioning Observer Design Using Exogenous Kalman Filter". <https://doi.org/10.1115/OMAE2019-96490>
- Asgari, P., Fernandes, A.C., Low, Y.M., 2020. "Most often instantaneous rotation center (MOIRC) for roll damping assessment in the free decay test of a FPSO". *Appl. Ocean Res.* 95, 102014. <https://doi.org/https://doi.org/10.1016/j.apor.2019.102014>
- Avalos, G.O.G., Wanderley, J.B. V, 2018. "Numerical study of forced roll oscillation of FPSO with bilge keel". *Ocean Eng.* 147, 304–317. <https://doi.org/https://doi.org/10.1016/j.oceaneng.2017.10.034>
- Azcona, J., Bouchotrouch, F., González, M., Garcíandía, J., Munduate, X., Kelberlau, F., Nygaard, T.A., 2014. "Aerodynamic thrust modelling in wave tank tests of offshore floating wind turbines using a ducted fan", in: *Journal of Physics: Conference Series*. IOP Publishing, p. 12089.
- Bachynski, E.E., Thys, M., Sauder, T., Chabaud, V., Sæther, L.O., 2016. "Real-Time Hybrid Model Testing of a Braceless Semi-Submersible Wind Turbine: Part II — Experimental Results". <https://doi.org/10.1115/OMAE2016-54437>
- Banik, A.K., Roy, S., Saha, K., Dey, S., 2019. "Effect of wave spreading including

- multi-directional wave interaction on the responses of a spar platform". Mar. Syst. Ocean Technol. 14, 153–165.
- Batalla Toro, L.F., Reid, S.L., Tudela, A.S., Graham, D., 2018. "Integrated Decommissioning of a Pentagon Shaped Production Semisubmersible in the UK: A Unique Challenge". <https://doi.org/10.1115/OMAE2018-77831>
- Bayati, I., Belloli, M., Ferrari, D., Fossati, F., Giberti, H., 2014. "Design of a 6-DoF Robotic Platform for Wind Tunnel Tests of Floating Wind Turbines". Energy Procedia 53, 313–323. <https://doi.org/https://doi.org/10.1016/j.egpro.2014.07.240>
- Beauchesne, C., Parenteau, T., Septseault, C., Béal, P.-A., 2015. "Development & Large Scale Validation of a Transient Flow Assurance Model for the Design & Monitoring of Large Particles Transportation in Two Phase (Liquid-Solid) Riser Systems ". <https://doi.org/10.4043/25892-MS>
- Beveridge, M.C.M., 2008. Cage aquaculture. John Wiley & Sons.
- Bjerke, K.S., 1990. "Offshore fish-fanning platforms-development, design, construction and operation: the SEACON and SULAN concepts", in: Engineering for Offshore Fish Farming. Thomas Telford Publishing, pp. 153–169.
- Bjørnø, J., Heyn, H.-M., Skjetne, R., Dahl, A.R., Frederich, P., 2017. "Modeling, Parameter Identification and Thruster-Assisted Position Mooring of C/S Inocean Cat I Drillship". <https://doi.org/10.1115/OMAE2017-61896>
- Bugrov, L., 2006. "The" Sadco" underwater fish-farming system". Underw. Technol. Ocean World" Sci. Tech. J. about World Ocean Resour. Dev. 1, 34–45.
- Cahay, M., Roberts, B.A., Sadouni, S., Béal, P.-A., Septseault, C., Mravak, Z., Benoit, C., 2017. "Ice Load Calculation on Semi-Submersible Platform". <https://doi.org/10.1115/OMAE2017-61903>
- Carmo, B.S., Assi, G.R.S., Meneghini, J.R., 2013. "Computational simulation of the flow-induced vibration of a circular cylinder subjected to wake interference". J. Fluids Struct. 41, 99–108. <https://doi.org/https://doi.org/10.1016/j.jfluidstructs.2013.02.010>
- Chadwick, E.M.P., Parsons, G.J., Sayavong, B., 2010. Evaluation of closed-containment technologies for saltwater salmon aquaculture. NRC Research Press.
- Chang, S.-H.M., Isherwood, M., 2003. "Vortex-Induced Vibrations of Steel Catenary Risers and Steel Offloading Lines due to Platform Heave Motions ". <https://doi.org/10.4043/15106-MS>
- Chen, H., 2017. "Safety of Marine Operations Involving Dynamically Positioned Vessels". <https://doi.org/10.1115/OMAE2017-62708>
- Chen, L., Taylor, P.H., Draper, S., Wolgamot, H., Milne, I.A., Whelan, J.R., 2019. "Response based design metocean conditions for a permanently moored FPSO during tropical cyclones: Estimation of greenwater risk". Appl. Ocean Res. 89, 115–127. <https://doi.org/https://doi.org/10.1016/j.apor.2019.05.003>
- Chen, Y., Fu, S., Xu, Y., Fan, D., 2013. "High order force components of a near-wall circular cylinder oscillating in transverse direction in a steady current". Ocean Eng. 74, 37–47. <https://doi.org/https://doi.org/10.1016/j.oc>

eaneng.2013.09.009

Chen, Y., Yang, N., Jin, X., 2014. "Nonlinear Finite-Element Analysis of Flexible Marine Pipes for Deep-Sea Mining".

Cheng, J., Cao, P., Ren, H., Zhang, M., Fu, S., 2018. "Experimental Study of the Pipe With Buoyancy Modules".

Cheng, N., Gaudin, C., Cassidy, M.J., 2019. "Physical and numerical study of the combined bearing capacity of hybrid foundation systems". Ocean Eng. 179, 104–115.
<https://doi.org/10.1016/j.oceaneng.2019.03.002>

Choi, Y.-M., Nam, B.W., Hong, S.Y., Jung, D.W., Kim, H.J., 2018. "Coupled motion analysis of a tension leg platform with a tender semi-submersible system". Ocean Eng. 156, 224–239.
<https://doi.org/https://doi.org/10.1016/j.oceaneng.2018.01.031>

Chong, S.H., 2017. "Numerical simulation of offshore foundations subjected to repetitive loads". Ocean Eng. 142, 470–477.
<https://doi.org/10.1016/j.oceaneng.2017.07.031>

Chow, J.H., Ng, E.Y.K., Srikanth, N., 2019. "Numerical study of the dynamic response of a wind turbine on a tension leg platform with a coupled partitioned six degree-of-freedom rigid body motion solver". Ocean Eng. 172, 575–582.
<https://doi.org/https://doi.org/10.1016/j.oceaneng.2018.12.040>

Chu, Y.I., Wang, C.M., Park, J.C., Lader, P.F., 2020. "Review of cage and containment tank designs for offshore fish farming". Aquaculture 519, 734928.
<https://doi.org/https://doi.org/10.1016/j.aquaculture.2020.734928>

Cozijn, H., Choi, J.W., You, Y.-J., 2017.

"Thruster-Wave Interaction During DP Stationkeeping: Model Tests in Open Water and Under a Ship Hull".
<https://doi.org/10.1115/OMAE2017-62168>

da Silva Gomes, S., Pinheiro Gomes, S.C., 2021. "A new dynamic model of towing cables". Ocean Eng. 220, 107653.
<https://doi.org/https://doi.org/10.1016/j.oceaneng.2020.107653>

Day, A.H., Clelland, D., Oguz, E., Dai, S., Azcona Armendáriz, J., Bouchotrouch, F., Lopez, J.A., Sánchez, G., González Almeria, G., 2017. "Realistic simulation of aerodynamic loading for model testing of floating wind turbines".

Deepak, C.R., Ramji, S., Ramesh, N.R., Babu, S.M., Abraham, R., Shajahan, M.A., Atmanand, M.A., 2007. "Development And Testing of Underwater Mining Systems For Long Term Operations Using Flexible Riser Concept".

Deepak, C.R., Shajahan, M.A., Atmanand, M.A., Annamalai, K., Jeyamani, R., Ravindran, M., Schulte, E., Handschuh, R., Panthel, J., Grebe, H., Schwarz, W., 2001. "Developmental Tests On the Underwater Mining System Using Flexible Riser Concept".

Dehghani, A., Aslani, F., 2019. "A review on defects in steel offshore structures and developed strengthening techniques". Structures 20, 635–657.
<https://doi.org/10.1016/j.istruc.2019.06.002>

Detlefsen, O., Theilen, L., Abdel-Maksoud, M., 2017. "Static and Dynamic Analysis Methods of Position-Keeping Capability for Offshore Supply Vessels With Voith-Schneider Propellers".
<https://doi.org/10.1115/OMAE2017-61893>

DNV, 2010. Recommended Practice Global

Performance Analysis of Deepwater Floating Structures.

- Dong, Q., Lu, H., Yang, J., Guo, X., 2019. "Dynamic gangway responses between TLP and semi-submersible platform during tender-assisted drilling". Mar. Struct. 67, 102645. <https://doi.org/https://doi.org/10.1016/j.marstruc.2019.102645>
- Fang, S.M., Niedzwecki, J.M., Fu, S., Li, R., Yang, J., 2014. "VIV response of a flexible cylinder with varied coverage by buoyancy elements and helical strakes". Mar. Struct. 39, 70–89. <https://doi.org/https://doi.org/10.1016/j.marstruc.2014.06.004>
- Feng, X., Bai, W., Chen, X.B., Qian, L., Ma, Z.H., 2017. "Numerical investigation of viscous effects on the gap resonance between side-by-side barges". Ocean Eng. 145, 44–58. <https://doi.org/https://doi.org/10.1016/j.oceaneng.2017.08.060>
- Fernandes, A.C., Asgari, P., Sales Junior, J.S., 2018. "Linear and non-linear roll damping of a FPSO via system identification of a third order equation with sway-roll coupled damping effects". Ocean Eng. 166, 191–207. <https://doi.org/https://doi.org/10.1016/j.oceaneng.2018.08.006>
- Fernandez, C., Bhushan Kumar, S., Lok Woo, W., Norman, R., Kr. Dev, A., 2020. "Real-Time Prediction of Reliability of Dynamic Positioning Sub-Systems for Computation of Dynamic Positioning Reliability Index (DP-RI) Using Long Short Term Memory (LSTM)". <https://doi.org/10.1115/OMAE2020-18844>
- Fernandez, C., Dev, A.K., Norman, R., Woo, W.L., Kumar, S.B., 2019. "Dynamic Positioning System: Systematic Weight Assignment for DP Sub-Systems Using Multi-Criteria Evaluation Technique Analytic Hierarchy Process and Validation Using DP-RI Tool With Deep Learning Algorithm". <https://doi.org/10.1115/OMAE2019-95485>
- Fernandez, C., Kumar, S.B., Lok Woo, W., Norman, R., Kr. Dev, A., 2018. "Dynamic Positioning Reliability Index (DP-RI) and Offline Forecasting of DP-RI During Complex Marine Operations". <https://doi.org/10.1115/OMAE2018-77267>
- Fonseca, N., Stansberg, C.T., 2017. "Wave Drift Forces and Low Frequency Damping on the Exwave FPSO", in: Proceedings of the ASME 2017 36th International Conference on Ocean, Offshore and Arctic Engineering. Volume 1: Offshore Technology. Trondheim. <https://doi.org/10.1115/OMAE2017-62540>
- Føre, H.M., Dahle, S.W., Gaarder, R.H., 2018. "Tensile Strength of Nylon Netting Subjected to Various Concentrations of Disinfecting Chemicals". J. Offshore Mech. Arct. Eng. 141. <https://doi.org/10.1115/1.4040562>
- Fredriksen, A.G., Bonnemaire, B., Nilsen, Ø., Aspelund, L., Ommundsen, A., 2018. "Irregular Wave and Current Loads on a Fish Farm System". <https://doi.org/10.1115/OMAE2018-77482>
- Fu, Z., Li, W., Sun, H., Yuan, M., Li, X., Cai, L., Wang, A., Guo, X., Wei, H., Tian, X., 2020. "Experiment-Scale Multi-Vessel Dynamic Positioning System for the Twin-Lift Decommissioning Operation". <https://doi.org/10.1115/OMAE2020-18631>
- Gang, C., Huan, Z., Yuhuan, W., Chao, W., Wei, Z., Yan, Y., 2018. "Float-Over Installation Analysis of Semisubmersible

- Production Platform Topside".
<https://doi.org/10.1115/OMAE2018-77347>
- Gansel, L.C., Endresen, P.C., Steinhovden, K.B., Dahle, S.W., Svendsen, E., Forbord, S., Jensen, Ø., 2017. "Drag on Nets Fouled With Blue Mussel (*Mytilus Edulis*) and Sugar Kelp (*Saccharina Latissima*) and Parameterization of Fouling".
<https://doi.org/10.1115/OMAE2017-62030>
- Gao, J., He, Z., Huang, X., Liu, Q., Zang, J., Wang, G., 2021. "Effects of free heave motion on wave resonance inside a narrow gap between two boxes under wave actions". *Ocean Eng.* 224, 108753.
<https://doi.org/https://doi.org/10.1016/j.oceaneng.2021.108753>
- Gao, W., Zhu, W., Dong, L., Qi, X., 2016. "A Study of Spar-FPSO VIM Phenomenon and Its Influence to Mooring System".
- Gao, Z., Efthymiou, M., Zhao, W., Cheng, L., Zhou, T., 2020. "Experimental Study of Hydrodynamic Damping for Water Intake Risers".
<https://doi.org/10.1115/OMAE2020-18119>
- Ghassempour, M., Failla, G., Arena, F., 2019. "Vibration mitigation in offshore wind turbines via tuned mass damper". *Eng. Struct.* 183, 610–636.
<https://doi.org/10.1016/j.engstruct.2018.12.092>
- Gonçalves, R.T., Suzuki, H., Marques, M.A., Silva, L.S.P., Tian, C., Hirabayashi, S., 2020. "Experimental Study of the Effect of the Pontoon Dimensions on the Flow-Induced Motions (FIM) of a Semi-Submersible Platform With Four Square Columns".
<https://doi.org/10.1115/OMAE2020-18009>
- Gundersen, G., Stuberg, P., Kendon, T.E., Reinholdtsen, S.-A., 2018. "Improved FPSO Offloading Strategy Based on Analysis Including DP System".
<https://doi.org/10.1115/OMAE2018-78465>
- Ha, Y.-J., Kim, K.-H., Nam, B.W., Hong, S.Y., Kim, H., 2021. "Experimental study for characteristics of slamming loads on bow of a ship-type FPSO under breaking and irregular wave conditions". *Ocean Eng.* 224, 108738.
<https://doi.org/https://doi.org/10.1016/j.oceaneng.2021.108738>
- Handschuh, R., Grebe, H., Panthel, J., Schulte, E., Wenzlawski, B., Schwarz, W., Atmanand, M.A., Jeyamani, R., Shajahan, M.A., Deepak, C.R., Ravindran, M., 2001. "Innovative Deep Ocean Mining Concept Based On Flexible Riser And Self-propelled Mining Machines".
- Harmsen, E., van Dijk, R., Stuberg, P., 2018. "DP-Stability During Heavy Lift Operations Using a Modified Kalman Filter".
<https://doi.org/10.1115/OMAE2018-77901>
- He, J., Wan, D., Hu, Z., 2018. "CFD Simulations of Helical Stakes Reducing Vortex Induced Motion of a Semi-Submersible".
<https://doi.org/10.1115/OMAE2018-78372>
- Hegseth, J.M., Bachynski, E.E., Karimirad, M., 2018. "Comparison and Validation of Hydrodynamic Load Models for a Semi-Submersible Floating Wind Turbine".
<https://doi.org/10.1115/OMAE2018-77676>
- Hill, H., 2018. "Future Proofing Fish Farming". *Mar. Rep.* 125.
- Horn, J.T., Leira, B.J., 2019. "Fatigue reliability assessment of offshore wind

- turbines with stochastic availability". Reliab. Eng. Syst. Saf. 191, 106550. <https://doi.org/10.1016/j.ress.2019.106550>
- Hu, X., Zhang, X., You, Y., 2017. "Numerical Studies on Vortex-Induced Motions of a Semi-Submersible With Four Columns Based on IDDES Model", in: Proceedings of the ASME 2017 36th International Conference on Ocean, Offshore and Arctic Engineering. Volume 1: Offshore Technology. ASME, Trondheim. <https://doi.org/10.1115/OMAE2017-62164>
- Hu, Z.-Q., Wang, S.-Y., Chen, G., Chai, S.-H., Jin, Y.-T., 2017. "The effects of LNG-tank sloshing on the global motions of FLNG system". Int. J. Nav. Archit. Ocean Eng. 9, 114–125.
- Hu, Z.Z., Mai, T., Greaves, D., Raby, A., 2017. "Investigations of offshore breaking wave impacts on a large offshore structure". J. Fluids Struct. 75, 99–116. <https://doi.org/10.1016/j.jfluidstructs.2017.08.005>
- Hu, Z.Z., Yan, S., Greaves, D., Mai, T., Raby, A., Ma, Q., 2020. "Investigation of interaction between extreme waves and a moored FPSO using FNPT and CFD solvers". Ocean Eng. 206, 107353. <https://doi.org/https://doi.org/10.1016/j.oceaneng.2020.107353>
- Huang, A.S., Tannuri, E.A., Queiroz Filho, A.N., Ianagui, A.S.S., Yuba, D.G.T., Nogueira, S., Abdalla, T.C., 2017. "The Influence of Hold-Back Vessels on the Operation of a DP Drilling Rig: Control System and Stability Analysis". <https://doi.org/10.1115/OMAE2017-61153>
- Huang, X.-H., Liu, H.-Y., Hu, Y., Yuan, T.-P., Tao, Q.-Y., Wang, S.-M., Liu, Z.-X., 2020. "Hydrodynamic performance of a semi-submersible offshore fish farm with a single point mooring system in pure waves and current". Aquac. Eng. 90, 102075. <https://doi.org/https://doi.org/10.1016/j.aquaeng.2020.102075>
- Ji, X., Li, Y., Tang, Y., Tong, B., 2019. "Viscous damping effect and vortex shedding performance of the novel anti-motion structures on a cylindrical FPSO". Ocean Eng. 190, 106430. <https://doi.org/https://doi.org/10.1016/j.oceaneng.2019.106430>
- Jiang, S.-C., Liu, H., Sun, T.-Z., Gu, Q., 2020. "Numerical simulation for hydrodynamic behavior of box-systems with and without narrow gaps". Ocean Eng. 214, 107698. <https://doi.org/https://doi.org/10.1016/j.oceaneng.2020.107698>
- Jin, R., Xiong, Y., Wang, Y., 2018. "Motion response analysis of Truss spar platform with small-scale cylinders under bichromatic waves", in: The 28th International Ocean and Polar Engineering Conference. International Society of Offshore and Polar Engineers.
- Jin, X., Wang, A.M., Li, H., Yu, W., He, M., Wang, A., 2018. "Floatover Installation Technology With a DP2 Class Dynamic-Positioning Semisubmersible Vessel".
- Jin, Y., Chai, S., Duffy, J., Chin, C., Bose, N., 2019. "Hydrodynamics of a conceptual FLNG system in side-by-side offloading operation". Ships Offshore Struct. 14, 104–124. <https://doi.org/10.1080/17445302.2018.1482041>
- Jin, Y., Chai, S., Duffy, J., Chin, C., Bose, N., 2018. "URANS predictions on the hydrodynamic interaction of a conceptual FLNG-LNG offloading system in regular waves". Ocean Eng. 153, 363–386. <https://doi.org/https://doi.org/10.1016/j.oceaneng.2018.01.102>
- Ju, S.H., Huang, Y.C., 2019. "Analyses of

- offshore wind turbine structures with soil-structure interaction under earthquakes". Ocean Eng. 187, 106190.
<https://doi.org/10.1016/j.oceaneng.2019.106190>
- Kang, Z., Zhang, C., Sun, L., 2017. "Research on truncation method of FPSO and offloading system in model test". Appl. Ocean Res. 67, 94–108.
<https://doi.org/https://doi.org/10.1016/j.apor.2017.06.007>
- Karimirad, M., Bachynski, E.E., 2017. "Sensitivity Analysis of Limited Actuation for Real-time Hybrid Model Testing of 5MW Bottom-fixed Offshore Wind Turbine", in: Energy Procedia. Elsevier, pp. 14–25.
<https://doi.org/10.1016/j.egypro.2017.10.331>
- Karimirad, M., Bachynski, E.E., Berthelsen, P.A., Ormberg, H., 2017. "Comparison of Real-Time Hybrid Model Testing of a Braceless Semi-Submersible Wind Turbine and Numerical Simulations".
<https://doi.org/10.1115/OMAE2017-61121>
- Kato, T., Kawamura, Y., Tahara, J., Baba, S., Sanada, Y., 2020. "Development of Side Thruster System for ASV".
- Kawahashi, T., Arai, M., Wang, X., Cheng, L.-Y., Nishimoto, K., Nakashima, A., 2019. "A study on the coupling effect between sloshing and motion of FLNG with partially filled tanks". J. Mar. Sci. Technol. 24, 917–929.
<https://doi.org/10.1007/s00773-018-0596-5>
- Kaynia, A.M., 2019. "Seismic considerations in design of offshore wind turbines". Soil Dyn. Earthq. Eng. 124, 399–407.
<https://doi.org/10.1016/j.soildyn.2018.04.038>
- Kerkeni, S., Liferov, P., Serré, N., Bridges, R., Jorgensen, F., 2018. "Station-Keeping Trials in Ice: Dynamic Positioning in Ice — Results and Learnings".
<https://doi.org/10.1115/OMAE2018-78556>
- Kiamini, S., Jalilvand, A., Mobayen, S., 2018. "LMI-based robust control of floating tension-leg platforms with uncertainties and time-delays in offshore wind turbines via T-S fuzzy approach". Ocean Eng. 154, 367–374.
<https://doi.org/https://doi.org/10.1016/j.oceaneng.2018.02.027>
- Kim, J.-S., Yoo, S.O., Kim, H.J., Lee, J.H., Han, S.L., Lee, D.Y., 2019. "Experimental and Numerical Study of Horizontal Wave Impact Loads for a Semi-Submersible Drilling Unit".
<https://doi.org/10.1115/OMAE2019-96236>
- Kim, M., Jung, K.H., Park, S.B., Lee, G.N., Duong, T.T., Suh, S.-B., Park, I.-R., 2020. "Experimental and numerical estimation on roll damping and pressure on a 2-D rectangular structure in free roll decay test". Ocean Eng. 196, 106801.
<https://doi.org/https://doi.org/10.1016/j.oceaneng.2019.106801>
- Kitazawa, D., Mizukami, Y., Kanehira, M., Takeuchi, Y., Ito, S., 2017. "Water Tank and Field Tests on the Performance of a Submersible Fish Cage for Farming Silver Salmon".
<https://doi.org/10.1115/OMAE2017-61631>
- Koop, A., 2020. "Using CFD to determine scale effects on current loads of offshore vessels in side-by-side configuration". Ocean Eng. 195, 106707.
<https://doi.org/https://doi.org/10.1016/j.oceaneng.2019.106707>
- Koop, A., Cozijn, H., Schrijvers, P., Vaz, G., 2017. "Determining Thruster-Hull Interaction for a Drill-Ship Using CFD".

- <https://doi.org/10.1115/OMAE2017-61485>
- Krishnan, R., Seeninaidu, N., 2017. "Hydrodynamic Response of Three Column Semi-Submersible Floater Supporting Vertical Axis Wind Turbine". <https://doi.org/10.1115/OMAE2017-62452>
- Kristiansen, D., Aksnes, V., Su, B., Lader, P., Bjelland, H. V., 2017. "Environmental Description in the Design of Fish Farms at Exposed Locations". <https://doi.org/10.1115/OMAE2017-61531>
- Kristiansen, D., Lader, P., Endresen, P.C., Aksnes, V., 2018. "Numerical and Experimental Study on the Seakeeping Behavior of Floating Closed Rigid Fish Cages". <https://doi.org/10.1115/OMAE2018-77254>
- Kumar, N., Kumar Varma Kolahalam, V., Kantharaj, M., Manda, S., 2018. "Suppression of vortex-induced vibrations using flexible shrouding—An experimental study". *J. Fluids Struct.* 81, 479–491. <https://doi.org/https://doi.org/10.1016/j.jfluidstruct.2018.04.018>
- Kvittem, M.I., Berthelsen, P.A., Eliassen, L., Thys, M., 2018. "Calibration of Hydrodynamic Coefficients for a Semi-Submersible 10 MW Wind Turbine". <https://doi.org/10.1115/OMAE2018-77826>
- Lader, P., Kristiansen, D., Alver, M., Bjelland, H. V., Myrhaug, D., 2017. "Classification of Aquaculture Locations in Norway With Respect to Wind Wave Exposure". <https://doi.org/10.1115/OMAE2017-61659>
- Larsen, K., Vigesimal, T., Bjørkli, R., Dalane, O., 2018. "Mooring of Semi Submersibles in Extreme Sea States: Simplified Models for Wave Drift Forces and Low Frequency Damping". <https://doi.org/10.1115/OMAE2018-77178>
- Laugesen, R., Hansen, A.M., 2015. "Experimental study of the dynamic response of the DTU 10 MW wind turbine on a tension leg platform", in: DTU Wind Energy. Phys Conf Ser. p. 92007.
- Lee, D., Lee, S.-J., 2019. "Adaptive PD for Dynamic Positioning System Based on DDPG ".
- Lee, J., Choi, S.-M., Lee, S.J., Jung, K.H., 2019. "Tension Based Heading Control Strategy of the Arctic FPSO With DP Assisted Mooring System". <https://doi.org/10.1115/OMAE2019-96557>
- Li, B., 2020. "Multi-body hydrodynamic resonance and shielding effect of vessels parallel and nonparallel side-by-side". *Ocean Eng.* 218, 108188. <https://doi.org/https://doi.org/10.1016/j.oceaneng.2020.108188>
- Li, B., Wang, L., Wang, X., Xu, S., Li, X., 2018. "Estimation of Thruster-Thruster/Current Interaction in a Dynamic Positioning System Through Supervised Learning With Neural Networks ".
- Li, D.-J., Fu, Q., Du, Z.-F., Xiao, Y., Han, R.-G., Sun, H.-H., 2018. "Structural Configuration Selection and Optimization of 7th Generation Semi-Submersible Drilling Unit". <https://doi.org/10.1115/OMAE2018-78688>
- Li, L., Jiang, Z., Ong, M.C., 2017. "A Preliminary Study of a Vessel-Shaped Offshore Fish Farm Concept". <https://doi.org/10.1115/OMAE2017-61665>

- Li, L., Jiang, Z., Ong, M.C., Hu, W., 2019a. "Design optimization of mooring system: An application to a vessel-shaped offshore fish farm". Eng. Struct. 197, 109363. <https://doi.org/https://doi.org/10.1016/j.engstruct.2019.109363>
- Li, L., Jiang, Z., Vangdal Høiland, A., Chen Ong, M., 2018a. "Numerical Analysis of a Vessel-Shaped Offshore Fish Farm". J. Offshore Mech. Arct. Eng. 140. <https://doi.org/10.1115/1.4039131>
- Li, L., Jiang, Z., Wang, J., Ong, M.C., 2019b. "Numerical Study on the Heading Misalignment and Current Velocity Reduction of a Vessel-Shaped Offshore Fish Farm". J. Offshore Mech. Arct. Eng. 141. <https://doi.org/10.1115/1.4042266>
- Li, L., Jiang, Z., Wang, J., Ong, M.C., 2018b. "Predicting the Heading Misalignment of a Vessel-Shaped Offshore Fish Farm Under Waves and Currents". <https://doi.org/10.1115/OMAE2018-77476>
- Li, Q., Wang, J., Yan, S., Gong, J., Ma, Q., 2018. "A zonal hybrid approach coupling FNPT with OpenFOAM for modelling wave-structure interactions with action of current". Ocean Syst. Eng. 8, 381–407. <https://doi.org/10.12989/ose.2018.8.4.381>
- Li, W., Tang, Y., Wang, B., Li, Y., 2018. "Internal Resonances for the Heave Roll and Pitch Modes of a Spar Platform Considering Wave and Vortex Exciting Loads in Heave Main Resonance". J. Mar. Sci. Appl. 17, 265–272. <https://doi.org/10.1007/s11804-018-0023-7>
- Li, Y., Liu, S.-J., Li, L., 2007. "Dynamic analysis of deep-ocean mining pipe system by discrete element method". China Ocean Eng. 21, 175–186.
- Li, Z.X., Wu, K., Shi, Y., Ning, L., Yang, D., 2019. "Experimental study on the interaction between water and cylindrical structure under earthquake action". Ocean Eng. 188, 106330. <https://doi.org/10.1016/j.oceaneng.2019.106330>
- Liang, Y., Tao, L., 2018. "Hydrodynamics Around a Deep-Draft Semi-Submersible With Various Corner Shapes". <https://doi.org/10.1115/OMAE2018-77135>
- Liang, Y., Tao, L., Xiao, L., Liu, M., 2017. "Experimental and numerical study on vortex-induced motions of a deep-draft semi-submersible". Appl. Ocean Res. 67, 169–187. <https://doi.org/https://doi.org/10.1016/j.apor.2017.07.008>
- Liao, K., Duan, W., Ma, Q., Ma, S., Zhao, B., Hu, C., 2017. "Numerical Analysis of Wave Impact Loads on Semi-Submersible Platform". <https://doi.org/10.1115/OMAE2017-62464>
- Lim, D.-H., Kim, Y., 2019. "Probabilistic analysis of air gap of tension-leg platforms by a nonlinear stochastic approach". Ocean Eng. 177, 49–59. <https://doi.org/https://doi.org/10.1016/j.oceaneng.2019.02.054>
- Liu, M., Xiao, L., Kou, Y., Lu, H., 2017a. "Numerical Study on Vortex-Induced Motions of Semi-Submersibles With Various Types of Columns". <https://doi.org/10.1115/OMAE2017-62355>
- Liu, M., Xiao, L., Liang, Y., Tao, L., 2017b. "Experimental and numerical studies of the pontoon effect on vortex-induced motions of deep-draft semi-submersibles". J. Fluids Struct. 72, 59–79. <https://doi.org/https://doi.org/10.1016/j.jfluidstructs.2017.04.007>
- Liu, M., Xiao, L., Yang, J., Tian, X., 2017c.

- "Parametric study on the vortex-induced motions of semi-submersibles: Effect of rounded ratios of the column and pontoon". Phys. Fluids 29, 55101. <https://doi.org/10.1063/1.4983347>
- Liu, W., Wang, J., Huang, J., Liu, Y., Li, Y., 2017. "Spar Platform Oil Storage and Offloading System Design".
- Luo-Theilen, X., Rung, T., 2019. "Numerical analysis of the installation procedures of offshore structures". Ocean Eng. 179, 116–127. <https://doi.org/10.1016/j.oceaneng.2019.03.004>
- Lyu, B., Wu, W., Yao, W., Wang, Y., Zhang, Y., Tang, D., Yue, Q., 2019. "Multibody dynamical modeling of the FPSO soft yoke mooring system and prototype validation". Appl. Ocean Res. 84, 179–191. <https://doi.org/https://doi.org/10.1016/j.apor.2019.01.011>
- Lyu, N., Ding, J., 2020. "Numerical Research on Thrust Deduction of Submerged Waterjet Propelled Transport Vessels on Inland Rivers".
- Manikandan, R., Saha, N., 2019. "Dynamic modelling and non-linear control of TLP supported offshore wind turbine under environmental loads". Mar. Struct. 64, 263–294. <https://doi.org/https://doi.org/10.1016/j.marstruc.2018.10.014>
- Martin, T., Kamath, A., Bihs, H., 2020. "A Lagrangian approach for the coupled simulation of fixed net structures in a Eulerian fluid model". J. Fluids Struct. 94, 102962. <https://doi.org/https://doi.org/10.1016/j.jfluidstructs.2020.102962>
- Matoug, C., Augier, B., Paillard, B., Maurice, G., Sicot, C., Barre, S., 2020. "An hybrid approach for the comparison of VAWT and HAWT performances for floating offshore wind turbines", in: Journal of Physics: Conference Series. IOP Publishing, p. 32026.
- Meng, L., Sun, C., Zhang, M., Han, H., Li, Y., 2021. "Dynamic mesh simulation on the effect of sloshing on concurrent two-phase flow fields for two-dimensionally packed columns simulations". Cryogenics (Guildf). 113, 103231. <https://doi.org/https://doi.org/10.1016/j.cryogenics.2020.103231>
- Molin, B., Remy, F., Kimmoun, O., Stassen, Y., 2002. "Experimental study of the wave propagation and decay in a channel through a rigid ice-sheet". Appl. Ocean Res. 24, 247–260. [https://doi.org/https://doi.org/10.1016/S0141-1187\(03\)00005-1](https://doi.org/https://doi.org/10.1016/S0141-1187(03)00005-1)
- Montasir, O.A., Yenduri, A., Kurian, V.J., 2019. "Mooring System Optimisation and Effect of Different Line Design Variables on Motions of Truss Spar Platforms in Intact and Damaged Conditions". China Ocean Eng. 33, 385–397. <https://doi.org/10.1007/s13344-019-0037-1>
- Moreno, F.M., Amendola, J., Tannuri, E.A., Ferreira, M.D., 2019. "Development of a Control Strategy for Underway Tandem-Like Oil Transfer Operation Between a Conventional and a DP Tanker". <https://doi.org/10.1115/OMAE2019-96335>
- Moulas, D., Shafiee, M., Mehmanparast, A., 2017. "Damage analysis of ship collisions with offshore wind turbine foundations". Ocean Eng. 143, 149–162. <https://doi.org/10.1016/j.oceaneng.2017.04.050>
- Müller, K., Sandner, F., Bredmose, H., Azcona, J., Manjock, A., Pereira, R., 2014. "Improved tank test procedures for scaled floating offshore wind turbines".

- Murai, M., Takahashi, K., 2017. "The Influence of an Arrangement of an Array of Semi-Submersible Type FOWTs to Their Hydrodynamic Responses". <https://doi.org/10.1115/OMAE2017-61614>
- Neale, P., Nagy, T., Grepaly, I., Tóth, P., Kristóf, G., Csobán, A., 2017. "Long-Term Abrasion Test for Seabed Mining Hose Liners ". <https://doi.org/10.4043/27707-MS>
- Niewiarowski, A., Adriaenssens, S., Pauletti, R.M., Addi, K., Deike, L., 2018. "Modeling underwater cable structures subject to breaking waves". *Ocean Eng.* 164, 199–211. <https://doi.org/https://doi.org/10.1016/j.oceaneng.2018.06.013>
- Nijun, Y., Bin, C., Jianxin, X., 2017. "Pressure Loss of Flexible Hose in Deep-Sea Mining System", in: 18th International Conference on Transport and Sedimentation of Solid Particles. Prague, Czech Republic, pp. 393–400.
- O’Connell, K., Thiebaut, F., Kelly, G., Cashman, A., 2018. "Development of a free heaving OWC model with non-linear PTO interaction". *Renew. Energy* 117, 108–115. <https://doi.org/https://doi.org/10.1016/j.renene.2017.10.027>
- O’Leary, K., Pakrashi, V., Kelliher, D., 2019. "Optimization of composite material tower for offshore wind turbine structures". *Renew. Energy* 140, 928–942. <https://doi.org/10.1016/j.renene.2019.03.101>
- Oguz, E., Clelland, D., Day, A.H., Incecik, A., López, J.A., Sánchez, G., Almeria, G.G., 2018. "Experimental and numerical analysis of a TLP floating offshore wind turbine". *Ocean Eng.* 147, 591–605. <https://doi.org/https://doi.org/10.1016/j.oceaneng.2017.10.052>
- Parenteau, T., 2012. "Flow Assurance for Deep Ocean Mining: Large-Scale Experiment for Flow Correlation Validation and Abrasion Testing ". <https://doi.org/10.4043/23250-MS>
- Parenteau, T., 2010. "Flow Assurance for Deepwater Mining". <https://doi.org/10.1115/OMAE2010-20185>
- Parenteau, T., Lemaire, A., 2011. "Flow Assurance for Deep Ocean Mining - Pressure Requirement Through S-Shape Riser and Jumper ". <https://doi.org/10.4043/21237-MS>
- Park, S.H., Lee, S.J., Lee, S., 2021. "Experimental investigation of towing- and course-stability of a FPSO towed by a tug-boat with lateral motion". *Int. J. Nav. Archit. Ocean Eng.* 13, 12–23. <https://doi.org/https://doi.org/10.1016/j.ijnaoe.2020.11.003>
- Peng, Y., Xia, J.X., Cao, B., Ren, H.T., Wu, Y., 2015. "Spatial Configurations and Particle Transportation Parameters of Flexible Hose in Deep-sea Mining System ".
- Pessoa, J., Stansberg, C.T., Fonseca, N., Laranjinha, M., 2018. "Experimental and Numerical Study of the Free Surface Elevation Over the pontoons of a Semisubmersible Platform in Waves". <https://doi.org/10.1115/OMAE2018-78009>
- Pires, O., Azcona, J., Vittori, F., Bayati, I., Gueydon, S., Fontanella, A., Liu, Y., De Ridder, E.J., Belloli, M., Van Wingerden, J.W., 2020. "Inclusion of rotor moments in scaled wave tank test of a floating wind turbine using SiL hybrid method", in: *Journal of Physics: Conference Series*. IOP Publishing, p. 32048.
- Pivano, L., Nguyen, D., Smøgeli, Ø., 2017. "Full-Scale Validation of a Vessel’s

- Station-Keeping Capability With DynCap".
<https://doi.org/10.1115/OMAE2017-62666>
- Qin, H., Xu, Z., Li, P., Yu, S., 2020. "A physical model approach to nonlinear vertical accelerations and mooring loads of an offshore aquaculture cage induced by wave-structure interactions". Ocean Eng. 197, 106904.
<https://doi.org/https://doi.org/10.1016/j.oceaneng.2019.106904>
- Ramesh, N.R., Thirumurugan, K., Rajesh, S., Deepak, C.R., Atmanand, M.A., 2013. "Experimental and Computational Investigation of Turbulent Pulsatile Flow through a Flexible Hose ".
- Rao, Q., Wang, Z., Liu, S., Fang, M., 2009. "Interaction of fluid-solid coupled flexible hose and mining machine in deep-ocean mining system", in: Eighth ISOPE Ocean Mining Symposium. International Society of Offshore and Polar Engineers.
- Ren, H., Xu, Y., Cheng, J., Cao, P., Zhang, M., Fu, S., Zhu, Z., 2019a. "Vortex-induced vibration of flexible pipe fitted with helical strakes in oscillatory flow". Ocean Eng. 189, 106274.
<https://doi.org/https://doi.org/10.1016/j.oceaneng.2019.106274>
- Ren, H., Xu, Y., Zhang, M., Deng, S., Li, S., Fu, S., Sun, H., 2019b. "Hydrodynamic forces on a partially submerged cylinder at high Reynolds number in a steady flow". Appl. Ocean Res. 88, 160–169.
<https://doi.org/https://doi.org/10.1016/j.apor.2019.04.025>
- Ren, N., Ma, Z., Fan, T., Zhai, G., Ou, J., 2018. "Experimental and numerical study of hydrodynamic responses of a new combined monopile wind turbine and a heave-type wave energy converter under typical operational conditions". Ocean Eng. 159, 1–8.
<https://doi.org/https://doi.org/10.1016/j.oceaneng.2018.03.090>
- Rhee, C. van, Munts, E., Bosch, J. van den, Lotman, R., Heeren, J., 2013. "New Developments in the Simulation of Slurry Behaviour in Spooled Hoses for Offshore Mining Applications ".
<https://doi.org/10.4043/24082-MS>
- Rindarøy, M., Selvik, Ø., Ross, A., 2020. "Hybrid DP Simulations".
<https://doi.org/10.1115/OMAE2020-18309>
- Robertson, A.N., Bachynski, E.E., Gueydon, S., Wendt, F., Schünemann, P., Jonkman, J., 2018. "Assessment of Experimental Uncertainty for a Floating Wind Semisubmersible Under Hydrodynamic Loading".
<https://doi.org/10.1115/OMAE2018-77703>
- Rodríguez, C.A., Ramos, I.S., Esperança, P.T.T., Oliveira, M.C., 2020. "Realistic estimation of roll damping coefficients in waves based on model tests and numerical simulations". Ocean Eng. 213, 107664.
<https://doi.org/https://doi.org/10.1016/j.oceaneng.2020.107664>
- Rongau, J., Viale, S., 2017. "Development of a Flexible Pipe for Deep Sea Mining ".
<https://doi.org/10.4043/27658-MS>
- Rosetti, G.F., Pinto, M.L., de Mello, P.C., Sampaio, C.M.P., Simos, A.N., Silva, D.F.C., 2019. "CFD and experimental assessment of green water events on an FPSO hull section in beam waves". Mar. Struct. 65, 154–180.
<https://doi.org/https://doi.org/10.1016/j.marstruc.2018.12.004>
- Samadi, M., Ghodsi Hassanabad, M., 2017. "Hydrodynamic response simulation of Catenary mooring in the spar truss floating platform under Caspian Sea conditions". Ocean Eng. 137, 241–246.

<https://doi.org/https://doi.org/10.1016/j.oceaneng.2017.03.004>

95406

Sanchez-Mondragon, J., Vázquez-Hernández, A.O., Cho, S.K., Sung, H.G., 2018. "Yaw motion analysis of a FPSO turret mooring system under wave drift forces". Appl. Ocean Res. 74, 170–187.
<https://doi.org/https://doi.org/10.1016/j.apor.2018.02.013>

Silva, D.F.C., Coutinho, A.L.G.A., Esperança, P.T.T., 2017a. "Green water loads on FPSOs exposed to beam and quartering seas, part I: Experimental tests". Ocean Eng. 140, 419–433.
<https://doi.org/https://doi.org/10.1016/j.oceaneng.2017.05.005>

Sanchez-Mondragon, J., Vázquez-Hernández, A.O., Cho, S.K., Sung, H.G., 2017. "Motion behavior in a turret-moored FPSO caused by piston mode effects in moonpool". Ocean Eng. 140, 222–232.
<https://doi.org/https://doi.org/10.1016/j.oceaneng.2017.05.025>

Silva, D.F.C., Esperança, P.T.T., Coutinho, A.L.G.A., 2017b. "Green water loads on FPSOs exposed to beam and quartering seas, Part II: CFD simulations". Ocean Eng. 140, 434–452.
<https://doi.org/10.1016/j.oceaneng.2016.11.008>

Sauder, T., Chabaud, V., Thys, M., Bachynski, E.E., Sæther, L.O., 2016. "Real-Time Hybrid Model Testing of a Braceless Semi-Submersible Wind Turbine: Part I — The Hybrid Approach".
<https://doi.org/10.1115/OMAE2016-54435>

Skjong, S., Pedersen, E., 2017. "Co-Simulation of a Marine Offshore Vessel in DP-Operations Including Hardware-In-the-Loop (HIL)".
<https://doi.org/10.1115/OMAE2017-61164>

Sauder, T., Tahchiev, G., 2020. "From Soft Mooring System to Active Positioning in Laboratory Experiments".
<https://doi.org/10.1115/OMAE2020-19103>

Soeb, M.R., Islam, A.B.M.S., Jumaat, M.Z., Huda, N., Arzu, F., 2017. "Response of nonlinear offshore spar platform under wave and current". Ocean Eng. 144, 296–304.
<https://doi.org/https://doi.org/10.1016/j.oceaneng.2017.07.042>

Sayed, M., Islam, S., Watson, D., Kubat, I., Gash, R., Wright, B., 2017. "DP Drillship Stationkeeping in Ice - Comparison Between Numerical Simulations and Ice Basin Tests".

Song, H. Do, Kim, Y.-S., Suh, J.-C., 2019. "A Research of the DP Thruster Analysis with Various Duct Shapes for the Model Test".

Scott, D.C.B., Muir, J.F., 2000. "Offshore cage systems: A practical overview". Option Mediterr. Cent. Adv. Mediterr. Agron. Stud. 79–89.

Subbulakshmi, A., Sundaravadivelu, R., 2021. "Effects of damping plate position on heave and pitch responses of spar platform with single and double damping plates under regular waves". Ocean Eng. 224, 108719.
<https://doi.org/https://doi.org/10.1016/j.oceaneng.2021.108719>

Seo, M.-G., Ha, Y.-J., Kim, N.-W., Nam, B.W., Lee, K.-S., 2019. "Experimental Evaluation of Wave Impact Loads on Semi-Submersible Structure According to Trim Angle".
<https://doi.org/10.1115/OMAE2019->

Sun, L., Ding, Y.F., Zheng, J.T., Zong, Z., Liu, C.F., 2018. "Numerical Study of Vortex Induced Motions of Spar and Semi-

- Submersible Platforms at High Reynolds Numbers".
<https://doi.org/10.1016/j.apor.2019.01.003>
- Takano, S., Ono, M., Masanobu, S., 2015. "Evaluation of Wearing Pipe for Subsea Mining With Large Particles in Slurry Transportation".
<https://doi.org/10.1115/OMAE2015-41217>
- Tan, J.H.C., Teng, Y.J., Kiprawi, F., 2017. "Vortex Induced Motion of a Dry Tree Semisubmersible".
<https://doi.org/10.1115/OMAE2017-61653>
- Tang, Z., Wang, L., Yi, F., He, H., 2020. "An Optimized Thrust Allocation Algorithm for Dynamic Positioning System Based on RBF Neural Network".
<https://doi.org/10.1115/OMAE2020-18267>
- Thorsen, M.J., Challabotla, N.R., Sævik, S., Nydal, O.J., 2019. "A numerical study on vortex-induced vibrations and the effect of slurry density variations on fatigue of ocean mining risers". *Ocean Eng.* 174, 1–13.
<https://doi.org/https://doi.org/10.1016/j.oceaneng.2019.01.041>
- Thys, M., Chabaud, V., Sauder, T., Eliassen, L., Sæther, L.O., Magnussen, Ø.B., 2018. "Real-Time Hybrid Model Testing of a Semi-Submersible 10MW Floating Wind Turbine and Advances in the Test Method".
<https://doi.org/10.1115/IOWTC2018-1081>
- Thys, M., Fontanella, A., Taruffi, F., Belloli, M., Berthelsen, P.A., 2019. "Hybrid Model Tests for Floating Offshore Wind Turbines".
<https://doi.org/10.1115/IOWTC2019-7575>
- Tian, X., Wang, Q., Liu, G., Liu, Y., Xie, Y., Deng, W., 2019. "Topology optimization design for offshore platform jacket structure". *Appl. Ocean Res.* 84, 38–50.
<https://doi.org/10.1016/j.apor.2019.01.003>
- Tidwell, J.H., 2012. Aquaculture production systems. Wiley Online Library.
- Tsukada, Y., Ueno, M., Miyazaki, H., Takimoto, T., 2013. "An Auxiliary Thruster for Free-Running Model Ship Test".
<https://doi.org/10.1115/OMAE2013-10569>
- Tumen Ozdil, N.F., Akilli, H., 2019. "Flow comparison around horizontal single and tandem cylinders at different immersion elevations". *Ocean Eng.* 189, 106352.
<https://doi.org/https://doi.org/10.1016/j.oceaneng.2019.106352>
- Turner, A.A., Steinke, D.M., Nicoll, R.S., 2017. "Application of Wake Shielding Effects With a Finite Element Net Model in Determining Hydrodynamic Loading on Aquaculture Net Pens".
<https://doi.org/10.1115/OMAE2017-61330>
- Turner, A.A., Steinke, D.M., Nicoll, R.S., Stenmark, P., 2018. "Comparison of Taut and Catenary Mooring Systems for Finfish Aquaculture".
<https://doi.org/10.1115/OMAE2018-78261>
- Turner, R., 2000. "Offshore mariculture: Site evaluation". *Mediterr. offshore Maric.* 141–157.
- Uzunoglu, E., Guedes Soares, C., 2019. "A system for the hydrodynamic design of tension leg platforms of floating wind turbines". *Ocean Eng.* 171, 78–92.
<https://doi.org/https://doi.org/10.1016/j.oceaneng.2018.10.052>
- Vercrujssse, P.M., Verichev, S., 2011. "Vertical Hydraulic Transport for Deep Sea Mining Applications", in: Proceedings of 40th Underwater Mining Institute Conference. pp. 14–18.

- Vieira, D.P., de Mello, P.C., Dotta, R., Nishimoto, K., 2018. "Experimental investigation on the influence of the liquid inside the tanks in the wave behavior of FLNG vessels in side-by-side offloading operations". Appl. Ocean Res. 74, 28–39. <https://doi.org/https://doi.org/10.1016/j.apor.2018.02.019>
- Vittori, F., Bouchotrouch, F., Lemmer, F., Azcona, J., 2018. "Hybrid Scaled Testing of a 5MW Floating Wind Turbine Using the SiL Method Compared With Numerical Models". <https://doi.org/10.1115/OMAE2018-77853>
- Wang, A.-D., Bi, C.-W., Dong, G.-H., Guo, S.-A., 2020. "Numerical Study on the Dynamic Characteristics of a Fixed Horizontal Cylindrical Fish Cage under Earthquake Load".
- Wang, A.M., Chen, R., He, M., Zhu, X., Xu, J., van't Padje, W., 2019. "Virtual Reality Simulations for Dynamic Positioning Floatover Installation".
- Wang, C.M., Chu, Y.I., Park, J.C., 2019. "Moving offshore for fish farming". J. Aquac Mar Biol 8, 38–39.
- Wang, G., Liu, S., 2005. "Three-Dimensional DEM Model For Deep-Ocean Mining Pipe System".
- Wang, G., Liu, S., Li, L., 2007. "FEM modeling for 3D dynamic analysis of deep-ocean mining pipeline and its experimental verification". J. Cent. South Univ. Technol. 14, 808–813. <https://doi.org/10.1007/s11771-007-0154-5>
- Wang, S., Wang, X., Woo, W.L., 2019. "Effects of the asymmetric riser and bilge keel arrangements on FPSO green water assessment". Appl. Ocean Res. 86, 166–176. <https://doi.org/https://doi.org/10.1016/j.apor.2019.02.013>
- Wang, S., Wang, X., Woo, W.L., Seow, T.H., 2017. "Study on green water prediction for FPSOs by a practical numerical approach". Ocean Eng. 143, 88–96. <https://doi.org/https://doi.org/10.1016/j.oceaneng.2017.07.052>
- Wang, X., Zhou, J.-F., 2020. "Numerical and experimental study on the scale effect of internal solitary wave loads on spar platforms". Int. J. Nav. Archit. Ocean Eng. 12, 569–577. <https://doi.org/https://doi.org/10.1016/j.ijnaoe.2020.06.001>
- Wang, Z., Rao, Q., Liu, S., 2012. "Fluid-solid interaction of resistance loss of flexible hose in deep ocean mining". J. Cent. South Univ. 19, 3188–3193. <https://doi.org/10.1007/s11771-012-1394-6>
- Wang, Z., Rao, Q., Liu, S., 2011. "Dynamic Analysis of Seabed-Mining Machine-Flexible Hose Coupling In Deep Sea Mining".
- Weiss, C.V.C., Castellanos, O., Ondiviela, B., Juanes, J.A., Guanche Garcia, R., 2018. "Development of a Tool to Identify Potential Zones for Offshore Aquaculture: A Global Case Study for Greater Amberjack". <https://doi.org/10.1115/OMAE2018-77870>
- Wu, X., Ge, F., Hong, Y., 2012. "A review of recent studies on vortex-induced vibrations of long slender cylinders". J. Fluids Struct. 28, 292–308. <https://doi.org/https://doi.org/10.1016/j.jfluidstruct.2011.11.010>
- Wu, X., Hu, Y., Li, Y., Yang, J., Duan, L., Wang, T., Adcock, T., Jiang, Z., Gao, Z., Lin, Z., Borthwick, A., Liao, S., 2019. "Foundations of offshore wind turbines: A review". Renew. Sustain. Energy Rev.

- 104, 379–393.
<https://doi.org/10.1016/j.rser.2019.01.012>
- Xu, N., Qin, L., Wang, Y., 2018. "Application of Dynamic Positioning Float-Over Technology to HZ25-8 DPP Topside Installation".
- Xu, S., Wang, X., Wang, L., Li, X., Yang, L., Li, B., 2017. "Investigation of the Positioning Performances for DP Vessels with Thruster Failure Modes by a Novel Synthesized Criterion".
- Xu, Z., Qin, H., 2020. "Fluid-structure interactions of cage based aquaculture: From structures to organisms". Ocean Eng. 217, 107961.
<https://doi.org/https://doi.org/10.1016/j.oceaneng.2020.107961>
- Yan, B., Luo, M., Bai, W., 2019. "An experimental and numerical study of plunging wave impact on a box-shape structure". Mar. Struct. 66, 272–287.
<https://doi.org/https://doi.org/10.1016/j.marstruc.2019.05.003>
- Yang, C.K., Kim, M., 2018. "Numerical assessment of the global performance of spar and FPSO connected by horizontal pipeline bundle". Ocean Eng. 159, 150–164.
<https://doi.org/https://doi.org/10.1016/j.oceaneng.2018.03.075>
- Yang, H., Xu, P., 2018. "Parametric Resonance Analyses for Spar Platform in Irregular Waves". China Ocean Eng. 32, 236–244.
<https://doi.org/10.1007/s13344-018-0025-x>
- Yang, L., Nestegård, A., Falkenberg, E., 2018. "Analysis of Semi-Submersible Under Combined High Waves and Current Conditions Compared With Model Tests".
<https://doi.org/10.1115/OMAE2018-78595>
- Yang, S.-H., Ringsberg, J.W., Johnson, E., 2018. "Parametric study of the dynamic motions and mechanical characteristics of power cables for wave energy converters". J. Mar. Sci. Technol. 23, 10–29.
<https://doi.org/10.1007/s00773-017-0451-0>
- Yang, S.-H., Ringsberg, J.W., Johnson, E., Hu, Z., 2017. "Biofouling on mooring lines and power cables used in wave energy converter systems—Analysis of fatigue life and energy performance". Appl. Ocean Res. 65, 166–177.
<https://doi.org/https://doi.org/10.1016/j.apor.2017.04.002>
- Yenduri, A., Magee, A.R., Liu, J., Xu, W., Choudhary, A., Hussain, A.A., 2019. "Realistic Adaptive DP Controller for Flotel Operating in Side-by-Side Configuration With FPSO".
<https://doi.org/10.1115/OMAE2019-96577>
- Yoon, C.-H., Lee, D.-K., Park, Y.-C., Kim, Y.-J., Kwon, S., 2006. "Flow Analysis of Lifting Pump And Flexible Hose For Sea-Test".
- Yoon, C.-H., Park, Y.-C., Park, J., Kim, Y.-J., Kang, J.-S., Kwon, S.-K., 2009. "Solid-Liquid Flow Experiment With Real And Artificial Manganese Nodules In Flexible Hoses". Int. J. Offshore Polar Eng. 19.
- Yoon, C.H., Kwon, K.S., Kwon, S.K., Lee, D.K., Park, Y.C., Kwon, O.K., Sung, W.M., 2001. "An Experimental Study On the Flow Characteristics of Solid-liquid Two-phase Mixture In a Flexible Hose".
- Yoon, C.H., Lee, D.K., Kwon, K.S., Kwon, S.K., Kim, I.K., Park, Y.C., Kwon, O.K., 2002. "Experimental and Numerical Analysis on the Flow Characteristics of Solid-Liquid Two-Phase Mixtures in a Curvature Pipe", in: The Twelfth International Offshore and Polar Engineering Conference. International Society of Offshore and Polar Engineers.

- Yoon, C.H., Park, J.-M., Kang, J.S., Kim, Y., Park, Y.C., Park, S.G., Kim, C., Kang, S.S., Kim, S.B., Kim, W.T., Kwon, S.K., Ahn, B.S., Ha, M.-K., 2011. "Shallow Lifting Test For the Development of Deep Ocean Mineral Resources In Korea".
- Yu, A., Cheng, Y., Eason, R., 2010. "Slurry Flow Simulation for Deepwater Mining Application", in: ASME 2010 29th International Conference on Ocean, Offshore and Arctic Engineering.
- Yu, J., Hao, S., Yu, Y., Chen, B., Cheng, S., Wu, J., 2019. "Mooring analysis for a whole TLP with TTRs under tendon one-time failure and progressive failure". Ocean Eng. 182, 360–385. <https://doi.org/https://doi.org/10.1016/j.oceaneng.2019.04.049>
- Yu, S., Yoshida, T., Han, J., Mizukami, Y., Kitazawa, D., Liu, L., 2018. "Model Experiment of a Controllable Depth Cage and its Mooring System". <https://doi.org/10.1115/OMAE2018-77757>
- Yu, T., Zhang, Y., Zhang, S., Shi, Z., Chen, X., Xu, Y., Tang, Y., 2019. "Experimental study on scour around a composite bucket foundation due to waves and current". Ocean Eng. 189, 106302. <https://doi.org/10.1016/j.oceaneng.2019.106302>
- Yu, Y., Feng, G., Ren, H., 2017. "Ultimate Strength Assessment of Semi-Submersible Platform Under Different Load Conditions". <https://doi.org/10.1115/OMAE2017-61696>
- Zamora-Rodriguez, R., Gomez-Alonso, P., Amate-Lopez, J., De-Diego-Martin, V., Dinoi, P., Simos, A.N., Souto-Iglesias, A., 2014. "Model Scale Analysis of a TLP Floating Offshore Wind Turbine". <https://doi.org/10.1115/OMAE2014-24089>
- Zanganeh, R., Thiagarajan, K., 2018. "Prediction of the mean heading of a turret moored FPSO in bi-modal and bi-directional sea states". Appl. Ocean Res. 78, 156–166. <https://doi.org/https://doi.org/10.1016/j.apor.2018.04.006>
- Zangeneh, R., Thiagarajan, K.P., Cameron, M., 2017. "Effect of Wind Loads and Damping on Heading Stability of FPSOs". <https://doi.org/10.1115/OMAE2017-62134>
- Zhang, Q., Ma, P., Liu, J., Kumar Jaiman, R., 2017. "Numerical Simulation of Single Thruster in Open Water". <https://doi.org/10.1115/OMAE2017-61635>
- Zhang, X., Song, X., Qiu, W., Yuan, Z., You, Y., Deng, N., 2018. "Multi-objective optimization of Tension Leg Platform using evolutionary algorithm based on surrogate model". Ocean Eng. 148, 612–631. <https://doi.org/https://doi.org/10.1016/j.oceaneng.2017.11.038>
- Zhao, D., Hu, Z., Chen, G., 2017. "Experimental investigation on dynamic responses of FLNG connection system during side-by-side offloading operation". Ocean Eng. 136, 283–293. <https://doi.org/https://doi.org/10.1016/j.oceaneng.2017.03.034>
- Zhao, D., Hu, Z., Chen, G., Chen, X., Feng, X., 2018. "Coupling analysis between vessel motion and internal nonlinear sloshing for FLNG applications". J. Fluids Struct. 76, 431–453. <https://doi.org/https://doi.org/10.1016/j.jfluidstructs.2017.10.008>
- Zhao, L., Tan, Z., Hou, Y., Yin, Y., Meng, W., 2018. "Experimental Research on Vortex-Induced Vibration of Flexible Catenary Riser Model". <https://doi.org/10.1115/OMAE2018->

78363

Zone for a Semi-Submersible".
<https://doi.org/10.1115/OMAE2018-77294>

Zhao, L., Xu, S., Wang, X., Ding, A., 2020. "A Novel Saturation Protocol on the Thrust Allocation Strategy for Dynamic Positioning of Marine Vessels Operating in Extreme Wave Conditions".

Zhao, W., Wan, D., 2018. "CFD Parametric Study of Geometrical Variations on the Vortex-Induced Motions of Deep-Draft Semi-Submersibles".
<https://doi.org/10.1115/OMAE2018-78377>

Zhao, Y., Guan, C., Bi, C., Liu, H., Cui, Y., 2019. "Experimental Investigations on Hydrodynamic Responses of a Semi-Submersible Offshore Fish Farm in Waves". *J. Mar. Sci. Eng.* 7, 238.
<https://doi.org/10.3390/jmse7070238>

Zhao, Z., Wang, W., Han, D., Shi, W., Si, Y., Li, X., 2020. "Structural Control of an Ultra-Large Semi-Submersible Floating Offshore Wind Turbine". *J. Offshore Mech. Arct. Eng.* 143.
<https://doi.org/10.1115/1.4048880>

Zheng, H., Zheng, X.Y., Lei, Y., 2020. "A Novel Floating Wind-Solar-Aquaculture Concept: Fully Coupled Analysis and Technical Feasibility Study".

Zhou, X., Mizukami, Y., Yoshida, T., Kitazawa, D., 2018. "Motion Analysis of Flexible Hose Based on Water Tank Experiment".
<https://doi.org/10.1115/OMAE2018-77597>

Zhu, S., 2018. "Optimization of Heave Motions for a Four Column Semi-Submersible Based on Genetic Algorithm".
<https://doi.org/10.1115/OMAE2018-77289>

Zhu, S., Rentsch, H.C., Lefranc, M., Haaheim, H., 2018. "Investigation of Fatigue Damage for Stiffened Plates in Splash